UNIVERSITÉ DE STRASBOURG

ÉCOLE DOCTORALE DE SCIENCES CHIMIQUES

Institut de Chimie UMR 7177

THÈSE présentée par :

Thiago Diamond REIS FIRMINO

soutenue le : **27 mai 2014**

pour obtenir le grade de : **Docteur de l'université de Strasbourg**

Discipline / Spécialité : Chimie / Chimie Théorique

The quantum dynamics of the diffusion of dissociatively adsorbed diatomic molecules

THÈSE dirigée par :
M. MARQUARDT Roberto Professeur, Université de Strasbourg

RAPPORTEURS :
M. MONNERVILLE, Maurice Professeur, Université de Lille
M. TREMBLAY, Jean-Christophe Emmy-Noether Junior Group Leader Freie Universität Berlin

---

AUTRES MEMBRES DU JURY :
M. BONNEFONT, Antoine Maître de Conférences-HDR, Université de Strasbourg

Remerciements

À la fin de ces trois ans de thèse au sein du laboratoire de Chimie Quantique (LCQ) de Strasbourg, je tiens à adresser mes remerciements à l'ensemble de l'équipe.

Je remercie Chantal Daniel et Vincent Robert, directeurs du LCQ pour leur accueil chaleureux.

Je remercie vivement le professeur Roberto Marquardt pour m'avoir encadré et guidé au cours de ces trois années de thèse et pour les qualités humaines et scientifiques dont il a fait preuve tout au long de ce travail.

Je remercie le Dr. Fabien Gatti, de l'Université de Montpellier et le Dr. David Zanutini de l'Université de Caen pour m'avoir formé à la manipulation du logiciel MCTDH et pour les nombreuses et fructueuses discussions scientifiques que nous avons eues.

Je remercie le Dr. Wei Dong, de l'École normale supérieure de Lyon pour les fructeuses discussions scientifiques concernant sa surface d'énergie potentielle de H_2/Pd(111).

Je remercie également l'ensemble des membres de l'équipe du LCQ: Sylvie Fersing, Étienne Gindensperger, Emmanuel Fromager, Christophe Gourlaouen et Paola Sager pour avoir facilité mon intégration dans l'équipe et pour m'avoir apporté le soutien scientifique et technique dont j'avais besoin.

Au terme de ces trois années, j'ai beaucoup enrichi ma culture scientifique grâce aux échanges avec les autres thésards et post-doctorants de l'équipe du LCQ. Je souhaite particulièrement remercier les Drs Yann Cornaton, Murali Krishna, David Sulzer et Alex Domingo avec qui j'ai partagé des très bons moments conviviaux et tout particulièrement Tim Krah pour les événements sportifs que nous avons partagés.

Je ne peux pas oublier mes camarades de l'équipe qui mettent toujours la bonne ambiance dans le LCQ: Julien Eng, Julia Lefevre, Odile Franck et Benjamin Meyer.

Enfin, je voudrais remercier toutes les personnes que j'ai rencontrées au cours de mon séjour à Strasbourg: Adrien Cornic, Alvise Sgaravatti, Anne-Iris Romens, Zoé Dherbassy, entre autres.

Je remercie l'ensemble des membres du jury pour avoir accepté de juger ce travail: Antoine Bonnefont, Maître de Conférences au Laboratoire d'Électrochimie de Strasbourg, Jean-Cristophe Tremblay, leader du groupe de recherche en dynamique quantique dissipative à la Freie Universität Berlin et Maurice Monnerville, Professeur de l'Université des Sciences et Technologies de Lille au Laboratoire PhLAM.

Finalement, j'aimerais remercier mes parents et Émilie Chevrier pour leur soutien moral.

“Le monde et la science ont leurs données propres,
qui se touchent et ne se pénètrent pas.
L’une nous montre à quel but nous devons viser,
l’autre, le but étant donné,
nous donne les moyens de l’attendre. ”

- Henri Poincaré

Contents

List of Figures

List of Tables

Résumé (French Abstract)

Les molécules gazeuses interagissent avec des surfaces solides dans presque tous les environnements de l'univers. Une fois ces molécules adsorbées sur ces surfaces, on se pose quelques questions comme: Comment bougent-elles sur ces surfaces? Dans quelle échelle de temps ce mouvement se passe-t-il? Est-ce que ce mouvement peut être interprété comme une diffusion classique? Si c'est une diffusion quantique, comment peut-on la caractériser? Étudier les interactions de ces molécules avec certains métaux a une importance pour la catalyse hétérogène (par exemple pour la synthèse de NH_3) , dans la microélectronique, ou encore dans le stockage d'hydrogène, pour n'en mentionner que quelques exemples.

Comprendre les réactions chimiques qui ont lieu sur la surface requiert une compréhension détaillée de sa structure au niveau atomique. La spectrométrie de perte d'énergie des électrons à haute résolution ("High Resolution Electron Energy-Loss Spectroscopy"), par exemple, permet d'étudier les modes de vibration de l'adsorbat et même d'identifier des espèces qui sont adsorbées. Par contre il n'y a pas beaucoup de techniques expérimentales capables de détailler le mécanisme de la diffusion latérale d'atomes ou de molécules sur une surface. Des études réalisées par spectroscopie Spin-Echo ^{3}He de la diffusion de CO sur Cu(001) ont montré que selon les directions $< 110 >$ et $< 100 >$ il y a une dépendance oscillatoire de l'élargissement quasi-élastique du facteur de structure dynamique en fonction du transfert de quantité de mouvement. Cela a été modélisé par un mécanisme appelé diffusion par saut, qui relève de la mécanique classique. De ce modèle il a été conclut que la relation entre les énergies de barrières des sites «hollow» et «bridge» est environ $\frac{E_{\mathrm{H}}}{E_{\mathrm{B}}} \approx 1$. Cependant ce résultat n'est pas en accord avec les données actuelles disponibles à partir de calculs de structures électronique. Un traitement quantique de la diffusion

pourrait expliquer les données expérimentales et en même temps garder l'accord avec les calculs de structure électronique. Les effets quantiques sur la dynamique et la cinétique des adsorbats n'ont même pas été bien éclaircis. Dans ce travail, nous aborderons, pour mieux comprendre les possibles effets quantiques sur la diffusion des espèces adsorbées, le cas de l'adsorption dissociative de H_2 sur Pd(111), parce que ce système s'est avéré le plus simple à étudier. En fait, dû à la dissociation de la molécule lors de son adsorption, il sera possible d'apporter des réponses aux questions posées ci-dessus par l'étude plus simple d'un seul atome d'hydrogène sur le substrat.

Surface de potentiel

La surface de potentiel (SEP) est l'énergie électronique d'un système en fonction des coordonnées des atomes. La variation d'une SEP, montre le résultat de la compétition entre l'attraction et la répulsion, par exemple, entre la molécule et la surface.

H_2/Cu**(100)**

Le premier système étudié dans ce travail a été celui de H_2 sur Cu(100) où (100) représente le plan selon les indices de Miller. Pour réaliser ces études sur le substrat, il a fallu bien comprendre les fonctions multidimensionnelles des SEP qui existent sous forme analytique. Afin de s'assurer que la SEP [Somers *et al.*, *J. Chem. Phys.* , vol. 116, n. 9, pp. 3841, 2002; *J. Chem. Phys.* , vol. 121, n. 22, pp. 11379, 2004.] pouvait être utilisée pour réaliser ces études, plusieurs résultats de la référence ont été reproduits. Il a donc été constaté que la SEP n'est pas globale, comme le montre la Figure 1a. Cette figure montre la variation de l'énergie électronique en fonction de r, la distance entre deux atomes d'hydrogène, et ce pour une configuration parallèle de H_2 à la surface d'adsorption. Le résultat obtenu pour cette coupe nous fait penser que la diffusion des atomes de H sur la surface de Cu(100) est totalement libre, soit, sans aucune barrière d'énergie. Cela, n'est pas physique. C'est la conséquence d'un traitement mathématique artificiel fait dans les références Somers *et al.* [*J. Chem. Phys.* , vol. 116, n. 9, pp. 3841, 2002; *J. Chem. Phys.* , vol. 121, n. 22,

pp. 11379, 2004]. On attend en fait une variation de l'énergie lorsque les atomes de H s'approchent d'un atome de Cu. La ligne en pontillé montre cette fonction attendue, où l'interaction $H - H$ est plus faible que l'interaction $H - Cu$. On devrait même attendre une périodicité avec un période $2r_e$ ($r_e = 255$ pm, est la distance entre deux atomes de Cu). Par conséquence, la SEP de H_2/Cu(100) est inappropriée pour les études de diffusion quantique sur le substrat que l'on souhaite faire. Le résultat de cette étude a été communiqué aux auteurs des références.

H_2/Pd**(111)**

Comme le but du projet n'est pas de développer une nouvelle SEP mais d'étudier la diffusion d'un adsorbat sur une surface avec une SEP déjà existante, il a été décidé d'étudier le système H_2/Pd(111). La SEP de H_2/Pd(111) a été développée par Dong *et al* [*J. Chem. Phys.* , vol. 132, n. 1, pp. 014704, 2010; *Phys. Rev. B*, vol. 83, n. 22, pp. 125418, 2011.] en utilisant la théorie de la fonctionnelle de la densité [Dong et Hafner, *Phys. Rev. B* , vol. 56, n. 23, pp. 15396, 1997.], représentée analytiquement selon la théorie REBO "Reactive Bond Order". La fonctionnelle utilisée dans le travail de Dong *et al*, est celle développée par Perdew et Wang (PW91). Cette SEP décrit l'adsorption dissociative de H_2 sur la surface de Pd dont le plan réticulaire selon les indices de Miller est (111). La Figure 1b montre une coupe unidimensionnelle en r où l'on voit la périodicité attendue lorsque les atomes d'hydrogène se déplacent le long du substrat. La sous-routine de ce potentiel a été réécrite en FORTRAN 90, et modifiée pour pouvoir décrire la diffusion d'un seul atome d'hydrogène et pour en faire l'interface avec le logiciel MCTDH, discuté ci-dessous, qui permet d'aborder la dynamique quantique du système.

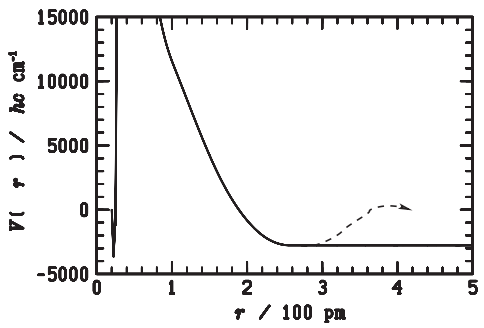

(a) SEP de H_2/Cu(100) lorsque z = 60 pm. Le dessin à la main en pointillé représente la fonction attendue.

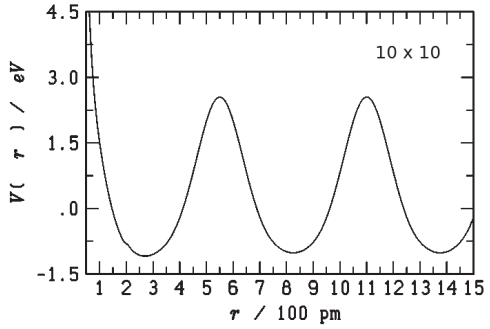

(b) SEP de H_2/Pd(111) lorsque z = 100 pm.

Figure 1 – Coupes unidimensionnelles des SEP de H_2/Cu(100) (a) et de H_2/Pd(111) (b) en fonction de r, la distance entre les deux atomes d'hydrogène. Dans les deux coupes, le dihydrogène est orienté parallèlement à la surface aux distances z indiquées.

Dynamique quantique

Méthodes

Dans ce travail, le logiciel MCTDH ("Multi-Configuration Time-Dependent Hartree") a été utilisé pour étudier la dynamique quantique. Le logiciel MCTDH permet de décrire le mouvement des atomes au vu d'une SEP, selon les règles de la mécanique quantique. Le logiciel résout l'équation de Schrödinger dépendant du temps $\mathrm{i}\hbar\frac{\partial}{\partial t}\,\Psi(t,\boldsymbol{x}) = \hat{H}\,\Psi(t,\boldsymbol{x})$ où i est l'unité imaginaire, $\hbar$ est la constate de Planck réduite, égal à $\frac{h}{2\pi}$, et $\hat{H}$ est l'hamiltonien. C'est un opérateur différentiel qui dépend de l'énergie cinétique et de l'énergie potentielle. Cette dernière est justement la SEP discutée auparavant. $\Psi(t,\boldsymbol{x})$ est la fonction d'onde qui décrit l'état du noyau d'hydrogène à l'instant t en fonction de sa position dans l'espace ($\boldsymbol{x}$), qui peut être le vecteur à trois dimensions des coordonnées cartésiennes. Pour le dihydrogène, c'est un vecteur à six dimensions. Plusieurs types de coordonnées ont été testées pour décrire le mouvement d'hydrogène: les coordonnées polaires, les coordonnées cartésiennes et les coordonnés "twisted". Pour ces dernières, l'axe y fait un angle de 120 degrés avec la coordonnée cartésienne $x = x_c$ (voir la Figure 2a). L'espace ainsi formé est non-euclidien. Les coordonnées "twisted" ont finalement été

retenues car la périodicité du système est beaucoup mieux exploitée dans cet espace. Les coordonnées cartésiennes sont représentées par x_c et y_c. Un atome adsorbé peut faire des vibrations le long de x_c et y_c, que l'on appelle vibrations parallèles au substrat, et une vibration le long de z, perpendiculaire au substrat. Les termes vibrationnels ont été calculés par la méthode de relaxation améliorée en bloc ("*improved relaxation in block form*"). La relaxation améliorée ("*improved relaxation*") optimise les fonctions de base par une propagation en temps imaginaire $\tau = -it$ où les coefficients sont obtenus par diagonalisation d'une matrice réduite qui représente l'hamiltonien par l'algorithme de Davidson. La propagation et la relaxation dans MCTDH utilisent la décomposition $\Psi(t, \boldsymbol{x}) = \sum_L b_L(t)\, \Phi_L(t, \boldsymbol{x})$, où $b_L(t)$ sont des coefficients complexes dépendant du temps et $\Phi_L(t, \boldsymbol{x})$ sont les fonctions de base dépendant du temps et du vecteur $\boldsymbol{x}$. Le fait que les fonctions de base sont dépendant du temps permet de représenter la fonction d'onde $\Psi(t, \boldsymbol{x})$ de forme très compacte. Cela est le grand avantage de la méthode MCTDH, qui permet ainsi de décrire des problèmes de grande dimensionalité. Le désavantage est que pour obtenir les fonctions $b_L(t)$ et $\Phi_L(t, \boldsymbol{x})$, il faut résoudre un système complexe d'équations différentielles non-linéaires. La résolution de ces équations est effectuée au sein du logiciel, mais un très grand nombre des calculs préliminaires a été nécessaire pour s'assurer de la convergence et exactitude des résultats finaux.

Résultats et discussions

Le traitement le plus simple de la dynamique quantique, est celui d'une cellule minimale, appelée aussi grille 1. Sur la Figure 2a on peut voir les coordonnées x et y choisies pour décrire le mouvement parallèle sur le substrat. Le losange est la structure la plus petite qui peut être répétée périodiquement. Dans le losange on voit les sites d'adsorption d'hydrogène sur Pd(111) les plus stables, "fcc" ("face centered cubic") et "hcp" ("hexagonal close-packed"). Comme le système étudié est périodique, on voit en pointillé où ces sites sont trouvés en dehors du losange. La Figure 2b montre une coupe unidimensionnelle de la SEP le long de la coordonnée cartésienne y_c. On y voit les deux sites d'adsorption "fcc" et "hcp", séparés par une barrière de 13 kJ mol^{-1} ($\sim$ 1140 $hc\,\mathrm{cm}^{-1}$). La différence d'énergie entre ces deux puits vaut 2 kJ mol^{-1} ($\sim$ 160 $hc\,\mathrm{cm}^{-1}$). La courbe pleine

donne l'énergie électronique. La courbe pointillée représente le premier canal adiabatique quand on ajoute l'énergie de vibration point zéro (EPZ) des coordonnées autres que celles montrées dans la Figure 2b. On constate qu'après avoir ajouté l'EPZ à la barrière électronique, la barrière effective augmente de 3,2 kJ mol^{-1} ($\sim$ 256 $hc\,\mathrm{cm}^{-1}$). Cela est déjà un phénomène quantique constaté dans ce travail.

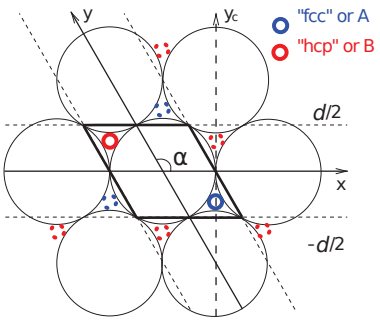

(a) Cellule unitaire de Pd(111) et les sites d'adsorption les plus stables "fcc" et "hcp" (d = 274 pm est la distance entre les deux atomes de Pd).

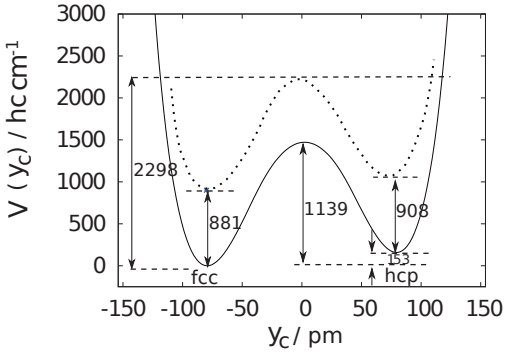

(b) Coupe unidimensionelle de la SEP le long de y_c quand x_c vaut $\frac{d}{2}$.

Figure 2 – Schéma de la cellule minimale et la coupe unidimensionnelle de la SEP le long de y_c.

Le spectre vibrationnel de H sur Pd(111) obtenu par spectrométrie de perte d'énergie des électrons à haute résolution [Conrad *et al*, *J. Electron. Spectrosc. Relat. Phenom.* , vol. 38, n. 0, pp. 289, 1986.] montre deux pics importants, l'un en 96 meV (774 $hc\,\mathrm{cm}^{-1}$) et l'autre en 126 meV (1016 $hc\,\mathrm{cm}^{-1}$). Saalfrank et Tremblay [*J. Chem. Phys.* , vol. 131, n. 8, pp. 084716, 2009.] ont calculé les termes vibrationnels fondamentaux pour le système H/Pd(111) et ont obtenu 717,4 cm^{-1} et 922,4 cm^{-1} . Ils ont attribué le premier terme à la vibration parallèle sur le site "fcc" ($\nu_{\mathrm{p,fcc}}$) et le deuxième à la vibration perpendiculaire sur le site "fcc" ($\nu_{\mathrm{z,fcc}}$). Ils ont calculé aussi les termes vibrationnels concernant les vibrations parallèle et perpendiculaire sur le site "hcp" (928,2 et 1117,7 cm^{-1} , respectivement). Les transitions spectrales fondamentales correspondant à ces termes ne peuvent pas être distinguées expérimentalement pour cause de la basse résolution de la technique expérimentale. Les termes vibrationnels issus du présent travail par l'utilisation de MCTDH, en particulier par la relaxation améliorée en bloc, sont 743,6 et 1047,6 cm^{-1} pour les modes

de vibration parallèle et perpendiculaire, respectivement, sur le site "fcc" 920,2 ainsi que 1200,2 cm^{-1} , sur le site "hcp". Ces résultats théoriques sont en bon accord avec le spectre expérimental et même mieux que ceux obtenus dans les travaux de Saalfrank et Tremblay.

Un autre résultat original de ce travail est la découverte que les états stationnaires de vibration perpendiculaire ne sont pas localisés aux sites "fcc" et "hcp". Ces états sont le résultat d'une interaction entre 4 modes de vibration localisés; ces modes localisés sont: un mode avec 1 quantum d'énergie de vibration perpendiculaire et un autre mode avec 2 quanta d'énergie de vibration parallèle, et ce pour les deux sites. Les états correspondant aux termes 1047,6 et 1200,2 cm^{-1} susmentionnés ne sont que deux membres de cet ensemble de 4 états délocalisés. Cette découverte a été faite par l'analyse de la densité de probabilité des états vibrationnels. Les Figures 3a et 3b donnent les positions d'isodensité et montrent la densité de probabilité dans les plans $x_c y_c$ et xz pour l'état correspondant à environ 1200 cm^{-1} . On aperçoit que la densité de probabilité est délocalisée et qu'il y a un mélange de modes localisés sur le sites "fcc" et "hcp". Sur la Figure 3a on voit qu'au site "hcp", pour lequel x_c est négatif, il y a un étalement important dans le plan $x_c y_c$ tandis que sur le site "fcc", pour lequel x_c est positif, la densité est plutôt localisée. Ce premier étalement correspond à l'harmonique d'un mode parallèle le long de $x_c y_c$. La nature de la densité sur le site "fcc" ne peut correspondre qu'à l'état ayant 1 quantum d'énergie dans le mode de vibration perpendiculaire. Si l'on regarde la Figure 3b, on confirme cette attribution. On y voit qu'effectivement sur le site "hcp" on trouve un n£ud sur z et un n£ud net sur x. Mais sur le site "fcc" on ne trouve qu'un n£ud sur z. Ainsi, cet état de vibration possède un mode avec 1 quantum d'énergie dans le mode de vibration perpendiculaire sur le site "fcc", un mode avec 1 quantum d'énergie dans le mode de vibration perpendiculaire sur le site "hcp" et un mode avec 2 quanta d'énergie dans le mode de vibration parallèle sur le site "hcp".

Les termes vibrationnels ont aussi été calculés pour une grille 2 et pour une grille 3. La grille 2 contient 4 sites "fcc" et 4 sites "hcp" et correspond ainsi à un degré de recouvrement égal à 12,5 %. La grille 3 contient 9 sites "fcc" et 9 sites "hcp", avec un degré de recouvrement égal à 5,6 %. Ainsi pour la grille 2 il y a une dégénérescence égale à 4 pour le niveau fondamental sur le site "fcc" et 4 pour le site "hcp". Pour la grille 3 il y a une

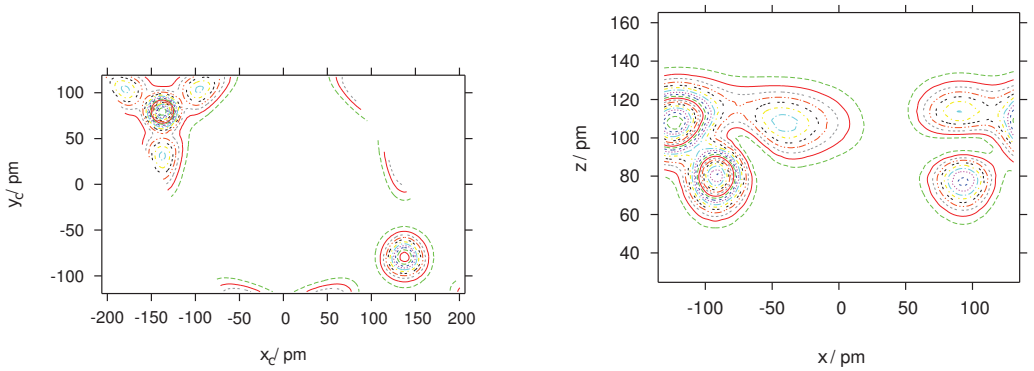

(a) Plan $x_c y_c$. (b) Plan xz

Figure 3 – Densité de probabilité pour la grille 1. Dans (a), seulement la densité au sein de la cellule minimale est montrée.

dégénérescence égale à 9 pour le site "fcc" et 9 pour le site "hcp". Pour les grilles 2 et 3, à mesure que l'énergie des niveaux augmente, on a constaté un éclatement des niveaux vibrationnels et la formation de bandes dont la largeur est donnée par la différence entre la borne minimale et la maximale de l'éclatement. La dégénérescence égale à 2, observée pour le mode vibrationnel parallèle (le long de x_c et y_c) pour la grille 1, n'est plus observée ni pour la grille 2 ni pour la grille 3. Cet éclatement de la dégénérescence constaté lorsque l'on diminue le degré de recouvrement (grille 2 et 3) et que l'on s'approche de la barrière d'énergie est dû à l'effet tunnel quantique. Cet effet est lié au couplage entre les modes localisés de même symétrie.

Une simulation de la dynamique quantique en fonction du temps, où le mode de vibration perpendiculaire sur le site "fcc" est excité avec un quantum d'énergie, a été faite. L'état donc initialement localisé sur le site "fcc" possède un mouvement perpendiculaire au substrat selon la dynamique classique. La modélisation quantique de la dynamique de diffusion montre qu'au bout de quelques dizaines de femtosecondes (1 fs = 10^{-15} s) l'atome commence à bouger parallèlement au substrat, ce qui correspond à un mouvement latéral de diffusion. Ce mouvement ne peut pas être expliqué par la mécanique classique, car en même temps que la diffusion commence à avoir lieu sur le site "fcc", l'atome commence à apparaître sur le site "hcp" qui se situe à environ 200 pm de distance du premier (2b). Cette délocalisation instantanée est caractéristique de la mécanique quantique, ce qui nous permet de dire que la diffusion de l'atome suit intimement les règles de cette mé-

canique. À la suite de cette modélisation on constate que l'état initial est partiellement rétabli au bout d'une centaine de femtosecondes ($\sim$ 150 fs) et que la diffusion recommence à nouveau. Cette quasi-périodicité du mouvement est une autre caractéristique de la dynamique quantique. Le mouvement serait strictement périodique s'il résultait de la superposition de deux états stationnaires uniquement. Cet étude montre, par contre, que les modes localisés sont décrits par plusieurs états stationnaires ou, inversement, que les états stationnaires sont décrits par plusieurs modes localisés qui sont quasirésonants et fortement couplés. En spectroscopie vibrationnelle, ce phénomène est appelé résonance de Fermi, en l'honneur d'Enrico Fermi qui a expliqué les bandes d'infrarouge interdites de l'étirement symétrique de CO_2. La liaison chimique est un autre exemple d'une résonance quantique, où l'état lié d'une molécule est le résultat d'un fort couplage entre les orbitales frontière, localisées sur les atomes entre lesquels la liaison est formée.

Conclusion et perspectives

Ce travail a permis une meilleure description du spectre infrarouge de H_2/Pd(111) qui peut être confondu avec le système H/Pd(111) à bas degré de recouvrement, puisque l'adsorption du dihydrogène est dissociative. Quand le degré de recouvrement est grand, des interactions entre les atomes d'hydrogène peuvent être importantes. L'étude du système H_2/Pd(111) à six dimensions devrait permettre de savoir si les interactions entre les atomes d'hydrogène sur le substrat sont vraiment importantes. Or, les données expérimentales ne sont pas capables pour l'instant de distinguer ces deux systèmes. La théorie est donc le seul moyen de comprendre la nature des états. Ce travail a en particulier mis en évidence un important phénomène de résonance quantique entre des états localisés sur différents sites d'adsorption. Dans le présent exemple de l'adsorption de H sur Pd(111), ce phénomène gouverne la diffusion de l'atome dans une échelle de temps ultra rapide (fs) que nous devrons donc nommer diffusion quantique.

Introduction

This thesis deals specifically with quantum dynamical calculations of the lateral diffusion of hydrogen atoms on Pd(111) and a complete description of infra-red spectrum of H_2 and H on this substrate. It is known that molecules and atoms in the gas phase interact with solid surfaces in almost every environment in the universe. This interaction often leads to the adsorption of the gas phase species on the solid surface. The latter is then called the substrate, the former the adsorbate. To understand the dynamics of a surface process, it is in general necessary to systematically study the elementary steps of the process in terms of simple model systems. A surface process is often quite complex, but can be decomposed into a number of elementary processes, such as adsorption, vibration, diffusion, rotation, reaction and desorption of the adsorbate. In practice, these elementary processes are studied by identifying and considering simple model systems.

One of the goals in theoretical studies of adsorbate-substrate interactions is to understand the nature of the forces that act on them. Several important physical and chemical processes may occur such as reaction (dissociation), or the back scattering (diffraction) into the gas phase in a vibrationally or rotationally excited state, or with a quantized change in the momentum parallel to the surface. In addition, coupling to the phonons and to electron-hole pair excitations may be important [5, 6].

Very few basic studies of the dynamics of molecular adsorption have been undertaken, to date, at a microscopic level and several fundamental questions remain without proper answer. When the molecules or the atoms are adsorbed we do not really know how they move on the surface. In what time-scale is this movement going on? Can this movement be interpreted as a classical diffusion? If it is a quantum diffusion, how can it

be characterized?

According on the strength of the adsorbate-substrate interaction, the adsorption can be called physisorption or chemisorption. Normally, during the physisorption (often also considered as non dissociative adsorption) the adsorbate does not react much with the substrate and it can be easily desorbed when the surface temperature is increased. The interaction between the adsorbate and the substrate is maximally about 20 kJ mol^{-1} [7]. However, during the chemisorption (often also considered as dissociative adsorption), the adsorbate reacts with the substrate, forming a rather strong chemical bonding (often covalent, with about 200 kJ mol^{-1}) [7]. Examples are H_2/Pt(111) [2], H_2/Cu(100) [2,3,8–11], H_2/Pd(111) [1,12], but also CO/Cu(100) [13], which is an example of non-dissociative chemisorption.

Surface dynamical processes are microscopic pathways in technologically important macroscopic processes such as the synthesis of ammonia from the elements $N_2 + 3\,H_2 \xrightarrow{Fe} 2\,NH_3$ [14, 15], a very famous example for heterogeneous catalysis, the hydrogen storage by physisorption [16] on graphenes or zeolites, the development of microelectronics and computer technologies [17].

These processes are related to the motion of the adsorbates on the substrate. At low energies, these are essentially vibrations around the equilibrium adsorption site. Today, there are techniques of high-sensitivity able to study of adsorbate vibrations. We mention here Fourier transform infra-red (FT-IR) spectrometry [18], energy loss spectroscopy (EELS) [19, 20] and High-Resolution Electron Energy Loss Spectroscopy (HREEL) [21–24]. On the other hand, few experimental techniques are capable to detail the mechanism of the lateral diffusion of atoms or molecules on a surface. Ellis *et al* [25] used ^{3}He Spin-Echo Spectroscopy to study the motion of CO on Cu(001) and observed both along the $\langle 110 \rangle$ and $\langle 100 \rangle$ directions an oscillatory dependence of the quasielastic broadening of the dynamical structure factor of the signal due to the scattered helium atoms as a function of momentum transfer.

This was modeled by a jump diffusion mechanism which allowed them to conclude that the ratio between the barrier energy of hollow and bridge site is approximately $E_H/E_B \simeq 1$. While this result is in disagreement with current available data from electronic structure

calculation [13], it shows how relevant are genuine quantum dynamical calculations for the description of the frustrated translational motion of adsorbed molecules. A quantum treatment of the diffusion could explain the experimental data and at the same time keep the agreement with the electronic structure calculations. Quantum effects of the dynamics and of the kinetics of adsorbates have not even been clarified.

The thesis is organized as follows: In Chapter 1, we present the principal methods used to perform the study of quantum dynamics with particular emphasis on the representation of the potential energy surface as a linear combination of products of one-dimensional functions especially for the systems that are bigger than three-dimensional (3D), the calculation of vibrational eigenstates and the propagation of wave packets. In Chapter 2, we present the potential energy surfaces and grids considered for the dynamical studies. We start to present the plan (111) of the face-centered cubic lattice for palladium where the hydrogen atoms are adsorbed and the diffusion process takes place. Some details pertaining to the potential energy surface (PES) of H_2/Pd(111) and the PW91 functional used to develop this PES from first principle calculations are summarized here. It is important to emphasize that the PES, which was used in this thesis, was developed and analytically represented by Dong [1, 12, 26–28]. This PES considers the palladium atoms rigid, phonons are hence neglected. The analysis of the PES of H/Pd(111), also carried out in this Chapter, shows which adsorption sites are more stable and the the barrier energy. In Chapter 3, we present the vibrational eigenstates of the adsorbed hydrogen atom and its isotopes on Pd(111). Following the study of this 3D system, we present the wave-packet propagation of H, D and T on Pd(111) and thermal wave packet propagation of H/Pd(111). In Chapter 4, we present the 6D system, i.e. the H_2/Pd(111) system. In Chapter 5 we show that the PES of H_2/Cu(100) [2, 3, 11], originally planned to be used at the beginning of this thesis, is inadequate to study the lateral diffusion because it fails to be global. Finally, in Chapter 6, we show the principle of the quantum calculations of the diffusion rate of adsorbates and the calculations that are necessary to simulate the ^{3}He spin-echo technique by considering the vibrational eigenstates and eigenfunctions of the adsorbed species.

Chapter 1

Methods

In this chapter a brief overview of the methods used in this work is presented.

1.1 Potential energy surface

The potential energy surface (PES) is a very useful conceptual tool in physical chemistry that allows us to model chemical reactions and interactions in simple systems. The time-independent Schrödinger Eq. (1) can be separated into one part which describes the electronic wave function for a fixed nuclear geometry, and a second part which describes the nuclear wave function, where the energy from the electronic wave function plays the role of a potential for the nuclear motion. This approximation is very often good because in a molecule the nuclei are essentially stationary compared to the electrons (the mass of the proton is about 1800 times larger than that of the electron). This separation is called the Born-Oppenheimer approximation. In practice, the electronic wave function depends parametrically on the nuclear coordinates [29].

The total, time-independent Schrödinger equation reads :

$$E_n \Psi_n = \hat{H} \Psi_n \tag{1}$$

where $\hat{H}$ is the Hamiltonian operator for a system of nuclei and electrons, that acts on certain wave function Ψ_n and E_n is the energy of the state Ψ_n. The subscript n denotes the state of system. The total Hamiltonian can be written as the sum of the electronic Hamiltonian and the kinetic energy of the nuclei, Eq. (2), where the subscript n is used for nuclei and e for electron.

$$\hat{H}_{\mathrm{tot}} = \hat{H}_{\mathrm{e}} + \hat{T}_{\mathrm{n}} \tag{2}$$

$$\hat{H}_{\mathrm{e}} = \hat{T}_{\mathrm{e}} + \hat{V}_{\mathrm{ne}} + \hat{V}_{\mathrm{ee}} + \hat{V}_{\mathrm{nn}} \tag{3}$$

$$\Psi_{\mathrm{tot}} = \Psi_{\mathrm{n}} \Psi_{\mathrm{e}} \tag{4}$$

$$E_{\mathrm{e}} \Psi_{\mathrm{e}} = \hat{H}_{\mathrm{e}} \Psi_{\mathrm{e}} \tag{5}$$

$$(\hat{T}_{\mathrm{n}} + E_{\mathrm{e}}) \Psi_{\mathrm{n}} = E_{\mathrm{tot}} \Psi_{\mathrm{n}} \tag{6}$$

In Eq. (3), the first term is the operator for the kinetic energy of the electrons; the second term represents the Coulomb attraction between electrons and nuclei; the fourth and fifth terms represent the repulsion between electrons and between nuclei, respectively. In Eq. (4), the electron wave function Ψ_{e} is supposed to vary parametrically with the position of the nuclei. Similarly, the electronic energy E_{e} will be a function of the position of the nuclei. In the Born-Oppenheimer approximation, one neglects the action of $\hat{T}_{\mathrm{n}}$, the kinetic energy operator of the nuclei, on the electronic wave function Ψ_{e}. Eq. (6) shows finally that the electronic energy can be interpreted as a potential surface for the motion of the nuclei. Electronic structure theory [29] deals with computational methods to solve Eq. (1). The PES used for the dynamical calculations in this thesis was developed by the density-functional theory, and will be addressed later.

1.2 Quantum dynamics

For the description of the hydrogen motion in the lowest adiabatic electronic state as a function of time, one solves the time-dependent Schrödinger equation

$$\mathsf{i}\hbar\frac{\partial}{\partial t}\,\Psi(\{x_i,y_i,z_i\},t) \;=\; \hat{H}\,\Psi(\{x_i,y_i,z_i\},t) \tag{7}$$

where i is the imaginary unit, $\hbar$, the reduced Planck constant equals $\frac{h}{2\pi}$. $\Psi(\{x_i,y_i,z_i\},t)$ is the wave function that describes the state of hydrogen nuclei at time t in function of this position in space ($\{x_i,y_i,z_i\}$). For one hydrogen atom ($i=1$) and for the hydrogen molecule ($i=1,2$).

To simplify the representation of time-dependent Schrödinger equation (eq. (7)), I will adopt in the following the bra-ket notation. The position in space ($\{x_i,y_i,z_i\}$) will be associated to the vector-ket $\mid \Psi \rangle$ then we can re-write the Eq. (7) as

$$\mathsf{i}\hbar\frac{\partial}{\partial t}\mid \Psi(t)\rangle \;=\; \hat{H}\mid \Psi(t)\rangle \tag{8}$$

The Hamiltonian $\hat{H}$ is the differential operator that depends on the kinetic energy operator $\hat{T}$ and the potential energy operator $\hat{V}$ (Eq. (9)).

In this work a set of coordinates was chosen that is non-Euclidean, in order to exploit the periodicity of the elementary cell on the (111) surface. The primitive cell is formed by skewed axes, which form an angle $\alpha = 120^0$ (see Fig. 9 or page 45). The Hamiltonian $\hat{H}$ which represents the twisted coordinate system for M nuclei is

$$\hat{H} = -\sum_{i=1}^{M}\frac{2}{3M_i}(\partial^2_{x_i}+\partial_{x_i}\partial_{y_i}+\partial^2_{y_i}) - \sum_{i=1}^{M}\frac{1}{2M_i}\frac{\partial^2}{\partial_{z_i^2}} + V(\{x_i,y_i,z_i\}) \tag{9}$$

where x_i, y_i, are the coordinates for the motion parallel to the substrate, the "frustrated translation" and z_i defines the distance of the each atom from the plane formed by the first layer of frozen Pd atoms. $V(\{x_i,y_i,z_i\})$ is the $\mathrm{H}-\mathrm{Pd}(111)$ interaction potential involving

all hydrogen atoms. The calculation of expectation values of the twisted coordinates x_i and y_i is carried out, within the MCTDH program, as if these coordinates were Cartesian. The volume element ratio between the Cartesian and the skewed elementary cell, $\frac{1}{\sin(120^0)} = (\frac{2}{\sqrt{3}})$, must therefore be multiplied to all observable quantities obtained from the MCTDH code using these coordinates.

1.3 Multiconfiguration Time-Dependent Hartree

To determine the time evolution of the nuclei wave function, $\Psi(\{x_i, y_i, z_i\}, t)$, we use the algorithm implemented in the Multiconfiguration Time-Dependent Hartree program (MCTDH) [30] that represents the Hamiltonian in terms of products of time dependent, one dimensional functions ϕ, the so called "single particle" functions (SPF) [31–33]. In the case of one hydrogen atom, the development of the wave function is then given as

$$\Psi(x,y,z,t) = \sum_{m_x=1}^{M_x} \sum_{m_y=1}^{M_y} \sum_{m_z=1}^{M_z} A_{m_x,m_y,m_z}(t)\phi_{m_x}^{(x)}(x,t)\phi_{m_y}^{(y)}(y,t)\phi_{m_z}^{(z)}(z,t) \tag{10}$$

To reduce the size of the coefficient vector $A_{m_{\kappa_i}}$, the coordinates ($\{x_i, y_i, z_i\}$) can be combined to a logical one, Q_i, also called combined mode of particles. Mode combination becomes interesting in the case of molecular hydrogen, the development of the wave function is then given as

$$\Psi(Q_1,Q_2,Q_3,t) = \sum_{m_{\kappa_1}=1}^{M_{\kappa_1}} \sum_{m_{\kappa_2}=1}^{M_{\kappa_2}} \sum_{m_{\kappa_3}=1}^{M_{\kappa_3}} A_{m_{\kappa_1},m_{\kappa_2},m_{\kappa_3}}(t)\phi_{m_{\kappa_1}}^{(\kappa_1)}(Q_1,t)\phi_{m_{\kappa_2}}^{(\kappa_2)}(Q_2,t)\phi_{m_{\kappa_3}}^{(\kappa_3)}(Q_3,t) \tag{11}$$

where $Q_1 = [x_1, y_1], Q_2 = [x_2, y_2]$ and $Q_3 = [z_1, z_2]$ represent the mode of the combination of coordinates chosen. We combined the modes of the frustrated translation (parallel motion) (x_i, y_i) for each hydrogen atom separately because these coordinates are coupled. The coordinates z_i that represent the distance of hydrogen atoms to the substrate are combined.

In practice, for the case of one hydrogen atom, the SPF are in their turn developed in terms of time independent primitive basis functions (PBF) χ :

$$\left.\begin{array}{l} \phi^{(x)}_{m_x}(x,t) = \sum_{n_x=1}^{N_x} c_{n_x m_x}(t)\chi^{(x)}_{n_x}(x) \\ \phi^{(y)}_{m_y}(y,t) = \sum_{n_y=1}^{N_y} c_{n_y m_y}(t)\chi^{(y)}_{n_y}(y) \\ \phi^{(z)}_{m_z}(z,t) = \sum_{n_z=1}^{N_z} c_{n_z m_z}(t)\chi^{(z)}_{n_z}(z) \end{array}\right\} \tag{12}$$

and for the case of molecular hydrogen, the developed in terms of time independent primitive basis functions (PBF) χ is give as

$$\left.\begin{array}{l} \phi^{\kappa_1}_{m_{\kappa_1}}(x_1,y_1,t) = \sum_{n_{x_1}=1}^{N_{x_1}} \sum_{n_{y_1}=1}^{N_{y_1}} c_{n_{x_1} n_{y_1} m_{\kappa_1}}(t)\chi^{(x_1)}_{n_{x_1}}\chi^{(y_1)}_{n_{y_1}} \\ \phi^{\kappa_2}_{m_{\kappa_2}}(x_2,y_2,t) = \sum_{n_{x_2}=1}^{N_{x_2}} \sum_{n_{y_2}=1}^{N_{y_2}} c_{n_{x_2} n_{y_2} m_{\kappa_2}}(t)\chi^{(x_2)}_{n_{x_2}}\chi^{(y_2)}_{n_{y_2}} \\ \phi^{\kappa_3}_{m_{\kappa_3}}(z_1,z_2,t) = \sum_{n_{z_1}=1}^{N_{z_1}} \sum_{n_{z_2}=1}^{N_{z_2}} c_{n_{z_1} n_{z_2} m_{\kappa_3}}(t)\chi^{(z_1)}_{n_{z_1}}\chi^{(z_2)}_{n_{z_2}} \end{array}\right\} \tag{13}$$

If $\chi^{(\alpha)}_{n_\alpha}$ and $\chi^{(\beta)}_{n_\beta}$ are Discrete Variable representations (DVR) functions (see section 1.7), the product of the PBF $\chi^{(\alpha)}_{n_\alpha}\chi^{(\beta)}_{n_\beta}$ defines a two dimensional DVR.

The equations determining the time evolution of the coefficients $A_{m_{\kappa_1},m_{\kappa_2},m_{\kappa_3}}(t)$ (the "A-vector") where ($\kappa_1 = (x_1,y_1), \kappa_2 = (x_2,y_2)$ and $\kappa_3 = (z_1,z_2)$), as well as these of the PBF expansion coefficients $c_{\ldots m_{\kappa_i}}(t)$ ($i = 1,2,3$) of the single particle functions are derived from the Dirac-Frenkel variational principle [31] ($\langle\ \delta\Psi \mid i\hbar\frac{\partial}{\partial t} - \hat{H} \mid \Psi\ \rangle = 0$).

The advantage of this program is that the total number of SPF, $M = M_{\kappa_1} \times M_{\kappa_2} \times M_{\kappa_3}$ can be made to be much smaller than the total number of PBF, which makes this program very attractive when compared to other programs [32–34] for the solution of the time dependent Schrödinger equation (Eq. (8)).

1.4 Product representation of potential energy surfaces

Normally the representations of potential energy surfaces (PES) are, by their nature, multidimensional and for an optimal performance of the MCTDH method, it is essential

to represent the Hamiltonian by a linear combination of products of one-dimensional functions similarly to the representation of the time dependent function, removing the need to calculate difficult multidimensional integrals in the solution of the equations of motion. As shown in Eq. (9), the kinetic energy operators are already in such form. However, the potential energy operator V needs to be re-fitted to a sum-of-products form. To obtain V in product-form, one can re-fit the V using the POTFIT procedure [35–37]. The most direct way to the product form is an expansion in a product basis. The expansion of potential energy operator of hydrogen atom (3D) $V(x, y, z)$ in sum-of-product form is given as

$$V(x,y,z) \approx V^{\text{app}}(x,y,z) \tag{14}$$

$$V^{\text{app}}(x,y,z) = \sum_{n_x=1}^{k_x}\sum_{n_y=1}^{k_y}\sum_{n_z=1}^{k_z} B_{n_x,n_y,n_z} v_{n_x}^{(x)}(x) v_{n_y}^{(y)}(y) v_{n_z}^{(z)}(z) \tag{15}$$

where $x, y,$ and z are the coordinates, B_{n_κ} are the coefficients, $v_{n_\kappa}^{(\kappa)}$ are the natural potentials and k_α ($\alpha = x, y, z$) are expansion numbers.

The expansion of potential energy operator of molecular hydrogen (6D) $V(x_1, y_1, z_1, x_2, y_2, z_2)$, where (x_1, y_1, z_1) are the twisted coordinates of the first hydrogen atom and (x_2, y_2, z_2) those of the second hydrogen atom, in sum-of-product form is given as

$$\begin{aligned} V(x_1,y_1,z_1,x_2,y_2,z_2) &\approx V^{\text{app}}(x_1,y_1,z_1,x_2,y_2,z_2) \\ &= \sum_{n_{\kappa_1}=1}^{k_{\kappa_1}}\sum_{n_{\kappa_2}=1}^{k_{\kappa_2}}\sum_{n_{\kappa_3}=1}^{k_{\kappa_3}} B_{n_{\kappa_1},n_{\kappa_2},n_{\kappa_3}} v_{n_{\kappa_1}}^{(1)}(x_1y_1) v_{n_{\kappa_2}}^{(2)}(x_2y_2) v_{n_{\kappa_3}}^{(3)}(z_1z_2) \end{aligned} \tag{16}$$

The expansion orders, n_{κ_i}, must be chosen large enough to achieve an accurate expansion. However this choice should be as small as possible, because the numerical effort of an MCTDH propagation grows (almost linearly) with the number of potential terms, that is, with the product of the expansion orders. Hence both the expansion coefficients and SPF should be optimized to provide the best approximative potential for a given set of expansion orders [33].

For the hydrogen atom (3D), the expansion coefficients B_{k_κ}, are determined by the overlaps between the potential $V(x,y,z)$ and the natural potentials $v^{(\kappa)}_{k_\kappa}$. Given the grid representation (DVR),

$$B_{k_x,k_y,k_z} \equiv \sum_{n_x=1}^{N_x}\sum_{n_y=1}^{N_y}\sum_{n_z=1}^{N_z} V(x_{n_x},y_{n_y},z_{n_z})v^{(x)}_{k_x}(x_{n_x})v^{(y)}_{k_y}(y_{n_y})v^{(z)}_{k_z}(z_{n_z}) \tag{17}$$

Since the orthonormal product basis set is complete over the grid points, the approximated and the exact potential are identical at the grid points, if the expansion orders and the number of grid points are equal, i.e., $V^{\mathrm{app}} \to V$ for $k_{\kappa_i} \to N_{\kappa_i}$. Note that the expansion coefficients are independent of the expansion orders.

To decrease the number of expansion terms $s = \prod_{i=1}^{f} n_{\kappa i}$ in Eq. (16) by a factor of n_{κ_i}, then, one contracts the expansion coefficients

$$D_{n_{\kappa_i}}(\chi^{(\kappa_i)}_{n_{\kappa_i}}) \;=\; \sum_{n_{\kappa_i=1}}^{k_{\kappa_i}} B_{n_{\kappa_i}} v^{(\kappa_i)}_{n_{\kappa_i}} \tag{18}$$

and re-write the expansion of the approximated potential as

$$V^{\mathrm{app}}(x_1,y_1,z_1,x_2,y_2,z_2) = \sum_{n_{\kappa_1}=1}^{k_{\kappa_1}}\sum_{n_{\kappa_2}=1}^{k_{\kappa_2}} v^{(1)}_{n_{\kappa_1}}(\chi^{(1)}_{n_{\kappa_1}})v^{(2)}_{n_{\kappa_2}}(\chi^{(2)}_{n_{\kappa_2}})\sum_{n_{\kappa_3}=1}^{k_{\kappa_3}} B_{n_{\kappa_3}} v^{(3)}_{n_{\kappa_3}} \tag{19}$$

The contraction of the coordinates is a very helpful trick, as it substantially reduces the numerical effort of the following MCTDH calculation without affecting the accuracy of the product expansion. In this work, it was chosen to contract the coordinate z for one hydrogen atom (system 3D) and z_1 and z_2 for the molecular hydrogen (6D system).

Results from POTFIT are not perfect for systems that are more than three-dimensional, but it was observed that the algorithm usually provides fits that are close to optimal. For two dimensional the expansion is perfect, i.e., the $\mathscr{L}^2$-error is minimal [31]. The $\mathscr{L}^2$-error is defined as the sum of the squares of the moduli of the fit errors on all product grid points.

The $\mathscr{L}^2$-error is given by [35, 36]

$$\begin{aligned}
\mathscr{L}^2 &= \sum_{n_{\kappa_1}=1}^{k_{\kappa_1}} \sum_{n_{\kappa_2}=1}^{k_{\kappa_2}} \sum_{n_{\kappa_3}=1}^{k_{\kappa_3}} \left(V(x_1, y_1, z_1, x_2, y_2, z_2) - V^{\mathrm{app}}(x_1, y_1, z_1, x_2, y_2, z_2)\right)^2 \\
&= \sum_{n_{\kappa_1}=1}^{k_{\kappa_1}} \sum_{n_{\kappa_2}=1}^{k_{\kappa_2}} \sum_{n_{\kappa_3}=1}^{k_{\kappa_3}} \left[\left(V(x_1, y_1, z_1, x_2, y_2, z_2)\right)^2 - \left(V^{\mathrm{app}}(x_1, y_1, z_1, x_2, y_2, z_2)\right)^2\right] \\
&= \sum_{n_{\kappa_1}=1}^{k_{\kappa_1}} \sum_{n_{\kappa_2}=1}^{k_{\kappa_2}} \sum_{n_{\kappa_3}=1}^{k_{\kappa_3}} |B_{n_{\kappa_1}, n_{\kappa_2}, n_{\kappa_3}}|^2 \qquad (20)
\end{aligned}$$

Typically, the $\mathscr{L}^2$-error, drops by $10 - 20$ % when fully optimizing the SPP. Only when too small values for the expansion orders were used, resulting in a rather inaccurate fit, we observe a lowering of the $\mathscr{L}^2$-error by about 40 %. However, these investigation could only be done on small three-dimensional systems [33].

To efficiently construct potential energy operators and to reduce the numerical effort of the following MCTDH calculation, a relevant region [37] can be chosen. In general, not all regions of the potential energy of surface are equally relevant for the process under investigation. The introduction of an appropriately chosen weight function w then allows the enhancement of regions of the surface with greater physical relevance. In this work the representation of the 3D potential $V(x, y, z)$ as a linear combination of products was made without choosing a relevant region. However, for the 6D system, $V(x_1, y_1, z_1, x_2, y_2, z_2)$, it was necessary to use a weight function w to define a relevant region because this representation becomes too expensive.

1.5 Propagation

Eigenstates of the Hamiltonian solve Eq. (21)

$$\hat{H} \mid \varphi_n \rangle = E_n \mid \varphi_n \rangle \tag{21}$$

E_n is the corresponding eigenvalue. Knowing the E_n and the $\mid \varphi_n \rangle$ we can solve the time-dependent Schrödinger equation, i.e., determine the time evolution of a state. Indeed, the $\mid \varphi_n \rangle$ form a basis, thus for each value of t, we can develop a state $\mid \Psi_t \rangle$ on the $\mid \varphi_n \rangle$:

$$\mid \Psi(t) \rangle \ = \sum_n C_n(t) \mid \varphi_n \rangle \tag{22}$$

with

$$C_n(t) = \langle \varphi_n \mid \Psi(t) \rangle \tag{23}$$

The $\mid \varphi_n \rangle$ do not depends on t thus the temporal dependence of $\mid \Psi(t) \rangle$ is contained in the $C_n(t)$. Therefore, to calculate the $C_n(t)$, we project the time-dependent Schrödinger equation on each state $\mid \varphi_n \rangle$, thus we have

$$\mathrm{i}\hbar \frac{\partial}{\partial t} \langle \varphi_n \mid \Psi(t) \rangle \ = \ \langle \varphi_n \mid \hat{H} \mid \Psi(t) \rangle \tag{24}$$

The observable $\hat{H}$ is Hermitian, therefore we can deduce from Eq. (21) that

$$\langle \varphi_n \mid \hat{H} = E_n \langle \varphi_n \mid \tag{25}$$

Eq. (24) can be re-written as

$$\mathrm{i}\hbar \frac{\partial}{\partial t} C_n(t) = E_n C_n(t) \tag{26}$$

The result of integration of Eq. (26) is given by

$$C_n(t) = C_n(t_0)e^{-\mathrm{i}E_n(t-t_0)/\hbar} \tag{27}$$

If we know the $\mid \Psi(t_0) \rangle$, to find $\mid \Psi(t) \rangle$, we have to develop $\mid \Psi(t_0) \rangle$ on the basis of eigenstates of $\hat{H}$

$$\mid \Psi(t_0) \rangle = \sum_n C_n(t_0) \mid \varphi_n \rangle \tag{28}$$

where $C_n(t_0)$ is given as

$$C_n(t_0) = \langle \varphi_n \mid \Psi(t_0) \rangle \tag{29}$$

$\mid \Psi(t) \rangle$, for some t, is given by

$$\mid \Psi(t) \rangle = \sum_n C_n(t_0)e^{-\mathrm{i}E_n(t-t_0)/\hbar} \mid \varphi_n \rangle \tag{30}$$

where E_n is the eigenvalue of $\hat{H}$ associated at the state $\mid \varphi_n \rangle$.

We can link the states of the system at two different times t and t_0 using a linear operator of propagation, $\mid \Psi(t) \rangle = U(t, t_0) \mid \Psi(t_0) \rangle$, thus we can go from $\mid \Psi(t_0) \rangle$ (vector of state at t_0) to $\mid \Psi(t) \rangle$ (vector of some later state). Integrating the time-dependent Schrödinger equation, we have

$$U(t, t_0) = e^{-\mathrm{i}H(t-t_0)/\hbar} \tag{31}$$

Applying the operator $U(t, t_0)$, we have

$$U(t,t_0) \mid \varphi_n \rangle = e^{-\mathrm{i}H(t-t_0)/\hbar} \mid \varphi_n \rangle = e^{-\mathrm{i}E_n(t-t_0)/\hbar} \mid \varphi_n \rangle \tag{32}$$

where $\mid \varphi_n \rangle$ is eigenvector of $\hat{H}$ with eigenvalue E_n.

The autocorrelation function is given as

$$\begin{aligned} A(t) &= \langle \Psi(t_0) \mid \Psi(t) \rangle = \sum_m \sum_n C_m^*(t_0) C_n(t_0) e^{-\mathrm{i}E_n(t-t_0)/\hbar} \langle \underbrace{\phi_m \mid \phi_n}_{\delta_{mn}} \rangle \\ &= \sum_n \mid C_n(t_0) \mid^2 e^{-\mathrm{i}E_n(t-t_0)/\hbar} \end{aligned} \tag{33}$$

Applying the Fourier transform (FT) to autocorrelation function $A(t)$ (Eq. (33)) when $t_0 = 0$, we have

$$\mathrm{F}[A(t)](E) = \sum_n \mid C_n(0) \mid^2 \delta_{mn}(E - E_n) \tag{34}$$

The FT of autocorrelation function $A(t)$ gives the peaks at the positions that correspond to the eigenvalues. The intensity of the peak gives the weight with which eigenstates participate at the state. For a propagation calculation, an initial wave packet $\mid \Psi_0 \rangle$ must be well chosen such as to find a desired eigenstate ϕ_n, the wave packet must have an important overlap C_n.

1.6 Calculation of vibrational eigenstates

The three-dimensional (3D) and six-dimensional (6D) anharmonic vibrational eigenstates for H/Pd(111) and H_2/Pd(111) and their energies are calculated using a variant of the *improved relaxation* method [38–40] called *improved relaxation in block form* [33, 41, 42]. In the block relaxation method the SPF are optimized to represent all states calculated therefore it is necessary to include more SPF to obtain results quantitative when it is calculated the excited states. However, this calculation takes a long time to finish and a larger consumption of memory but it requires much less human effort to run a block-relaxation as compared to run, i.e., 218 single relaxations. In practice, the *improved*

relaxation method use the SPF optimized by relaxation, i.e. a propagation of the wave packet in negative imaginary time: $\tau = -\mathrm{i}t$ and the coefficients are obtained by diagonalizing the resulting Hamiltonian matrix by the Davidson algorithm [43]. The propagator becomes a simple decreasing exponential:

$$\begin{aligned} U(t,0) &= e^{-\mathrm{i}\hat{H}\tau} \\ &= e^{-\hat{H}t} \end{aligned} \tag{35}$$

From Eq. (22), let $\mid \Psi(t_0) \rangle = \sum_n C_n(t_0) \mid \varphi_n \rangle$, where $\mid \varphi_n \rangle$ are (unknown) eigenstates. The MCTDH equations of motion are derived by applying the Dirac-Frenkel variational principle [31] to *ansatz* Eq. (10). This yields

$$\Psi(t_0) = \sum_I A_I(t_0)\Phi_I(t_0) \tag{36}$$

As explained above, the improved relaxation method computes the ground states by propagation in negative imaginary time, determining the A-vector and the SPF at t_0. Consider now the matrix $\boldsymbol{H}(t_0)$, with matrix elements

$$\boldsymbol{H}_{IJ}(t_0) = \langle\ \Phi_I(t_0) \mid \boldsymbol{H} \mid \Phi_J(t_0)\ \rangle \tag{37}$$

Diagonalization of this matrix yields a lowest eigenvalue $E_0^{(1)}$, where likely $E_0^{(1)} \neq E_1$, the lowest eigenvalue (unknown) that participates at the definition of $\Psi(t_0)$, thus, during a propagation in imaginary time until an adequate time t_1, all the states will be filtered out but φ_1. The initial wave packet $\Psi(t_0) = \sum_I A_I(t_0)\Phi_I(t_0)$ is decomposed in the stationary states φ_k. Applying the propagator (35) with $\hat{H} - E_1$, where $\hat{H}$ is the Hamiltonian and E_1 is the unknown eigenvalue corresponding to the eigenstate φ_1.

$$
\begin{aligned}
U(\tau,0;E_1) \mid \Psi(t_0) \rangle &= e^{-\mathrm{i}(H-E_1)t/\hbar}(\sum_k C_k \mid \varphi_k \rangle) \\
&= \sum_k C_k e^{-\mathrm{i}(E_k-E_1)t/\hbar} \mid \varphi_k \rangle) \\
&= \sum_{k\,>\,1} C_k e^{-\mathrm{i}(E_k-E_1)t/\hbar} \mid \varphi_k \rangle + C_1 \mid \varphi_1 \rangle
\end{aligned} \tag{38}
$$

and

$$
\begin{cases}
\sum_{k\,\neq\,1} C_k e^{-\mathrm{i}(E_k-E_1)t/\hbar} \mid \varphi_k \rangle \to 0 \quad t \to t_1 \\
\leftrightarrow U(\tau,0,E_1) \mid \Psi(t_0) \rangle \to |\varphi_1 \rangle \qquad t \to t_1
\end{cases} \tag{39}
$$

if t_1 is sufficiently large.

The cycle starts again by diagonalizing $\boldsymbol{H}(t_1)$, with matrix elements

$$
\boldsymbol{H}_{IJ}(t_1) = \langle\ \Phi_I(t_1) \mid \boldsymbol{H} \mid \Phi_J(t_1) \rangle \tag{40}
$$

Let the lowest eigenvalue $E_1^{(1)}$. Likely, $E_1^{(1)} \neq E_1$, but it can be expected that $|E_1^{(1)} - E_0^{(1)}| < |E_0^{(1)} - E_1|$, where E_1 is the exact energy of the state sought. Hereafter, one starts an other diagonalisation in the new configuration space built from the new SPF obtained and the propagation in imaginary time is made until time t_2, etc. This iteration method is repeated until convergence [39].

Indeed, it is possible to start with a block of initial vectors which then converge collectively to a set of eigenstates. Formally, the different wave functions are treated as different electronic states of one super-wavefunction. The mean fields are state-averaged mean fields, and the Davidson routine is replaced by a block-Davidson one. Block-relaxation requires more SPF to converge than single-vector relaxation because in block relaxation the SPF are optimized to represent all considered states simultaneously, while in single-vector relaxation they are optimized to represent a single state. However, we found that the required increase in the number of SPF is rather small. In fact, block relaxation is,

in general, more efficient than performing single-vector relaxations for each of the block states. However, the memory consumption of block relaxation is considerably larger. This limits the applicability of block improved relaxation when turning to larger systems. However, when block relaxation is feasible memorywise, it is certainly to be preferred over single-vector relaxation. Block relaxation can be run in a modus where the lowest n_{block} eigenenergies above some predefined energy threshold are computed. This feature is very convenient when all eigenstates within some energy interval are to be determined.

1.7 Discrete Variable representation (DVR)

The DVR basis which also called primitive basis in the following is the elementary representation basis of wave functions and operators used in this work. It corresponds essentially to a discretization of space and allocates a label to each degree of freedom in the system. DVR representations are used to set up the single-particle functions of an MCTDH (relaxation and propagation calculations) or the product grid (POTFIT) representation of the PES. With this representation one obtains diagonal matrices for the potential energy - at least approximatively. A more detailed discussion of the DVR technique can be found in Appendix B of the review [32]. The DVR chosen to describe operators and wave functions for the system in (3D) and (6D) are:

- for $\chi^{(x)}$ functions the EXP-DVR functions of x.
- for $\chi^{(y)}$ functions the EXP-DVR functions of y.
- for $\chi^{(z)}$ functions the Sine-DVR functions of z.

The exponential DVR is related to plane waves. It is therefore often used for dissociative degrees of freedom. Moreover, Exponential and Sine DVR functions are the only primitive basis representations within the MCTDH program that satisfy periodic boundary conditions. To describe the lateral movement of hydrogen atoms to the substrate (coordinates x and y) and the dissociation of molecular hydrogen, the periodic boundary conditions given by the exponential DVR functions are a good choice. The Sine-DVR was chosen to represent the distance of hydrogen from the plan of substrate (coordinate z). The choice of the system of coordinates to describe the dissociation of molecular hydrogen and the

"frustrated translation" of hydrogen atoms to the substrate will be discussed in Chapter 2.

1.8 Integration scheme

The efficiency of the MCTDH method depends on the algorithm used to solve a system of coupled nonlinear ordinary differential equations of first order. For the two systems studied in this work, was used for the evolution of the A-vector the "constant mean-field" (CMF) integration scheme such that during the integration, one may hold the Hamiltonian matrix elements and the products of the inverse density and mean-field matrices constant for some time τ.

For imaginary time propagations within the block relaxation method for the determination of eigenstates, the Davidson integrator (DAV) was used. The convergence is hence toward that eigenstate that has the largest overlap with the initial guess. A technical remark is in order. As the dimension of the space spanned by the configurations is rather large typical values range from 2000 to 2 000 000, the Davidson algorithm [43] is employed for diagonalization. When excited states are computed, especially by the block relaxation method, because it allows us to calculate several eigenstates at the same time, one may additionally improve the preconditioner by inverting a, say 1000×1000, block around the energy of interest. This accelerates the convergence of the Davidson iterations. In fact the routine used in this work is called (rrDAV), that uses the same Davidson routine, but the (rrDAV) is employed to performed the matrix product ($\hat{H} * A$-vector) and uses only real Hamiltonians and real wave-functions. This routine is faster, because it uses more real arithmetic, but works only for simple Hamiltonians (only real operators).

The SPF were propagated with the Runge-Kunta integrator to eighth order (RK8) for relaxation calculations in imaginary time.

A more detailed description of integration schemes can be found in [32, 33].

1.9 Statistical thermodynamics

Thermal initial conditions $\psi^T(0)$ can be simulated by the superposition wave function in Eq. (41):

$$\psi^{\mathrm{T}}(0) = \sum_j c_j \Phi_j \tag{41}$$

where ϕ_j are eigenfunctions at energy E_j and $c_j = \sqrt{P_j}\exp^{\mathrm{i}\propto_j}$, is the Boltzmann population of level j at the temperature T.

$$P_i = \frac{g_i e^{\frac{E_1 - E_i}{k_B T}}}{\sum g_i e^{\frac{E_1 - E_i}{k_B T}}} \tag{42}$$

where g_i is the degeneracy, k_B is the Boltzmann constant. $0 \leq \propto_j \leq 2\pi$ is generated randomly (with the BoltzmannCoeff.c routine, see Appendix B). The Boltzmann population of each level j at the temperature T is calculated with BoltzmannWeight.c routine (see Appendix A).

Chapter 2

Details on the potential energy surfaces and calculation grids for hydrogen on palladium

In this chapter, we present a brief introduction to the the plane (111) in the unit cell of Pd where this study is performed, a brief overview of the methods used to develop the PES of H_2/Pd(111) and H_2/Pd(111) and calculation grids.

2.1 Lattice geometry analysis

Metallic solids have periodic arrays of atoms which form a crystal lattice. Normally the structure of solids are described by the simplest repeating unit in a crystal, the so-called unit cells. Depending on the crystallization of the atoms, crystal structures, are named according to the Bravais lattice classification. In the Pd and Cu crystals, for example, atoms crystallize in the face-centered cubic lattice (fcc). Fig. 4 shows the unit cell of a face-centered cubic lattice. It shows the lattice planes and their orientation with respect to the unit cell using the Miller indices which are the inverse of cut segments of certain lengths on the crystallographic axes in the plane used to define the orientation [44]. In this figure, the plane (111) in the unit cell of Pd is represented by an equilateral triangle;

the length a is the lattice constant. The distance between the atoms 5 and 3 is $d = \frac{a}{\sqrt{2}}$. This is the distance between nearest neighbours. The constant a for Pd is 389 pm [45].

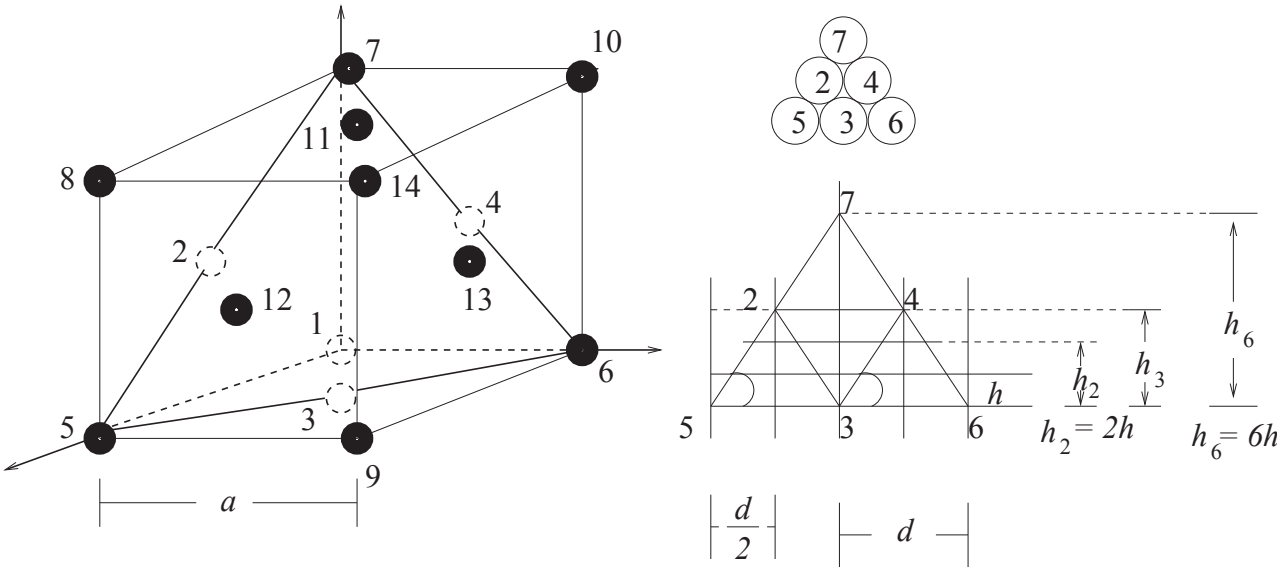

Figure 4 – Plane (111) of face-centered cubic lattice for palladium. The drawing on the right hand side shows the lengths d and $h_k = k.h$, where, $d = \frac{a}{\sqrt{2}} = 275.114$ pm, $h = \frac{d}{2\sqrt{3}} = \frac{a}{2\sqrt{6}} = 79.419$ pm.

The detail of Fig. 4 brings up a basic equilateral triangular pattern of maximum compactness. The side of the triangle is $2d = a\sqrt{2}$. Looking at the triangle formed by the atoms 5, 2, 7, 4, 6 and 3, one sees that:

$$\begin{aligned} q &= \frac{d}{2} \\ \frac{h}{q} &= \tan 30^0 = \frac{1}{2}\frac{2}{\sqrt{3}} = \frac{1}{\sqrt{3}} \\ \Rightarrow h &= \frac{1}{\sqrt{3}}q = \frac{d}{2\sqrt{3}} \qquad (43) \\ \frac{h_2}{2q} &= \tan 30^0 \\ \Rightarrow h_2 &= \frac{d}{\sqrt{3}} = 2h \qquad (44) \\ h_3 &= \sqrt{d^2 - q^2} \\ &= d\sqrt{1 - \frac{1}{4}} \\ &= \frac{d\sqrt{3}}{2} = 3h \qquad (45) \end{aligned}$$

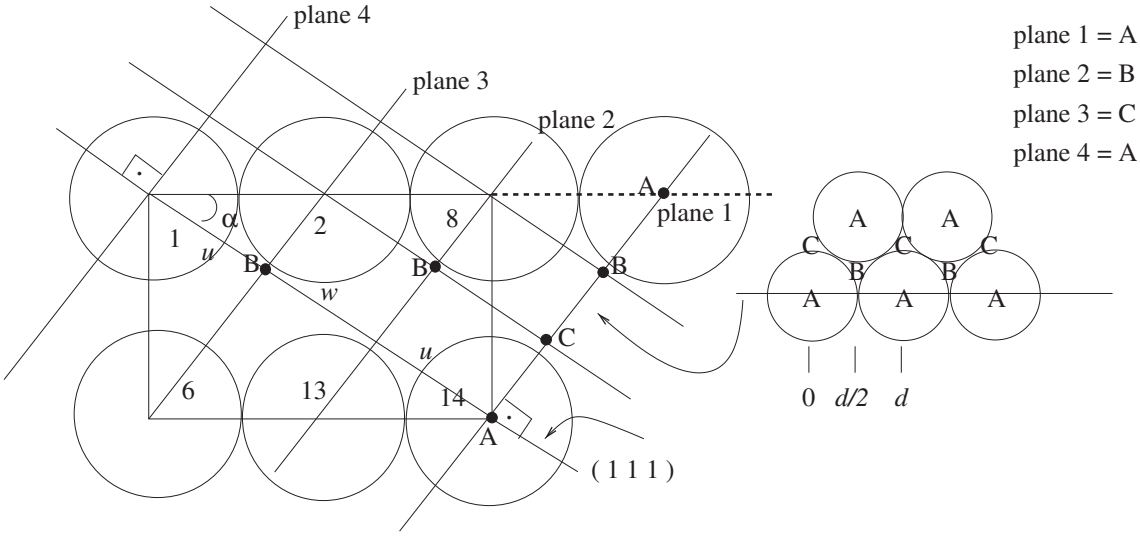

Figure 5 – Section showing of atoms in the plane (101) (left) and adsorption sites (right) ; in the hollow site : B, a Pd atom will follow in the next lowest plane (plane 2), this is the so-called "hcp" site (hexagonal close-packed); in the hollow site C, a Pd atom follows in plane 3, only, this is the so-called "fcc" site (face centered cubic); when a hydrogen atom is on a Pd atom, it occupies a so-called "top" site, (site A in this figure).

This motif is representative of all parallel planes of the zone named (111). To calculate the distance between these planes, we look at a section of the characteristic cube in the zone (101), Fig. 5. This plane contains the axis of the area (111) which passes through the atoms 1 and 14 in the Fig. 4. The planes orthogonal to this axis are also indicated by lines. They contain :

- atom 1 (plane 4)
- atoms 2 and 6 (plane 3)
- atoms 8 and 13 (plane 2)
- atom 14 (plane 1)

The distance between the planes is $u = w = \frac{\sqrt{6}}{3}d = \frac{\sqrt{3}}{3}a$. To demonstrate this, we set (see Figure 5) :

$$\begin{aligned} \cos\alpha &= \frac{u}{d} = \frac{2}{\sqrt{6}}d & (46)\\ u &= \frac{2}{\sqrt{6}}d = \frac{\sqrt{6}}{3}d = \frac{\sqrt{3}}{3}a & (47)\\ w &= \sqrt{6} - 2u = \sqrt{6}d - 2\frac{\sqrt{6}}{3}d \\ &= \frac{\sqrt{6}}{3}d \\ &= u & (48) \end{aligned}$$

2.2 H/Pd(111)

The PES that describes the dissociative adsorption of H_2 on Pd(111) [1,27,28] was written in FORTRAN 90. In this thesis, it was modified to study the diffusion of one hydrogen atom and also adapted to such implement in the MCTDH program [33]. In Appendix C the some lines of this routine is shown, as well as additional subroutines written to implement the code in the MCTDH program. All additional routines and modified parts of original code are duly indicated in Appendix C. The fifth line indicates the number of hydrogen atoms considered, (nH = 2). We modified it to nH = 1 to study the diffusion of just one hydrogen atom. This is the only change made in the program to adapt it from the description of the H_2/Pd(111) system to that of the H/Pd(111) system. The supercell used in the development of the PES (see below) consists of a slab of five Pd layers with a (10×10) Pd(111) surface cell and a vacuum space corresponding to five Pd layers [27].

In Appendix E a brief overview of the Density Functional Theory used to develop this PES is presented.

2.2.1 Analytical representation of the PES for H_2/Pd(111) and H/Pd(111)

The PES for the systems studied in this thesis were represented analytically by Dong [1, 27]. The analytical "reactive force field" potential used for constructing this PES was initially developed by Brenner [46] and parametrized to describe the dissociative adsorption of H_2 on Pd(111) by Dong *et al* [1, 26–28]. The subroutine H_2/Pd(111) was modified to describe the adsorption of one hydrogen atom on Pd(111) as described above.

In a very general way, the reactive force fields (RFF) represent the potential energy of a system as

$$E = E_{\mathrm{nr}} + E_{\mathrm{r}} \tag{49}$$

where E_{r} are RFF contribution and E_{nr} represents the long range interaction. The energy of system is described by RFF and it is decomposed into a repulsive energy (E_{rep} and a bonding energy (E_{bond})

$$E_{\mathrm{r}} = E_{\mathrm{rep}} + E_{\mathrm{bond}} \tag{50}$$

In subroutine H_2/Pd(111) the RFF used is called reactive bond order (REBO) potential and it is given by

$$E_{\mathrm{r}} = \sum_{\alpha=1}^{n} \sum_{\beta=1,\beta\geq\alpha}^{n} \sum_{i=1}^{N_\alpha} \sum_{j=1\ (j>i \text{ if } \alpha=\beta)}^{N_\beta} [V_{\alpha\beta}^{R}(r_{ij}^{\alpha\beta}) - \bar{b}_{ij}^{\alpha\beta} h_{\alpha\beta}(r_{ij}^{\alpha\beta})] \tag{51}$$

The molecules are denoted by Greek letters, n is the number of molecules, N_α and N_β are the number of atoms of species α and β, $r_{ij}^{\alpha\beta} = |r_i^\alpha - r_j^\beta|$ is the distance between atom i of molecule α and atom j of molecule β, $V_{\alpha\beta}^{R}(r_{ij}^{\alpha\beta})$ and $h_{\alpha\beta}(r_{ij}^{\alpha\beta})$ are the so called repulsive and hopping integral, respectively, which are approximated by

$$V_{\alpha\beta}^{R}(r_{ij}^{\alpha\beta}) = A_{\alpha\beta} f_{\alpha\beta}(r_{ij}^{\alpha\beta}) \left(1 + \frac{B_{\alpha\beta}}{r_{ij}\alpha\beta}\right) e^{-\sigma_{\alpha\beta} r_{ij}^{\alpha\beta}} \quad (52)$$

$$h_{\alpha\beta}(r_{ij}^{\alpha\beta}) = C_{\alpha\beta} f_{\alpha\beta}(r_{ij}^{\alpha\beta}) e^{-\omega_{\alpha\beta} r_{ij}^{\alpha\beta}} \quad (53)$$

where $A_{\alpha\beta}, B_{\alpha\beta}, C_{\alpha\beta}, \sigma_{\alpha\beta}and\omega_{\alpha\beta}$ are parameters to be determined by fitting. The potential is cut off beyond some distance and the cut off function used in this analytic representation is given by

$$f_{\alpha\beta}(r_{ij} = \begin{cases} 1 & r_{ij}^{\alpha\beta} \leq r_{s1}^{\alpha\beta} \\ \frac{1}{2}\{1 + \cos[\pi(r_{ij}^{\alpha\beta} - r_{s1}^{\alpha\beta})/(r_{s2}^{\alpha\beta} - r_{s1}^{\alpha\beta})]\} & r_{s1}^{\alpha\beta} < r_{ij}^{\alpha\beta} \leq r_{s2}^{\alpha\beta} \\ 0 & r_{ij}^{\alpha\beta} > r_{s2}^{\alpha\beta} \end{cases} \quad (54)$$

where $r_{s1}^{\alpha\beta}$ is the starting cut off distance from which the potential is attenuated gradually and $r_{s2}^{\alpha\beta}$ is the cut off distance beyond which there is no interaction.

$\bar{b}_{ij}^{\alpha\beta}$ is the symmetrized bond order term that describes the effect of chemical environment on the bonding strength between the ith atom of species α and the jth atom of species β,

$$\bar{b}_{ij}^{\alpha\beta} = \frac{1}{2}(b_{ij}^{\alpha\beta} + b_{ji}^{\beta\alpha}) \quad (55)$$

where

$$b_{ij}^{\alpha\beta} = \left(1 + \sum_{\gamma=1}^{n} \sum_{k=1,\ (k\neq i \text{ if } \gamma=\alpha;\ k\neq j,\ \text{if}\gamma=\beta)}^{N_\gamma} f_{\alpha\beta}(r_{ij}^{\alpha\beta}) g_{\alpha\beta\gamma}(\cos\theta_{ijk}) e^{-\lambda_{\alpha\beta\gamma}(r_{ik}^{\alpha\gamma} - r_{ij}^{\alpha\beta})}\right)^{\frac{1}{2}} \quad (56)$$

with θ_{ijk} the bond angle between the bonds ij and ik and $g_{\alpha\beta\gamma}(\cos\theta_{ijk})$ is described by a polynomial

$$g_{\alpha\beta\gamma}(y) = a_0^{\alpha\beta\gamma} + a_1^{\alpha\beta\gamma}(1+y) + a_2^{\alpha\beta\gamma}(1+y)^2 + a_3^{\alpha\beta\gamma}(1+y)^3 \quad (57)$$

For the $H_2 - Pd$ system, there are three types of interactions, i.e., $Pd - Pd$, $Pd - H$ and $H - H$, which leads to fifteen parameters in Eqs. (52) and (53). Moreover, there are five types of three-body terms, i.e., $Pd - Pd - Pd$, $Pd - Pd - H$, $H - Pd - H$, $H - H - Pd$ and $Pd - H - Pd$, which lead to twenty parameters in Eq. (57) and two parameters for $\lambda_{\alpha\beta\gamma}$ (one for $Pd - Pd - Pd$ and one for the other four types). Hence, there are in total 37 parameters for REBO potentials.

The reactive force field alone, i.e., E_{r}, is not capable of describing accurately the long range adsorbate-surface interaction, e.g., beyond a distance of 400 pm to the surface. The long range interaction is represented by E_{nr} (Eq. (49)). Since the surface corrugation effect is negligible when the adsorbate is far from the surface, the long range interaction can be described by a simple potential which is only function of the distance between the adsorbate's center of mass and the surface, Z, i.e.,

$$E_{\mathrm{nr}} = f_{\mathrm{L}}(Z)\left(c_0 - \frac{c_1}{Z^2}\right) \tag{58}$$

where c_0 and c_1 are two parameters to be determined by fitting and $f_{\mathrm{L}}(Z)$ is a rounded step function which is given by

$$f_{\mathrm{L}}(Z) = \begin{cases} 0 & Z \leq Z_1 \\ \frac{1}{2}\{1 - \cos[\pi(Z - Z_1)/(Z_2 - Z_1)]\} & Z_1 < Z \leq Z_2 \\ 1 & Z > Z_2 \end{cases} \tag{59}$$

with $Z_1 = 350$ pm and $Z_2 = 450$ pm. When the surface atoms are allowed to move, the coordinate Z in Eqs. (58) and (59) is defined with respect to the uppermost surface atom. The 37 parameters for REBO potential used for constructing the PES of H_2/Pd(111) are found in [1], Tab. 2, page 4.

2.2.2 Analysis of the PES for H/Pd(111)

A set of Cartesian coordinates chosen to describe the position of the hydrogen atom on the (111) surface is shown in Fig. 6a where x_c and y_c are the coordinates of H that describe the movement lateral to the substrate, the "frustrated translation" and z_c defines the distance of hydrogen from the plan formed by the first layer of frozen Pd atoms. Fig. 6b shows the possible adsorption sites of hydrogen on Pd(111) for an elementary unit cell where the intervals in x_c are $-\frac{d}{2}$ and $\frac{d}{2}$ and y_c are $-2h$ and $2h$.

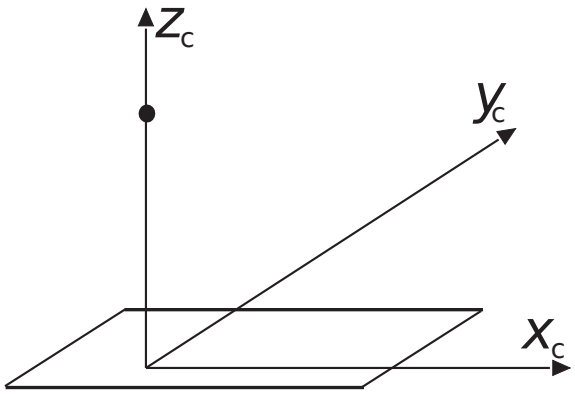

(a) Coordinate system for diffusion of H on a surface. In the schema, x_c and y_c are the coordinates of H on the substrate and z_c defines the distance of the hydrogen from the surface of Pd.

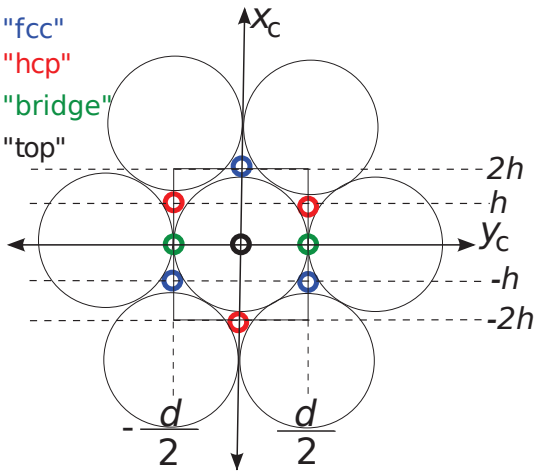

(b) Elementary unit cell of Pd(111) and the possible adsorption sites.

Figure 6 – (a) Coordinate of system for diffusion of hydrogen on Pd(111) and (b) elementary unit cell and the possible adsorption sites ($d = 275.114$ pm, $h = \frac{d}{2\sqrt{3}} = 79.419$ pm).

The one-dimensional section of the PES along the reaction coordinate $z = z_c$ when the atom of H is at fcc site (Fig. 7) shows two energy wells for $z < 0$. This PES is not developed to study the absorption of atoms therefore this results is not expected to be quantitatively exact but it corresponds qualitatively well to the PES discussed in [47–49]. So, to perform dynamical calculations we choose a limited range of values for z_c where the atom of H is adsorbed near the lowest well, see Fig. 7.

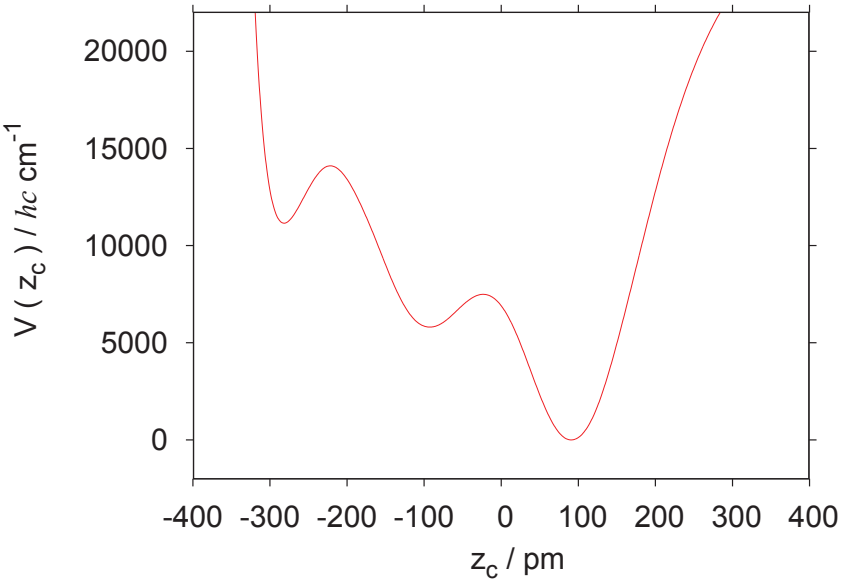

Figure 7 – One-dimensional section of the PES along z_c when x is $\frac{d}{3}$ and y is $-\frac{d}{3}$ ($d = \frac{a\sqrt{2}}{2}$, $a = 389$ pm is the Pd crystal parameter [45]). The range of values for z_c chosen to perform dynamical calculations is from 20 pm to 170 pm.

For convenience, the lowest well gives the zero reference energy value. The output of the REBO routine delivers -27687 $hc\,\mathrm{cm}^{-1}$ for this energy, which is the theoretical value of the energy released by the adsorption of a single H-atom on the Pd surface at its most stable adsorption site (electronic energy difference). From a simple thermodynamical cycle, one may estimate an experimental value ranging between -23200 and -22700 $hc\,\mathrm{cm}^{-1}$ for this energy (see Appendix D). It seems that the theoretical value obtained from the REBO routine is exaggerated. However the absolute value of the adsorption energy is not relevant for the work carried out in this thesis, and we will not consider it further.

For this set of Cartesian coordinates, the minima on the PES and the nth order saddle point (nth) of adsorption sites (Fig. 6b) were calculated by the algorithm described in [4], i.e. by searching those points whose the gradient of the PES are zero. The minima and the saddle points were distinguished via frequency calculations. For the "bridge" and "top" sites were found imaginary frequencies (Tab. 2). The saddle points are of order 1 and 2. For the adsorption "fcc" and "hcp" sites all frequencies are real (Tab. 3) and these adsorption sites are global minima (Tab. 1).

The difference between the adsorption "fcc" and "hcp" sites is $\sim 154\ hc\,\mathrm{cm}^{-1}$. The first energy barrier or transition structure, has one imaginary frequency (Tab. 2) and it is located at $\sim\ 1140\ hc\,\mathrm{cm}^{-1}$ above the "fcc" site ("bridge" site in Fig 6b. The second barrier is located at the "top" site, it has two imaginary frequencies (Tab. 2) and it is $\sim 5515\ hc\,\mathrm{cm}^{-1}$ above the "fcc" site.

Tab. 1 gives the values of Cartesian coordinates for some stationary points, the energies and the n order saddle point (n) of adsorption sites.

Table 1 – Cartesian coordinates, energies and nth order saddle point (nth) of adsorption sites.

sites	$x_\mathrm{c}\ /\ d$	y_c	z_c / pm	$V\ /\ hc\,\mathrm{cm}^{-1}$	$E^t_\mathrm{ZP}\ /\ hc\,\mathrm{cm}^{-1}$	n
fcc	$\frac{1}{2}$	$-h$	90.8	0	1273.9	0
hcp	$\frac{1}{2}$	h	90.1	153.4	1307.5	0
bridge	$\frac{1}{2}$	0	104.3	1139.1	1158.0	1
top	0	0	149.5	5515.1	1203.0	2

$d = 275.114$ pm, $h = \frac{d}{2\sqrt{3}} = 79.419$ pm, ^{t}harmonic ZPE

Table 2 – Vibrational wavenumbers (in cm^{-1}) of hydrogen, deuterium and tritium on Pd(111) obtained in the harmonic approximation [4] for the "bridge" and "top" sites. Negative values indicate imaginary wavenumbers.

sites	H/Pd(111)	D/Pd(111)	T/Pd(111)
	-364.7	-258.0	-210.8
bridge	1092.8	773.0	631.7
	1224.4	866.1	707.8
	-552.8	-296.1	-242.0
top	-552.8	-296.1	-242.0
	2405.5	1505.6	1230.3

It is noted that the vibrational wavenumbers calculated in the harmonic approximation [4] are in qualitatively good agreement with the experimental results [22] and the theoretical results [49]. The vibrational wavenumber calculated in Tab. 3 overestimates the anharmonic result [49], indicating that the system H/Pd(111) contains an important anharmonicity.

Table 3 – Vibrational wavenumbers (in cm^{-1}) of hydrogen on Pd(111) obtained in the harmonic approximation [4]. In reference [22] the vibrational wavenumber were obtained from High Resolution Energy Electron Loss Spectroscopy. In reference [49] the vibrational wavenumber were obtained from anharmonic calculations.

assignment	Experimental results [22]	Theoretical results [49]	This work
0_{fcc}	0	0	0
0_{hcp}		288.3	153.4
$\nu_{p,fcc}$	774	717.4	786.0
$\nu_{p,hcp}$		928.2	952.0
$\nu_{z,fcc}$	1016	922.4	975.5
$\nu_{z,hcp}$		1117.7	1172.1

Table 4 – Overview: Vibrational wavenumbers (in cm^{-1}) of hydrogen, deuterium and tritium atoms on Pd(111) obtained in the harmonic approximation [4].

assignment	H/Pd(111)	D/Pd(111)	T/Pd(111)
0_{fcc}	0	0	0
0_{hcp}	153.4	153.4	153.4
$\nu_{p,fcc}$	786.0	556.0	454.4
$\nu_{p,hcp}$	952.0	717.9	614.7
$\nu_{z,fcc}$	975.5	690.2	564.0
$\nu_{z,hcp}$	1172.1	874.0	742.3

The one-dimensional section of the PES along the reaction coordinate y_c (Fig.8) shows two energy wells ("fcc" and "hcp" sites) separated by a barrier $E_{\text{bridge}} = 1139\, hc\,\text{cm}^{-1}$ ("bridge" site). One observes that when the zero point energy (2D-ZPE) in the coordinates other than the coordinate shown in the section is added (see Fig. 8 in dashed line) the thus obtained energy barrier increases from 1139 to 1417 $hc\,\text{cm}^{-1}$ (=(2298-881)/$hc\,\text{cm}^{-1}$). The zero point energy (2D-ZPE) was calculated in the harmonic approximation ($\frac{E_{\text{ZP}}}{hc\,\text{cm}^{-1}} = \sum_i \frac{1}{2}\check{\nu}_i$).

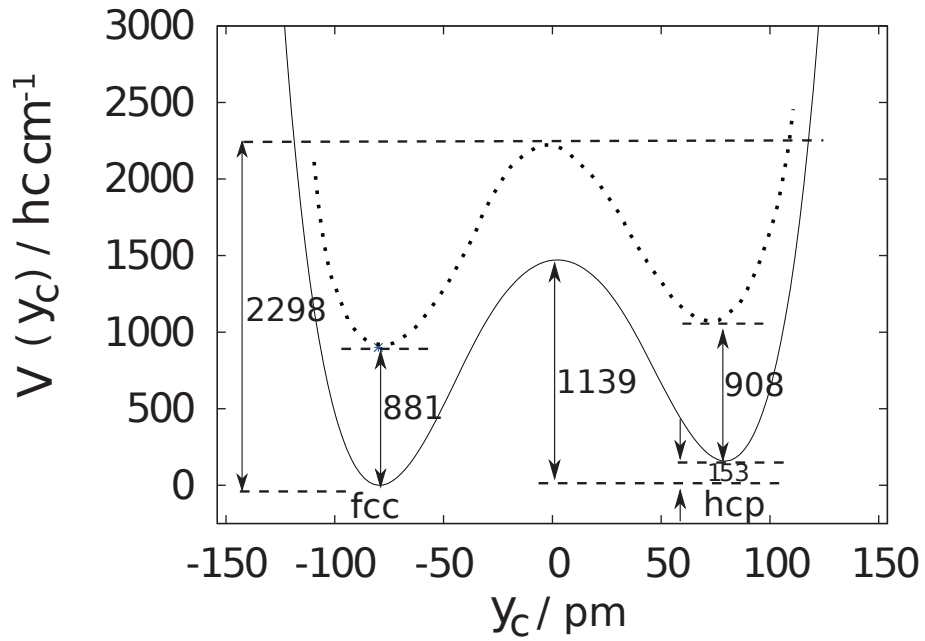

Figure 8 – One-dimensional section of the PES along y_c when x_c is $\frac{d}{2}$ ($d = \frac{a\sqrt{2}}{2}$, a = 389 pm is the Pd crystal parameter [45]) and z_c is 92.4 pm, in full line the electronic adiabatic energy and in dashed line the electronic adiabatic energy to which the 2D-ZPE was added. The dashed line is schematic, as calculated harmonic ZPE of all coordinates but y_c are reported here for stationary structures only.

The best set of coordinates to exploit the periodicity of the elementary cell and to describe the position of the hydrogen atom in the PES follows skewed axes of the primitive cell. They are shown as x and y axes in Fig. 9 form an angle $\alpha = 120^0$. We shall call then also twisted coordinates, where $x = x_c$ and $z = z_c$. The smallest possible periodically repeatable surface cell (elementary cell) is shown in Fig. 9. This cell will be used to define a first grid of calculations.

Its occupation by a hydrogen atom correspond to a 50% coverage of the substrate, as the atom can adsorb either in the "fcc" or in the "hcp" site.

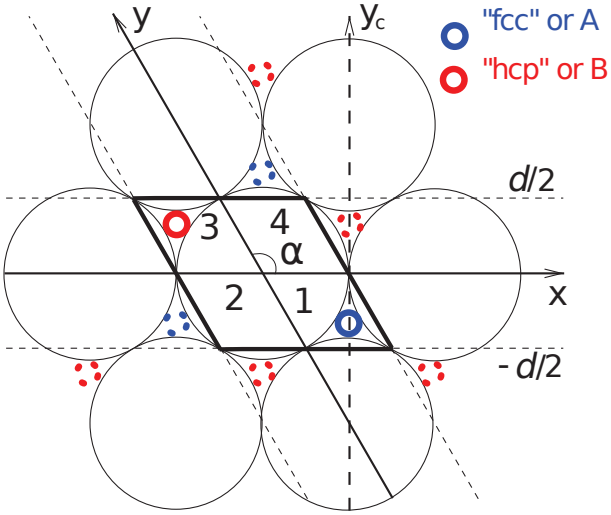

Figure 9 – Set of coordinates chosen to exploit the periodicity of the elementary cell of Pd(111). Numbers 1 to 4 define sub-cells that will be considered later.

The harmonic zero point energies in Tab. 5 were obtained summing up the corresponding values in Tabs. 2 and 3. The anharmonic zero point energies were obtained from the calculations of anharmonic eingenvalues using the MCTDH code as discussed below. For the bridge and top sites, Cartesian coordinates were used for the MCTDH calculations. Tab. 5 also gives the values of stationary points in the twisted coordinates.

Table 5 – Twisted coordinates, energies of adsorption sites and zero point energy anharmonic.

sites	x / d	y / d	z / pm	V / $hc\,\mathrm{cm}^{-1}$	E^t_{ZP} / $hc\,\mathrm{cm}^{-1}$
fcc	$\frac{1}{3}$	$-\frac{1}{3}$	90.8	0	1477.7
hcp	-$\frac{1}{3}$	$\frac{1}{3}$	90.1	153.4	1513.7
bridge	$\frac{1}{2}$	0	104.3	1139.1	1144.4
top	0	0	149.5	5515.1	968.1

d= 275.114 pm, a = 389 pm [45]; ^{t}anharmonic ZPE

2.2.3 Grid studies H/Pd(111)

The next largest periodically repeatable cells chosen for the quantum dynamics calculations are grid 2 and grid 3. The grid 2 contains 4 possible "fcc" sites and 4 possible "hcp" sites (represents a 12.5 % coverage of the substrate, Fig. 10a) and grid 3 contains 9 possible "fcc" sites and 9 possible "hcp" sites (represents a 5.6 % coverage of substrate, Fig. 10b).

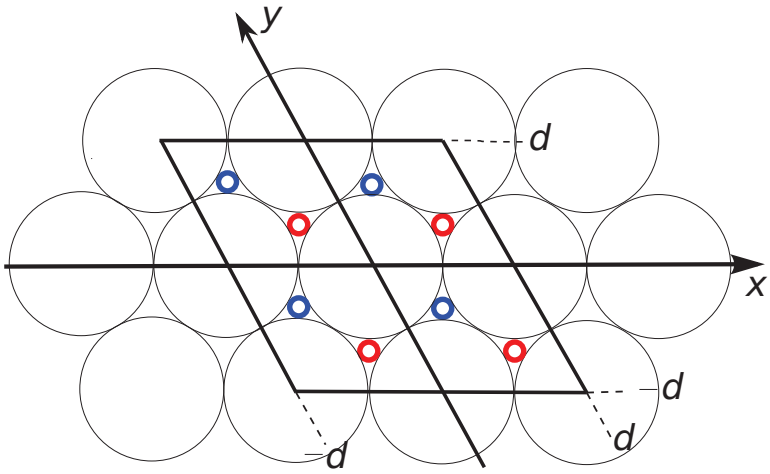

(a) Grid 2 with 12.5 % coverage of substrate.

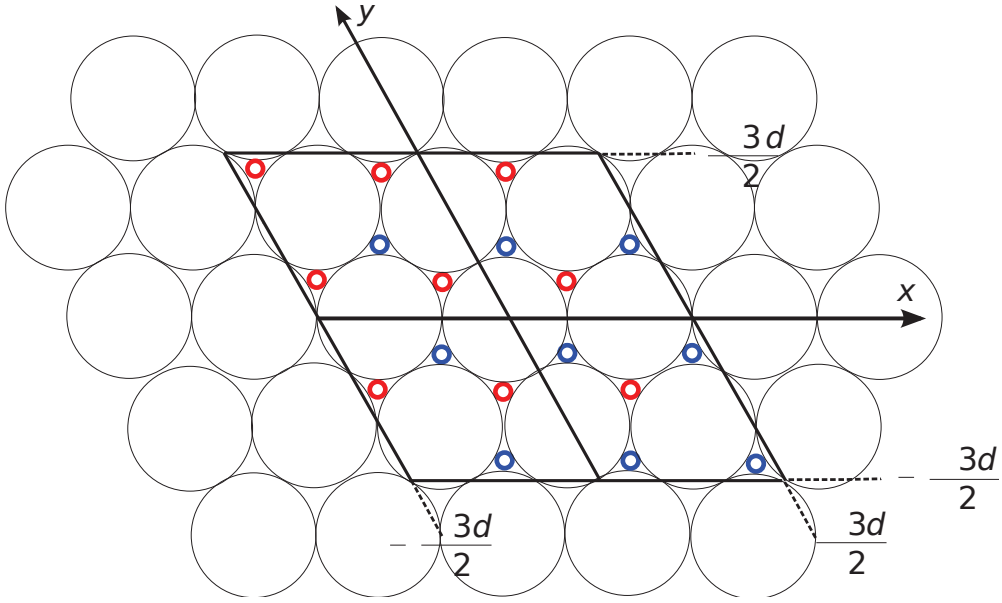

(b) Grid 3 with 5.6 % coverage of substrate.

Figure 10 – Next largest periodically repeatable cell: grid 2 (a) and grid 3 (b).

2.2.4 Potential representation using POTFIT

The product representations (see Eqs. (15) or (16)), for the (3D) and (6D) systems, respectively, do not in general guarantee the optimal solution (especially in the case of more than two dimensions) [36]. The representation of the potential of H/Pd(111) by a linear combination of products of one-dimensional functions using the POTFIT algorithm (discussed in Methods) for the grid 1, 2 and 3 shows a good approximation because the $\mathscr{L}^2$-error is small, showing that the V^{appr} is very close to the optimum. The representation of $V(x, y, z)$ as a linear combination of products (see that chapter Methods) was made without choosing any relevant region, i.e, all grid points are considered as relevant. The $\mathscr{L}^2$-error for grid 1 is 0.043 $hc\,\text{cm}^{-1}$, for grid 2 is 0.025 $hc\,\text{cm}^{-1}$ and for grid 3 is 0.022 $hc\,\text{cm}^{-1}$. The total time duration to perform the product representation with the POTFIT algorithm is about 1 hour for grid 1 and about 2 hours for grid 2 and 3.

The contour lines of the potential representations for each grid studied is given in Fig. 11. One sees for example in Fig. 11a (grid 1), the two more stables adsorption sites, "fcc" and "hcp", located at 50 and 300 $hc\,\text{cm}^{-1}$, respectively. The barrier energy is located at $\simeq$ 1200 $hc\,\text{cm}^{-1}$. In Figs. 11b and 11c one sees the 4 adsorption sites "fcc" and "hcp" for the grid 2 and 9 adsorption "fcc" and "hcp" sites for the grid 3, showing the difference of energy between the sites and the high symmetry when one increases the size of unit cells.

The parameters for this calculation are shown in Tab. 6.

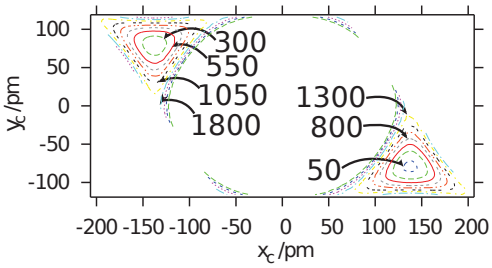

(a) Contour lines of PES for grid 1.

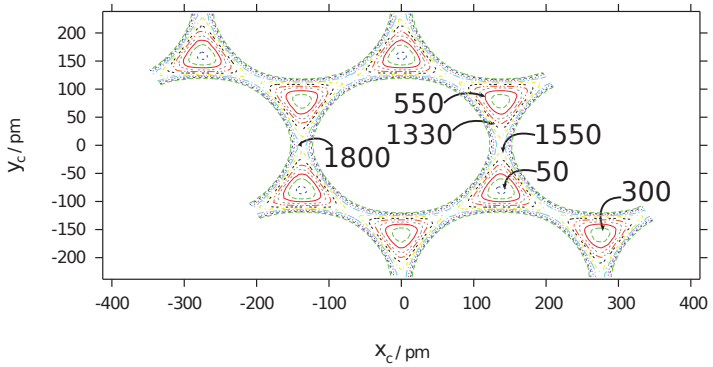

(b) Contour lines of PES for grid 2.

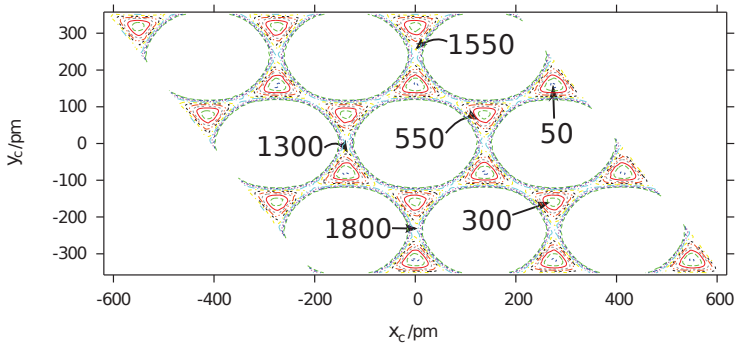

(c) Contour lines of PES for grid 3.

Figure 11 – Contour line representation of the potential and the adsorption sites the grid 1 (a), grid 2 (b) and grid 3 (c). The values of contour lines are in units of $hc\,\mathrm{cm}^{-1}$, $z_c = 90.8$ pm in all sections.

Table 6 – Calculation parameters. The DVR used are sine DVR (SIN) and Exponential (plane-wave) DVR. Masses used in the calculations are $m(^1\mathrm{H}) = 1.007825$ Da, $m(^2\mathrm{H}) = 2.014101$ Da, $m(^3\mathrm{H}) = 3.016049$ Da. CMF is the "constant mean field" integration scheme parameters, RRDAV is the Davidson diagonaliser, RK8 is the Runge-Kutta integration scheme to 8th order.

grid parameters

coordinate (κ)	DVR	DVR-parameters	N_κ [a)]	M_κ [a)]
x or y	EXP	$x^{(\min)} = y^{(\min)} = -j_\mathrm{g} \times d/2$,	61	
		$x^{(\max)} = y^{(\max)} = j_\mathrm{g} \times d/2$ [b)]		
		(1×1) grid: $j_\mathrm{g} = 1$		25
		(2×2) grid: $j_\mathrm{g} = 2$		40
		(3×3) grid: $j_\mathrm{g} = 3$		58
z	SIN	$z^{(\min)} = 20$ pm, $z^{(\max)} = 170$ pm	31	11

integration parameters

integration or extrapolation scheme	parameters
CMF	initial time interval 1.0 fs; accuracy parameter 10^{-3}
RRDAV/A	maximal order 5000; accuracy 10^{-9}; eps_inv = 10^{-9}
RK8/spf	accuracy 10^{-8}; initial step size 0.1 fs

"potfit" parameters

natural potentials	z is "contracted", $y = y = 50$
	$y = y = 50$ for (1×1)-grid
	$y = y = 55$ for (2×2)-grid
	$y = y = 58$ for (3×3)-grid
separable weights	x, y, z: weight type 0
correlated weights	no correlation
fit characteristics	weighted rms[c)] smaller than 0.047 $hc\,\mathrm{cm}^{-1}$ (all points)

[a)] N_κ is the number of primitive functions of coordinate κ, M_κ is the number of single particle functions.

[b)] $d = 275.114$ pm is the distance between nearest neighbour palladium atoms [45].

[c)] root mean square deviation

Chapter 3

Results for H/Pd(111) and isotopes: Vibrational eigenstates and time evolutions

In this Chapter, results for the vibrational spectrum and time evolution of initially localized wave packets are presented and discussed. The results allow us to have an unprecedented understanding of the diffusion dynamics.

3.1 Eigenstates of H, D and T on Pd(111)

3.1.1 Eigenstates of H on Pd(111)

Eigenenergies and eigenvectors are calculated with the improved block relaxation method (discussed in chapter Methods). All calculation parameters used for the grids studies are summarized in Tab. 6.

Fig. 10a for example, shows the grid 2. It is noted that when the hydrogen atom is located at "fcc" site (the blue circle), there are three channels of diffusion, i.e., the hydrogen atom can move to three "hcp" sites adjacent and equivalent (the red circles). Fig. 12 shows the three channels of diffusion. One can therefore describe the local vibrational structure arising at each equilibrium adsorption site with the aid of the C_{3v} point group, similarly to the point group of NH_3, where it is assumed to have a pyramidal molecular geometry.

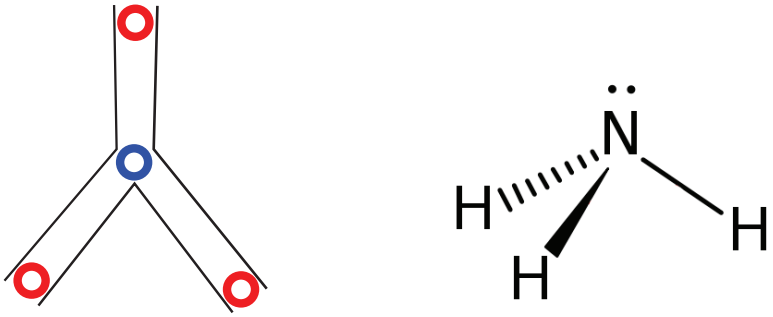

Figure 12 – Model for the representation of three channels of diffusion that look like the pyramidal molecular geometry of NH_3. The blue circle represents to "fcc" site and the three circles in red represent to "hcp" site.

A brief recall of group theory is given in the Appendix F. We shall use C_{3v} symmetry labels to characterize states that are localized in the three-fold symmetry sites.

Tab. 7 shows the eigenstates when the hydrogen atom is at "fcc" and "hcp" sites for the grids 1, 2 and 3. The parallel modes are indicated 2_{A} and 2_{B} and the perpendicular modes are indicated 1_{A} and 1_{B}, where the subscripts A and B mean "fcc" and "hcp" sites, respectively.

Table 7 – Band edges $\tilde{\nu}/\mathrm{cm}^{-1}$, band widths $\Delta\tilde{\nu}/\mathrm{cm}^{-1}$ and band degeneracies g for H/Pd(111).

band	label	modes	grid 1		grid 2		grid 3	
			band edge	(g)	band width	(g)	band width	(g)
1	A_1	0_A	0.0	(1)	0.0	(4)	0.0	(9)
2	A_1	0_B	189.4	(1)	0.0	(4)	0.0	(9)
3	E	2^1_A	743.6	(2)	0.5	(8)	0.5	(18)
4	E	2^1_B	920.2	(2)	4.1	(8)	4.6	(18)
5	A_1	$1^1_A+2^2_A$	1047.6	(1)	11.0	(4)	12.4	(9)
6	A_1	$1^1_A+1^1_B+2^2_B$	1200.1	(1)	10.5	(4)	11.9	(9)
7	E	$2^2_A+2^2_B$	1321.8	(2)	18.3	(8)	19.6	(18)
8	A_1	$1^1_A+1^1_B+2^2_A$	1336.8	(1)	21.3	(4)	22.9	(9)
9	A_1	$1^1_B+2^2_A+2^2_B$	1535.9	(1)	9.7	(4)	11.5	(9)
10	E	$2^2_A+2^2_B$	1572.8	(2)	4.1	(8)	4.5	(18)
⋮		⋮	⋮		⋮		⋮	
22	A_1	$1^2_A+2^3_A$	2188.7	(1)	1.1	(4)	1.5	(9)
⋮		⋮	⋮		⋮		⋮	
27	A_1	$1^2_B+2^3_B$	2342.8	(1)	0.5	(4)	0.8	(9)
⋮		⋮	⋮		⋮		⋮	

The vibrational spectrum of H on Pd(111) obtained by high resolution electron energy loss spectroscopy (HREELS) shows two important peaks, one at 96 meV (774 $hc\,\mathrm{cm}^{-1}$) and the other at 126 meV (1016 $hc\,\mathrm{cm}^{-1}$) [22]. Saalfrank and Tremblay [49] calculated fundamental vibrational modes for the system H/Pd(111) and obtained 717.4 cm^{-1} and 922.4 cm^{-1} . They related the first mode to the parallel vibration at the site "fcc" (we call this mode 2_{A}) and the second mode as perpendicular vibration at the site "fcc" (we call this mode 1_{A}). They also calculated the vibrational modes for parallel and perpendicular vibrations at the "hcp" site (2_{B} and 1_{B}, respectively). The fundamental spectral transitions for these modes can not be distinguished experimentally because of the low resolution of the experimental technique [22]. The vibrational modes presented in this work, obtained by MCTDH [30], in particular by improved relaxation in block [33, 41], are 743.6 and 1047.6 cm^{-1} at the site "fcc" and 920.2 and 1200.2 cm^{-1} at the site "hcp" for the parallel and perpendicular modes respectively, (see in Tab. 7). These theoretical results are in good agreement with the experimental spectrum [22] and slightly better than those obtained in the reference [49]. This difference of theoretical resultats of [49] can be atributed to the low quality of PES used [48].

An important finding of this work is the formation of bands when one decreases the coverage degree of the substrate, i.e., increasing the number of void sites of adsorption (see Fig. 10). For grid 1, for example, one expects a degeneracy (g) equal to 2 for the parallel mode at each one of the A or B sites, 2_{A} or 2_{B}, the symmetry label of which is E. For grid 2, there are 4 "fcc" and "hcp" sites (see Fig. 10a), a degeneracy (g) equal to 8 for each site is expected for mode 2, see the fifth column of the Tab. 7. For grid 3, there are 9 "fcc" and "hcp" sites (see Fig. 10b), a degeneracy (g) equal to 18 for each site could be reported in the sixth column of the Tab. 7. However the degeneracy (g) for the grids 2 and 3 is broken (see Tab. 7) as the levels approach the electronic barrier ($\sim$ 1140 $hc\,\mathrm{cm}^{-1}$, see Fig. (5)). The splitting of levels is due to the tunnel effect and is at the origin of the formation of bands. The band width is given by the maximal lift of degeneracy; it is calculated by the difference between the minimal and maximal eigenvalues of states that would otherwise be degenerate. The minimal eigenstate for the grids 2 and 3 corresponds normally to the band edge given by the minimal eigenstates obtained with grid 1.

Analysing the reduced probability density is very useful to understand the nature of each eigenstate and that the perpendicular vibration modes are not pure modes. For example, the Fig. 13 shows the reduced probability density for the ground states (0_A and 0_B) for the "fcc" and "hcp" sites, the symmetry label of which is A_1. One sees that the nature of the reduced probability density for the ground states in the "fcc" (0_A) and "hcp" (0_B) sites are highly localized.

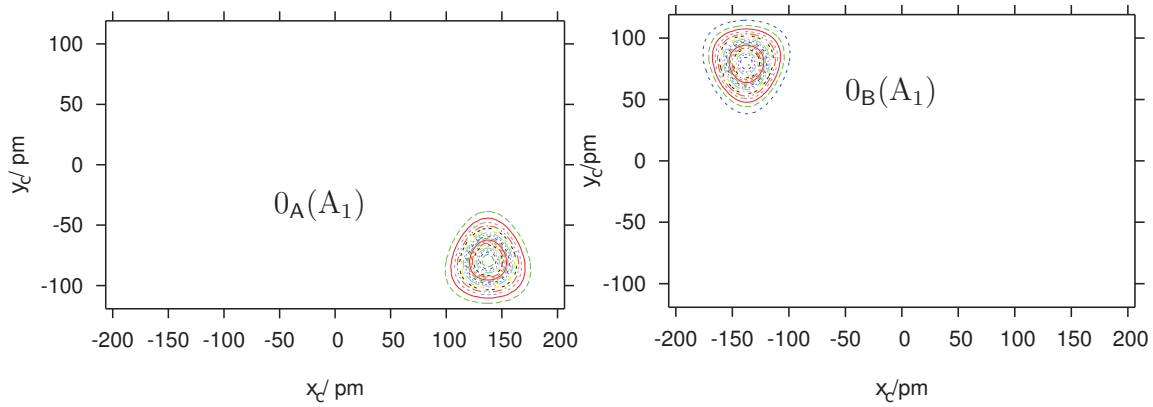

Figure 13 – Reduced probability density for the ground states 0_A and 0_B for the "fcc" and "hcp" sites, respectively, in the $x_c y_c$ plan.

Fig. 14 shows the reduced probability density for the parallel modes. It is expected a degeneracy of order 2, because there is a mode along x or y. It is possible to identify the vibrational direction parallel along x or y, by looking at the coordinate where the node of the probability distribution is localized. One observes also that the reduced probability density for the vibrational parallel modes remain localized at the "fcc" or "hcp" sites.

The fifth and sixth bands, which might naively be attributed to the perpendicular vibration modes (1047.6 and 1200.2 $hc\,\mathrm{cm}^{-1}$, Tab. 7) are in fact spread along the aforementioned channels localized at "fcc" and "hcp" sites. These modes are the result of a strong anharmonic interaction between 4 modes localized in the two sites : a mode with 1 quantum of perpendicular vibrational energy (1^1_A and 1^1_B) and a mode with 2 quanta of parallel vibration energy (2^2_A and 2^2_B).

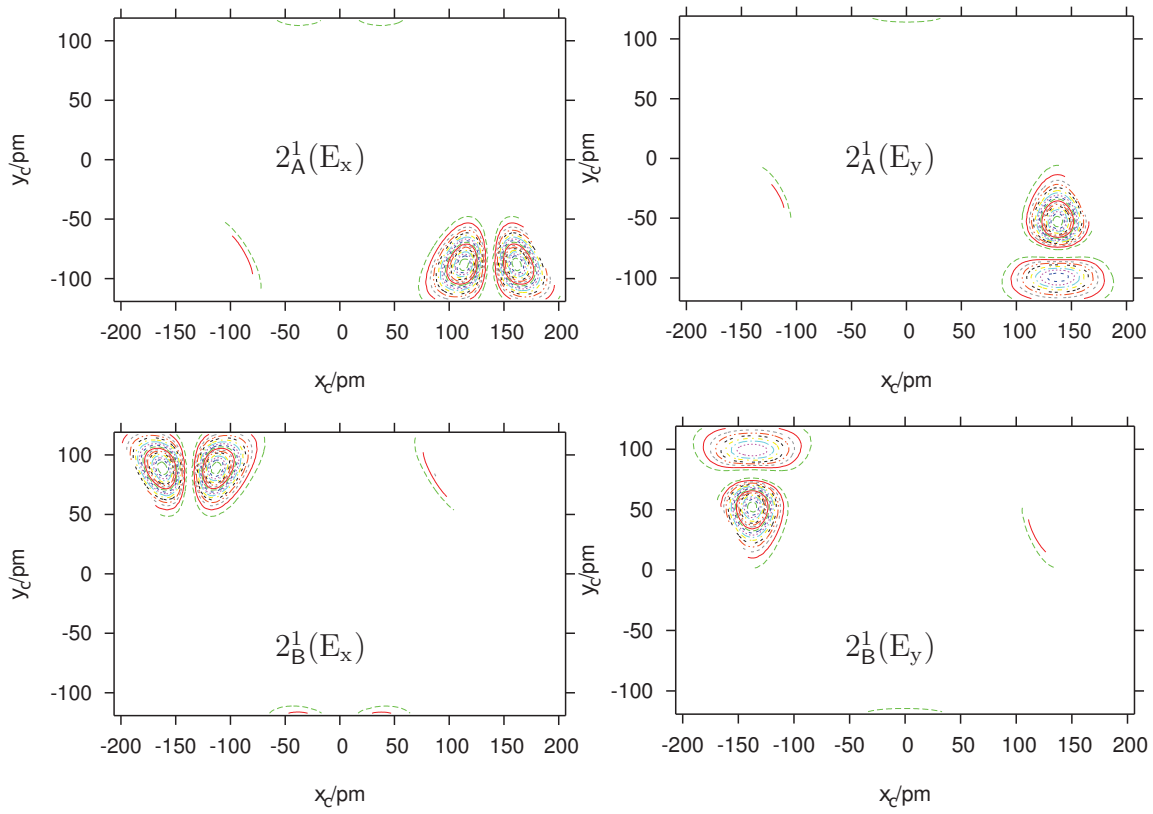

Figure 14 – Reduced probability density for the third and forth level that represent parallel modes with 1 quantum of energy (2^1_B and 2^1_B) in "fcc" and "hcp" sites, respectively, in the $x_c y_c$ plan.

Fig. 15 shows the reduced probability density in all the plans for the fifth level (1047.6 $hc\,\mathrm{cm}^{-1}$). Fig. 15a shows the reduced probability density in $x_c y_c$ plan. One observes that in this plan the probability density is localized at the "fcc" site (A) while fanning out importantly in the $x_c y_c$ plan. The form of this function must correspond to the parallel mode at "fcc" site. Due to the symmetry of the staggering, the function must be of the A_1 type. The first possible parallel vibration of A_1 type is the overtone 2^2_A.

Figs. 15b and 15c show the reduced probability density in the xz and yz plans, respectively. In these plans one observes that the probability density is localized at "fcc" site, where x is positive and y is negative. A node in z, corresponding to the perpendicular mode, can be clearly seen. Thus, the perpendicular vibrational mode (1047.6 $hc\,\mathrm{cm}^{-1}$) is a mixture of two modes localized at the "fcc" site (A) : a perpendicular vibrational mode with 1 quantum of energy (1^1_A) and a parallel vibrational mode with 2 quanta of energy (2^2_A).

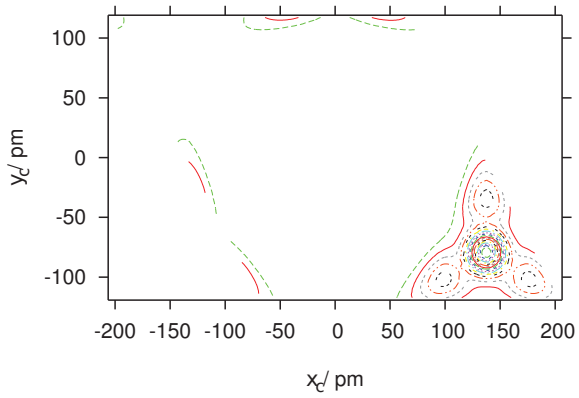

(a) Reduced probability density in $x_c y_c$ plan.

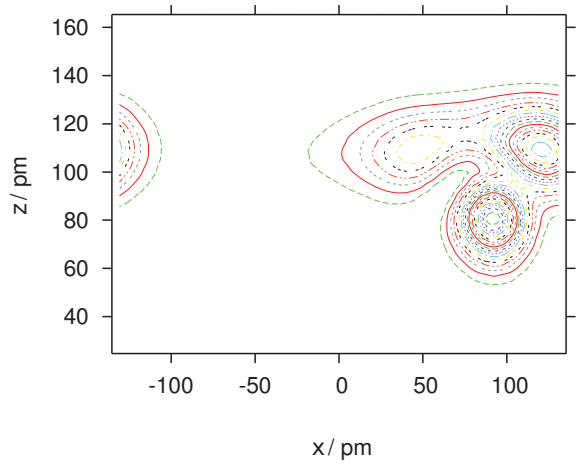

(b) Reduced probability density in xz plan.

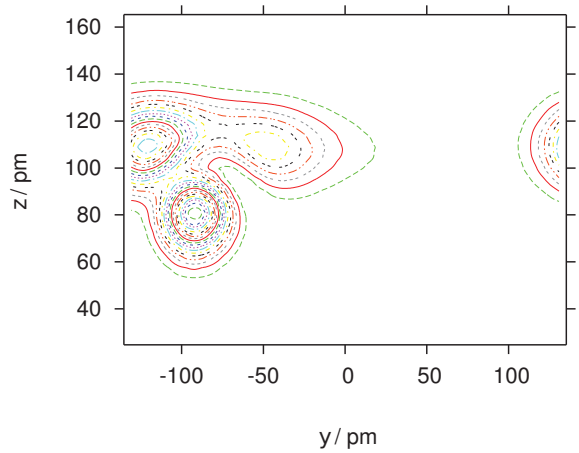

(c) Reduced probability density in yz plan.

Figure 15 – Reduced probability density for the fifth state at 1047.6 $hc\,\mathrm{cm}^{-1}$ assigned as $1^1_{\mathrm{A}} + 2^2_{\mathrm{A}}$.

Fig. 16 shows the reduced probability density in all the plans for the sixth state (1200.2 $hc\,\mathrm{cm}^{-1}$). One observes in the Fig. 16a that the reduced probability density is delocalized in the $x_\mathrm{c}y_\mathrm{c}$ plan. Focusing at the "fcc" site, (x_c positive and y_c negative) one sees that the shape of the probability of density is more localized, no unfolding or fanning out. However, in the "hcp" site, (x_c negative and y_c positive) the shape of the probability density is different, there is a fanning out as already seen above for the state at 1046.4 $hc\,\mathrm{cm}^{-1}$.

Figs. 16b and 16c show the reduced probability density in the xz and yz plans. One notes an important delocalization. In the region of positive x_c and negative y_c ("fcc" site), one can recognize the formation of a node in z, corresponding to the perpendicular mode (1^1_A). For x_c negative and y_c positive ("hcp" site), it is noted a perfectly formed node in z is noted, corresponding to the perpendicular mode (1^1_B). Combining with Fig. 16a, one can assign this reduced probability density as a mixture of : a perpendicular vibrational mode with 1 quantum of energy (1^1_A) in "fcc" site, a perpendicular vibrational mode with 1 quantum of energy (1^1_B) in "hcp" site and a parallel vibrational mode with 2 quanta of energy (2^2_A) in "hcp" site.

Fig. 17 shows the reduced probability density in all the plans for the sixth state (1336.8 $hc\,\mathrm{cm}^{-1}$). The reduced probability density in the $x_\mathrm{c}y_\mathrm{c}$ plan, Fig. 17a, shows that the two sites are similar. Again an important fanning out along the 3 channels at the "fcc" site (x_c positive and y_c negative) is noticed. One assigns this as a parallel vibration with 2 quanta of energy (2^2_A). In the "hcp" site, the probability density is more localized. This is hence a perpendicular vibration with 1 quantum of energy (1^1_B).

Figs. 16b and 16c show the reduced probability density in the xz and yz plans. An important delocalization in the two sites is noticed. Additionally, for the "fcc" site (x_c positive and y_c negative) one recognizes a well formed node in z, corresponding to the perpendicular vibration with 1 quantum of energy (1^1_A). This is also seen at the "hcp" site (x_c negative and y_c positive) a node in z, corresponding to the perpendicular vibration with 1 quantum of energy (1^1_B).

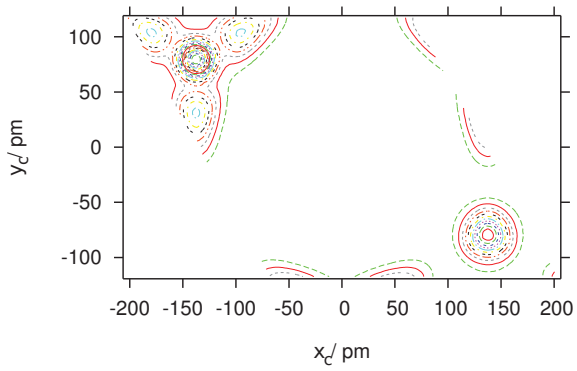

(a) Reduced probability density in $x_c y_c$ plan.

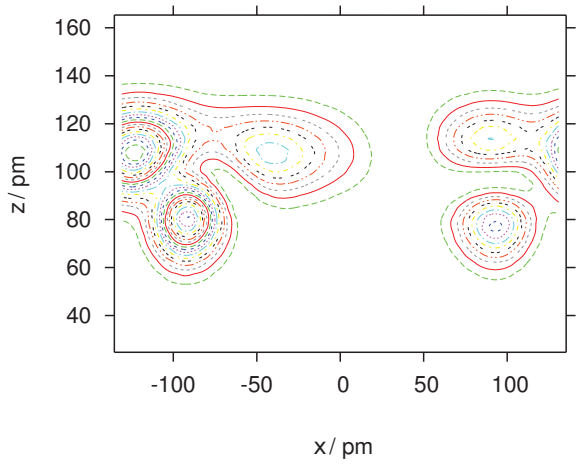

(b) Reduced probability density in xz plan.

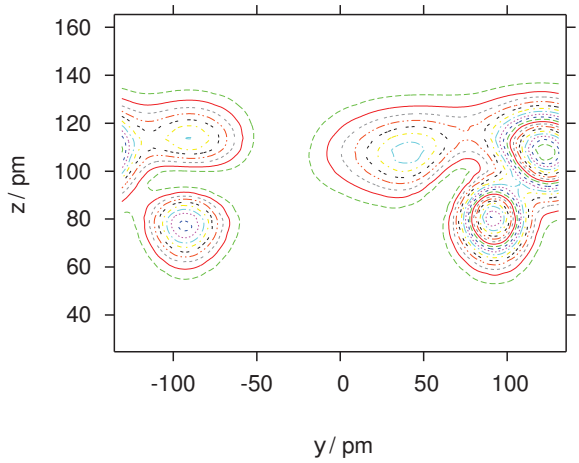

(c) Reduced probability density in yz plan.

Figure 16 – Reduced probability density for the sixth level (1200.1 $hc\,\mathrm{cm}^{-1}$), assigned as $1^1_{\mathrm{A}} + 1^1_{\mathrm{B}} + 2^2_{\mathrm{B}}$; symmetry label A_1.

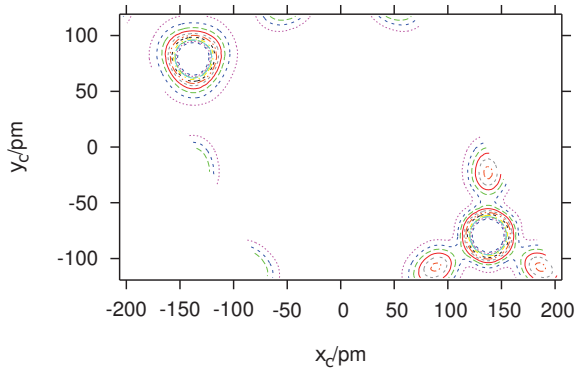

(a) Reduced probability density in $x_c y_c$ plan.

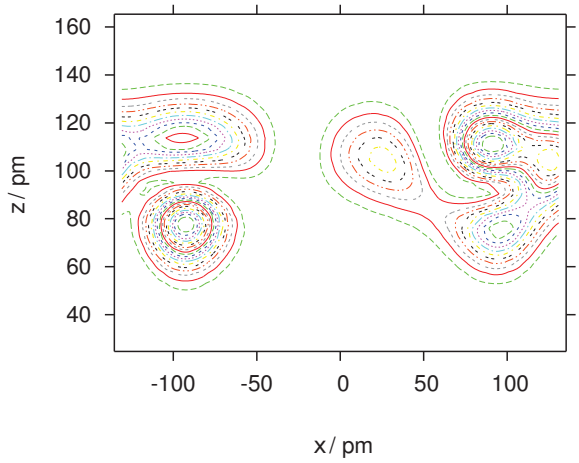

(b) Reduced probability density in xz plan.

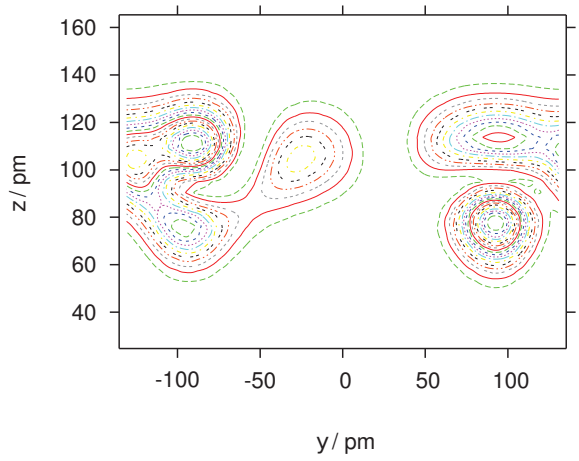

(c) Reduced probability density in yz plan.

Figure 17 – Reduced probability density for the eighth level (1336.8 $hc\,\mathrm{cm}^{-1}$), assigned as $1^1_{\mathrm{A}} + 1^1_{\mathrm{B}} + 2^2_{\mathrm{A}}$; symmetry label A_1.

Fig. 18 shows the reduced probability density for the ninth state at 1535.9 $hc\,\mathrm{cm}^{-1}$. Inspection of the shape of the probability density for at the two sites in the $x_\mathrm{c}y_\mathrm{c}$ plan (Fig. 18a), shows that the state can be assigned as a parallel vibration with 2 quanta of energy (2^2_A), a parallel vibration with 2 quanta of energy (2^2_B). Looking at the Figs. 18b and 18c one recognizes at the "hcp" site a node in z. However, for the "fcc" site, there is no node in z.

The mixed modes $1^1_\mathsf{A}+2^2_\mathsf{A}$, $1^1_\mathsf{A}+1^1_\mathsf{B}+2^2_\mathsf{B}$, $1^1_\mathsf{A}+1^1_\mathsf{B}+2^2_\mathsf{A}$ and $1^1_\mathsf{B}+2^2_\mathsf{A}+2^2_\mathsf{B}$ belong all to the same symmetry species A_1. The mixing of the pure modes is due to anharmonic coupling terms in the exact Hamiltonian operator. This type of interaction between vibrational modes of the same symmetry and similar energies is known as a Fermi resonance [50, 51].

The twenty-second and twenty-seventh levels (2188.7 and 2342.8 $hc\,\mathrm{cm}^{-1}$) also correspond to perpendicular vibrations and it is also noticed that these modes are not localized, rather they are mixtures of site localized modes. Fig. 19a shows that the reduced probability density in the $x_\mathrm{c}y_\mathrm{c}$ plan is localized at "fcc" site but it fans out considerably, which is interpreted as a parallel vibration mode with 3 quanta of energy (2^3_A). Figs. 19b and 19c show 2 nodes in z. It is noticed that the probability density is localized at "fcc" site, thus one interprets it as a perpendicular vibration mode with 2 quanta of energy 1^2_A. The twenty-sixth state (2342.8 $hc\,\mathrm{cm}^{-1}$) is composed of a parallel vibrational mode with 3 quanta of energy localized at "hcp" (2^3_B) and a perpendicular vibrational mode with 2 quanta of energy localized at "hcp" site 1^2_B.

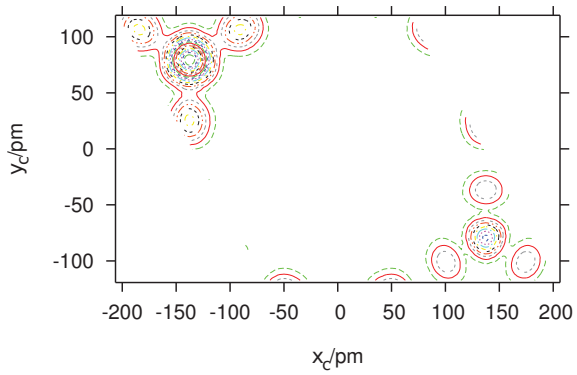

(a) Reduced probability density in $x_c y_c$ plan.

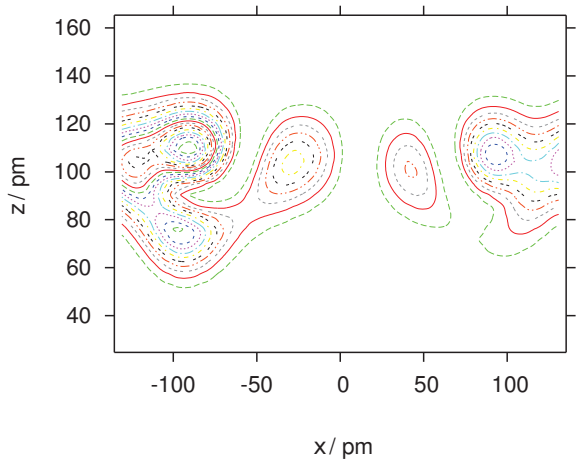

(b) Reduced probability density in xz plan.

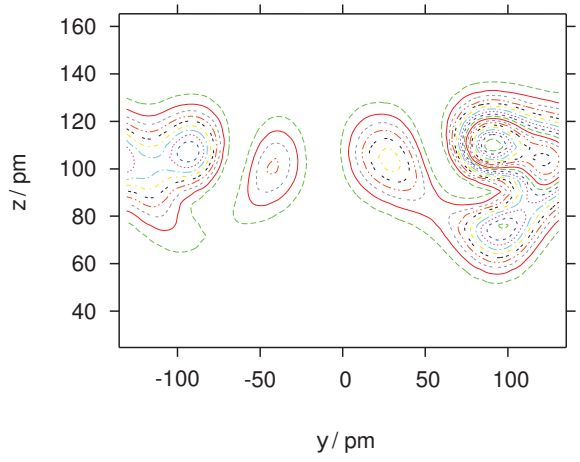

(c) Reduced probability density in yz plan.

Figure 18 – Reduced probability density for the ninth level (1535.9 $hc\,\mathrm{cm}^{-1}$), assigned as $1^1_{\mathrm{B}} + 2^2_{\mathrm{A}} + 2^2_{\mathrm{B}}$, its label of symmetry is A_1.

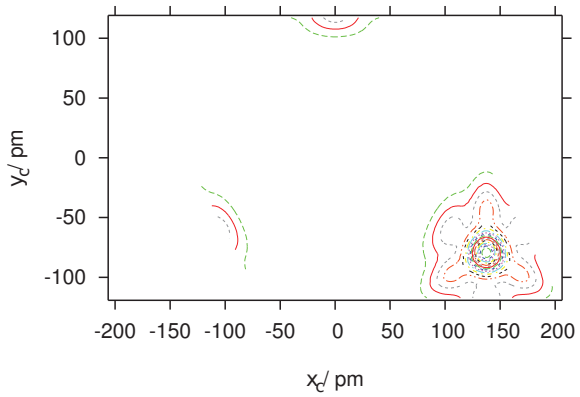

(a) Reduced probability density in $x_c y_c$ plan.

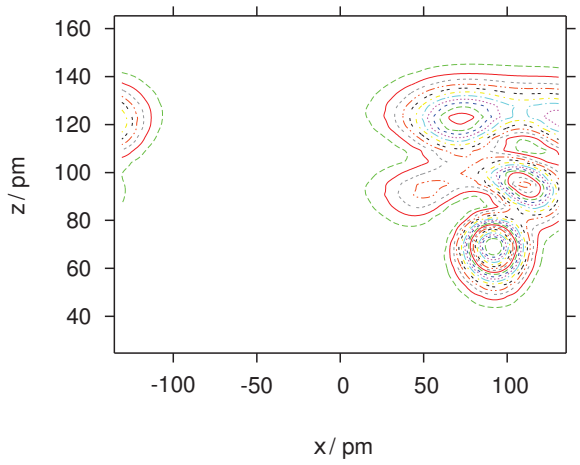

(b) Reduced probability density in xz plan.

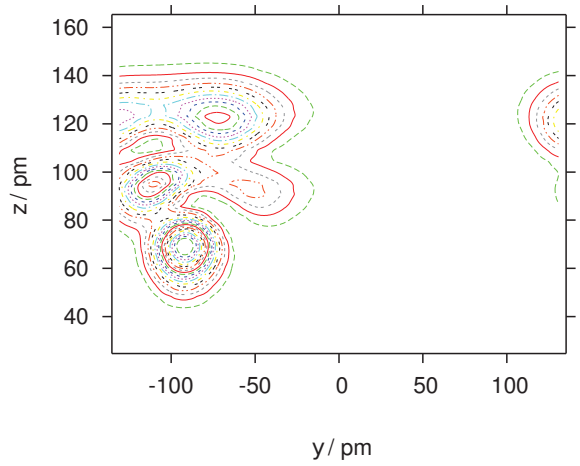

(c) Reduced probability density in yz plan.

Figure 19 – Reduced probability density for the twenty second level (2188.7 $hc\,\mathrm{cm}^{-1}$), assigned as $1^2_{\mathrm{A}} + 2^3_{\mathrm{A}}$, its label of symmetry is A_1.

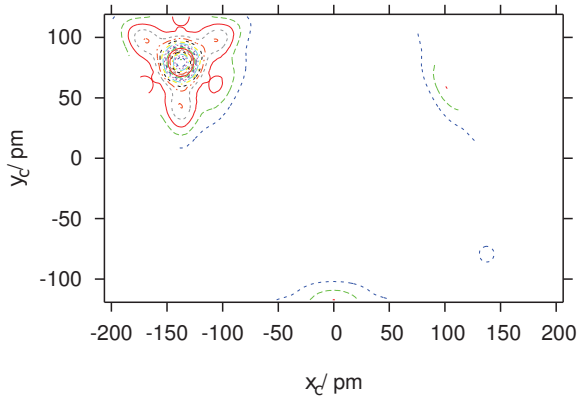

(a) Reduced probability density in $x_c y_c$ plan.

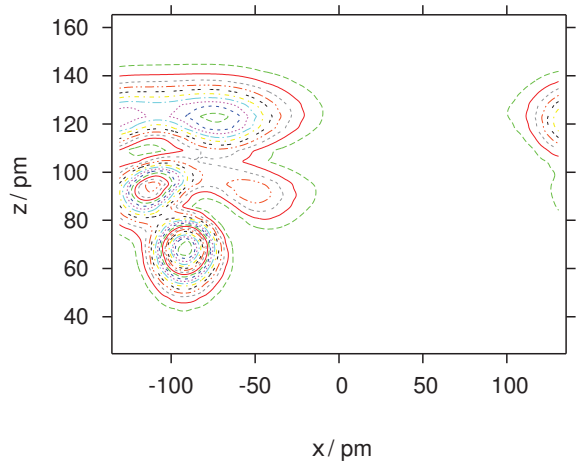

(b) Reduced probability density in xz plan.

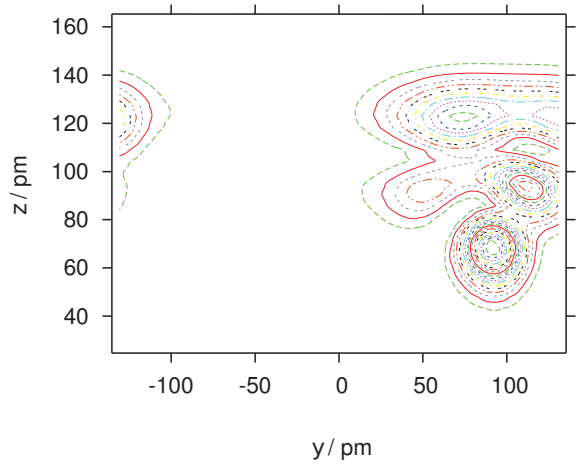

(c) Reduced probability density in yz plan.

Figure 20 – Reduced probability density for the twenty seventh level (2342.8 $hc\,\mathrm{cm}^{-1}$), assigned as $1^2_{\mathrm{B}} + 2^3_{\mathrm{B}}$, its label of symmetry is A_1.

In summary, each site has a local C_{3v} symmetry, such that per site two vibrational modes parallel to the substrate and one mode perpendicular to it can be expected. Per site type there will hence be 8 parallel and 4 perpendicular vibrational states arranged in levels of quasi-isoenergetic states. Tunneling may split these levels. Here, we summarize the results for the 2×2 surface cell grid, which we also call grid 2. The present calculations yield that the ground state level remains four-fold degenerate, at least within the accuracy defined by the number of digits reported in Tab. 8 below, both for the "fcc" and the "hcp" site, while the vibrationally excited levels split into two blocks, as indicated in this table.

Table 8 – Wavenumbers of the fundamental transitions for H/Pd(111) in cm^{-1} .

modes	site	theory			exp [22]
		this work[a]		ref. [49]	
parallel	fcc	743.6 (5)	744.1 (3)	717.4	774.3
	hcp	726.8 (3)	730.8 (5)		
perpendicular	fcc	1047.6 (1)	1058.6 (3)	922.4	1016.3
	hcp	1000.2 (3)	1010.8 (1)		

Column "this work" in Tab. 8 reports four sets of transitions for each mode. These sets arise from tunneling splitting of degenerate vibrationally excited levels and remaining degeneracies are indicated by the numbers in parentheses. The total degeneracy of levels is given by the product of site degeneracies arising from the (2×2) grid (see Fig. 10a) and the degeneracies of modes localized at each site (see text). Tunneling splits these transitions as indicated (numbers in parentheses give the remaining degeneracies). In refs [49] and [22], only one value is reported per transition. The present results for vibrational wavenumbers are comparable to previsouly reported values. Tab. 8 reports only the fundamental transitions and the present work has given evidence for the occurrence of strong anharmonic resonances in the overtone spectrum, which are include already present in the perpendicular modes presented in the table.

3.1.2 Eigenstates of D on Pd(111)

Normally a shift toward smaller wave numbers in the spectrum of the molecule is expected when an atom is replaced by an isotope of larger mass. Here, the hydrogen atom ^{1}H (1.007825 Da) is replaced by a deuterium atom ^{2}H (2.014101 Da) [52] and a decrease of the eigenvalues is indeed noticed. For example, one notes the decrease in the parallel vibrational modes (2^1_{A} or 2^1_{B}). The mode at 743.6 $hc\,\mathrm{cm}^{-1}$ (2^1_{A}) of hydrogen changes to 561.4 $hc\,\mathrm{cm}^{-1}$ (2^1_{A}) for the deuterium atom. Tab. 9 gives the eigenstates of D/Pd(111).

Table 9 – Band edges $\tilde{\nu}/\mathrm{cm}^{-1}$, band widths $\Delta\tilde{\nu}/\mathrm{cm}^{-1}$ and band degeneracies g for D/Pd(111).

band	label	modes	grid 1		grid 2	
			band edge	(g)	band width	(g)
1	A_1	0_{A}	0.0	(1)	0.0	(4)
2	A_1	0_{B}	188.8	(1)	188.8	(4)
3	E	2^1_{A}	561.4	(2)	561.4	(8)
4	E	2^1_{B}	748.5	(2)	748.5	(8)
5	A_1	$1^1_{\mathsf{A}}+(2^2_{\mathsf{A}})$	785.5	(1)	785.5	(4)
6	A_1	$1^1_{\mathsf{B}}+(2^2_{\mathsf{B}})$	966.2	(1)	966.2	(4)
7	A_1	$1^1_{\mathsf{A}}+2^2_{\mathsf{A}}$	1020.6	(1)	1020.6	(4)
8	E	2^2_{A}	1064.9	(2)	0.2	(4)
9	A_1	$1^1_{\mathsf{B}}+2^2_{\mathsf{B}}$	1181.6	(1)	0.6	(4)
10	E	$2^2_{\mathsf{A}}+2^2_{\mathsf{B}}$	1215.7	(2)	3.9	(8)
⋮		⋮	⋮		⋮	
22	A_1	$1^2_{\mathsf{A}}+(2^2_{\mathsf{A}})$	1590.8	(1)	0.3	(4)
⋮		⋮	⋮		⋮	
27	A_1	$1^2_{\mathsf{B}}+(2^2_{\mathsf{B}})$	1765.3	(1)	0.6	(4)
⋮		⋮	⋮		⋮	

It is noted that the perpendicular vibrational modes (785.5 and 966.2 $hc\,\mathrm{cm}^{-1}$) are rather localized (see Figs. 21 and 22). Furthermore, one observes that along $x_c y_c$ there is fanning out like it is noted for the H/Pd(111) (see Figs. 21a and 60a). One starts to note an important staggering along $x_c y_c$ at the seventh and ninth levels (1020.6 and 1181.6 $hc\,\mathrm{cm}^{-1}$) see the Figs. 23a and 24a but it continues localized on one site. Nevertheless the perpendicular vibrational modes of D/Pd(111) at "fcc" and "hcp" sites are derived of modes rather localized, $(1^1_{\mathsf{A}}+ 2^2_{\mathsf{A}})$ for the "fcc" site and $(1^1_{\mathsf{B}}+ 2^2_{\mathsf{B}})$ for the "hcp" site.

It is noted that the eighth and tenth levels consist of the parallel vibrational modes with 2 quanta of energy because they are two nodes along $x_c y_c$ (Fig. 25). The eighth level (1064.9 $hc\,\mathrm{cm}^{-1}$) is rather localized at the "fcc" site (Fig. 25) and is assigned to 2^2_{A}. The tenth level (1215.7 $hc\,\mathrm{cm}^{-1}$) is a mixture of parallel vibrations with 2 quanta of energy at "fcc" and "hcp" sites, thus, it is represented as $2^2_{\mathsf{A}} + 2^2_{\mathsf{B}}$.

Figs. 26 and 27 show the reduced probability density for the twenty second (1590.8 $hc\,\mathrm{cm}^{-1}$) and twenty sixth (1765.3 $hc\,\mathrm{cm}^{-1}$) levels. Theses modes represent the perpendicular vibrational modes with 2 quanta of energy in the "fcc" and "hcp" sites, respectively (Figs. 26b and 27b). It is noted that these modes are localized and that the density of probability along $x_c y_c$ do essentially not fan out. Therefore one represents these modes as 1^2_{A} and 1^2_{B} (Figs. 26 and 27).

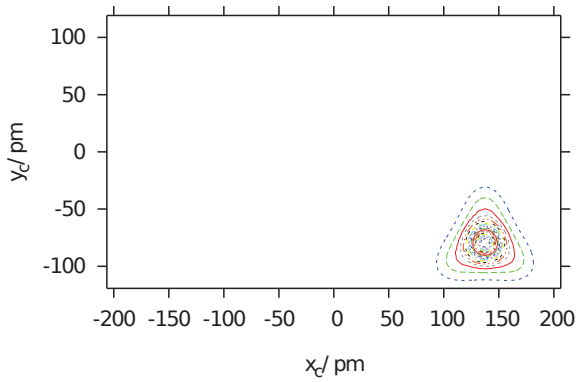

(a) Reduced probability density in $x_c y_c$ plan.

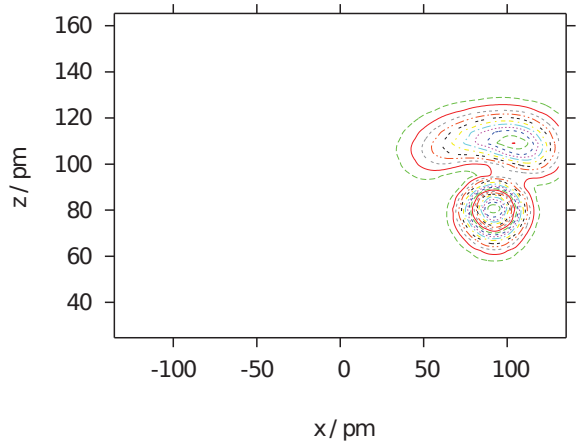

(b) Reduced probability density in xz plan.

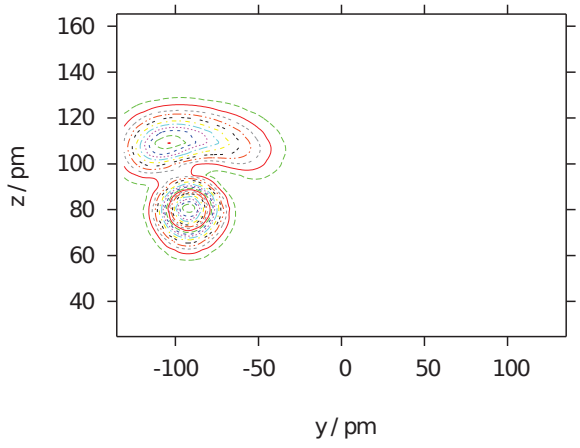

(c) Reduced probability density in yz plan.

Figure 21 – Reduced probability density for the fifth level (785.5 $hc\,\mathrm{cm}^{-1}$) for D/Pd(111) which can be assigned as $1^1_{\mathrm{A}} + 2^2_{\mathrm{A}}$, its label of symmetry is A_1. The 2^2_{A} component is very faint and can be put into brackets (see Tab. 9).

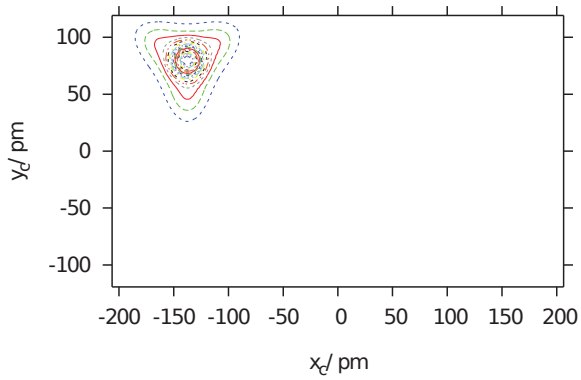

(a) Reduced probability density in $x_c y_c$ plan.

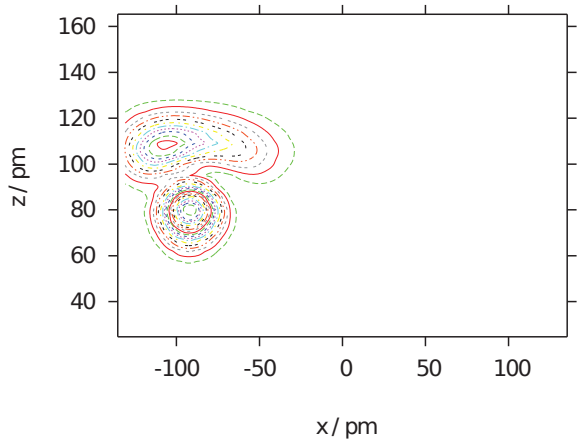

(b) Reduced probability density in xz plan.

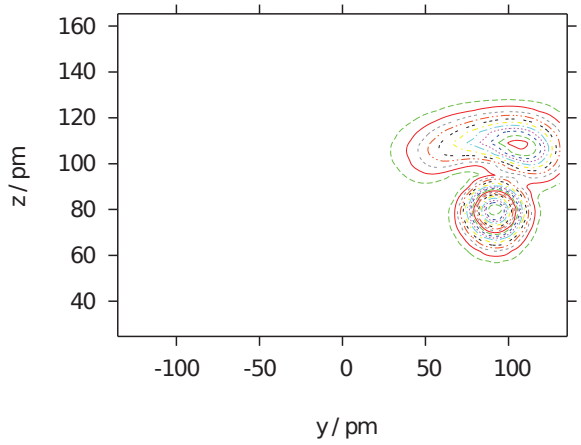

(c) Reduced probability density in yz plan.

Figure 22 – Reduced probability density for the sixth level (966.2 $hc\,\mathrm{cm}^{-1}$) for D/Pd(111) which can be assigned as $1^1_{\mathrm{B}} + 2^2_{\mathrm{B}}$, its label of symmetry is A_1. The 2^2_{B} component is very faint and can be put into brackets (see Tab. 9).

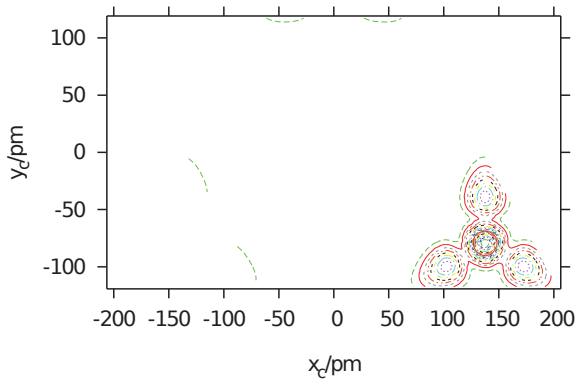

(a) Reduced probability density in $x_c y_c$ plan.

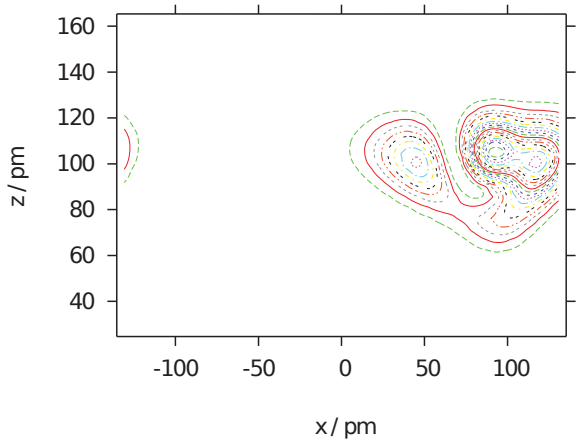

(b) Reduced probability density in xz plan.

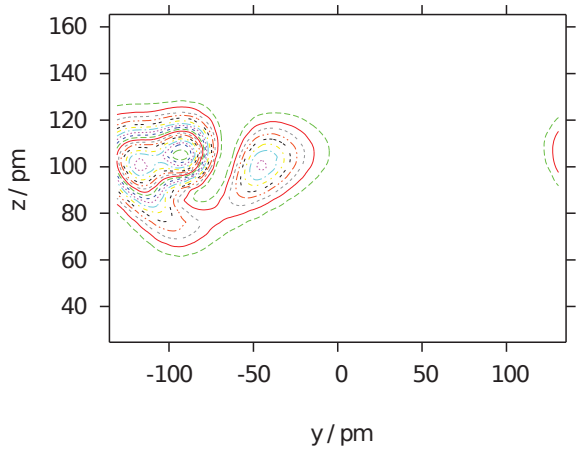

(c) Reduced probability density in yz plan.

Figure 23 – Reduced probability density for the seventh level (1020.6 $hc\,\mathrm{cm}^{-1}$) for D/Pd(111) which can be assigned as $1^1_{\mathrm{A}} + 2^2_{\mathrm{A}}$, its label of symmetry is A_1(see Tab. 9).

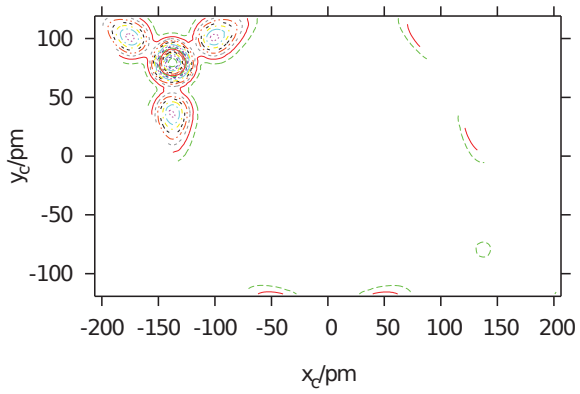

(a) Reduced probability density in $x_c y_c$ plan.

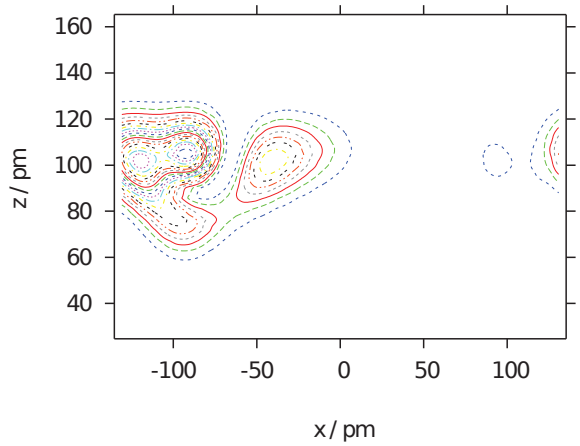

(b) Reduced probability density in xz plan.

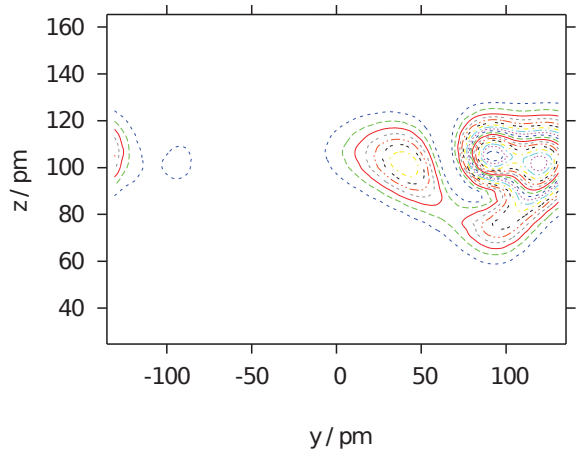

(c) Reduced probability density in yz plan.

Figure 24 – Reduced probability density for the ninth level (1181.6 $hc\,\mathrm{cm}^{-1}$) for D/Pd(111) which can be assigned as $1^1_{\mathrm{B}} + 2^2_{\mathrm{B}}$, its label of symmetry is A_1(see Tab. 9).

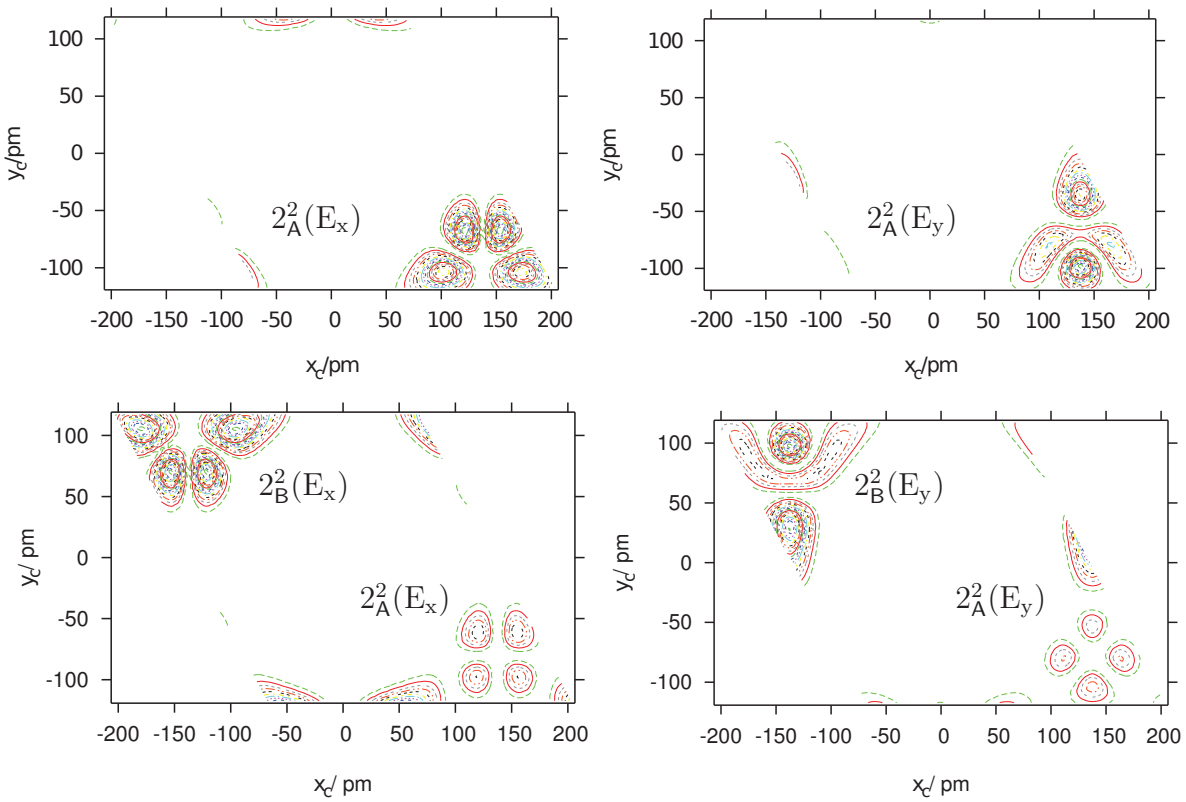

Figure 25 – Reduced probability density for the eighth and tenth levels (1064.9 and 1215.7 $hc\,\mathrm{cm}^{-1}$, respectively) that represent the vibrational parallel modes of D/Pd(111) with 2 quanta of energy. At 1064.9 $hc\,\mathrm{cm}^{-1}$ the mode is localized at the "fcc" site (2^2_A) and at 1215.7 $hc\,\mathrm{cm}^{-1}$ the mode is delocalized on two sites (2^2_A+2^2_B) (see Tab. 9).

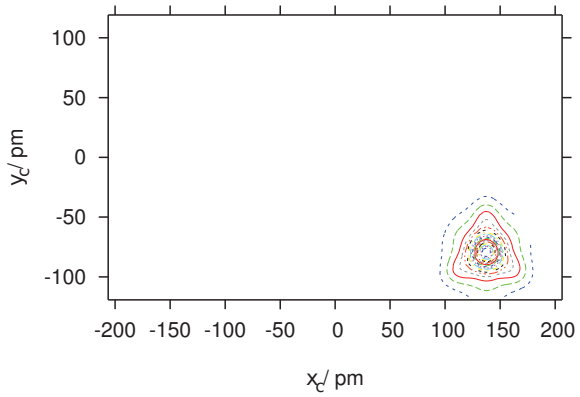

(a) Reduced probability density in $x_c y_c$ plan.

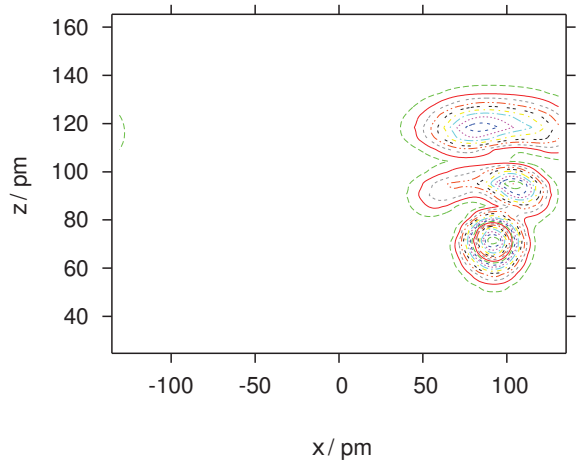

(b) Reduced probability density in xz plan.

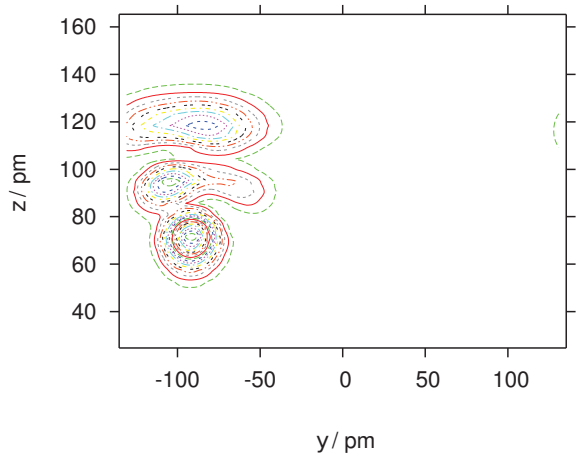

(c) Reduced probability density in yz plan.

Figure 26 – Reduced probability density for the twenty second level (1590.8 $hc\,\mathrm{cm}^{-1}$) for D/Pd(111) which can be assigned as 1^2_{A}, its label of symmetry is A_1(see Tab. 9).

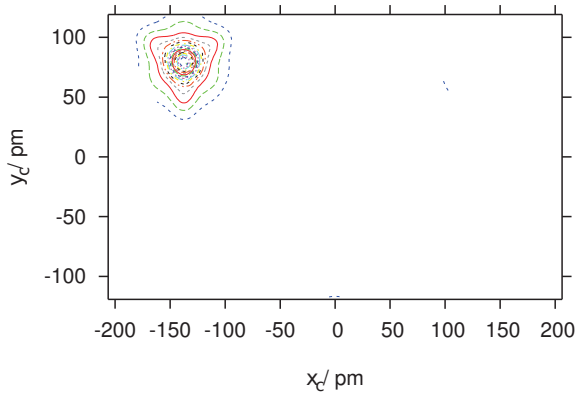

(a) Reduced probability density in $x_c y_c$ plan.

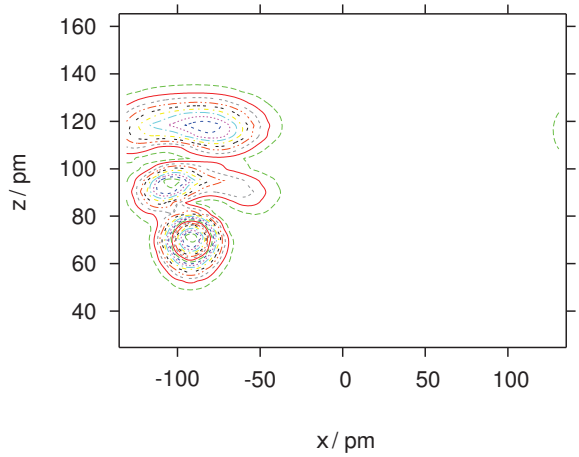

(b) Reduced probability density in xz plan.

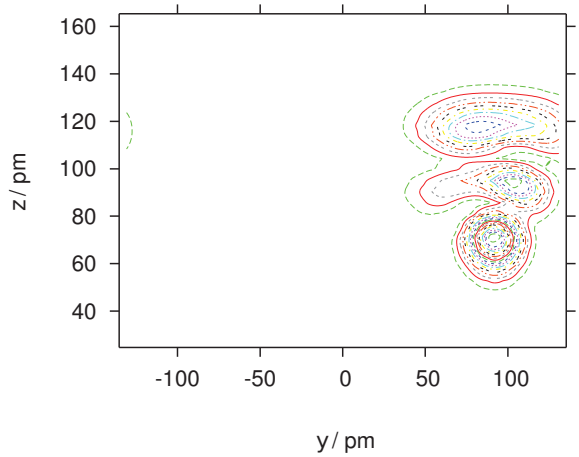

(c) Reduced probability density in yz plan.

Figure 27 – Reduced probability density for the twenty seventh level (1765.3 $hc\,\mathrm{cm}^{-1}$) for D/Pd(111) which can be assigned as 1^1_{B}, its label of symmetry is A_1.

3.1.3 Eigenstates of T on Pd(111)

The reduced probability densities show that the modes are rather localized similar to the findings for the modes of the deuterium atom. The eigenvalues decrease because of the isotope effect. Tab. 10 gives the eigenstates of T/Pd(111). The reduced probability density for the modes of vibration of T/Pd(111) can be found in Appendix G.

Table 10 – Band edges $\tilde{\nu}/\mathrm{cm}^{-1}$, band widths $\Delta\tilde{\nu}/\mathrm{cm}^{-1}$ and band degeneracies g for T/Pd(111).

band	label	modes	grid 1		grid 2	
			band edge	(g)	band width	(g)
1	A_1	0_A	0.0	(1)	0.0	(4)
2	A_1	0_B	187.9	(1)	187.9	(4)
3	E	2^1_A	471.2	(2)	471.2	(8)
4	A_1	$1^1_A + (2^2_A)$	650.4	(1)	650.4	(4)
5	E	2^1_B	660.1	(2)	660.1	(8)
6	A_1	$1^1_B + (2^2_B)$	837.1	(1)	837.1	(4)
7	A_1	$1^1_A + 2^2_A$	873.7	(1)	873.7	(4)
8	E	2^2_A	912.1	(2)	912.1	(8)
9	A_1	$1^1_B + 2^2_B$	1049.9	(1)	0.2	(4)
10	E	$2^2_A + 2^2_B$	1085.7	(2)	3.3	(8)
⋮		⋮	⋮		⋮	
22	A_1	$1^2_A + (2^2_A)$	1311.9	(1)	0.3	(4)
⋮		⋮	⋮		⋮	
29	A_1	$1^2_B + (2^2_B)$	1490.9	(1)	2.9	(4)
⋮		⋮	⋮		⋮	

The eigenvalue for the (2^1_A) mode of H/Pd(111) is 743.6 $hc\,\mathrm{cm}^{-1}$ (Tab. 7), which is about a factor 1.6 larger than the corresponding eigenvalue of the T/Pd(111) system from (Tab. 10), and a factor 1.3 larger that the eigenvalue of the D/Pd(111) system from Tab. 9. Similar ratios apply to the modes involving 1^1_A. These rations are slightly smaller

than the values $\sqrt{3}$ and $\sqrt{2}$ which might be naively expected from harmonic calculations and the classical isotope formula. This discrepancy hints at the strong anharmonicity of the PES.

3.2 Wave packet studies of H, D and T on Pd(111)

This section shows the results of a wave packet propagation using the MCTDH method. Some of the wave packet propagations in this work were calculated using a Gaussian function as an initial state, i.e., the first single particle function is a normalised Gaussian given an initial momentum of the form $f(x) = \mathrm{N}\exp(-\frac{1}{4}(x-x_0)/\sigma)^2)\ \exp(\mathrm{i}\,p\,(x-x_0))$, where x_0 is the center of an initial Gaussian wave packet, p is the initial momentum of the wave packet and σ denotes the width, N is a normalization factor. σ is defined as the standard deviation, i.e., $\sqrt{(\langle x^2\rangle - \langle x\rangle^2)}$ [32]. The Gaussian function is centred in coordinates of the "fcc" site, the width is 0.25 a_0^{-1} and $p = 0\ \hbar/a_0$. Here, x is a generic coordinate that stands for any of the three coordinates of the H-atom.

3.2.1 Propagation of H on grid 1 at $\langle E\rangle \simeq 1518\ hc\,\mathrm{cm}^{-1}$

For the first wave packet propagation, the initial state is localized at the "fcc" site and is essentially non-excited, its energy ($\simeq$ 1518 $hc\,\mathrm{cm}^{-1}$) being roughly the zero point energy, see Fig. 28. This state remains nearly stationary, as shown in the following snapshots. The energy of the wave packet is the quantum mechanical average energy that is obtained from the weighted average over the energies of all eigenstates that participate at its construction.

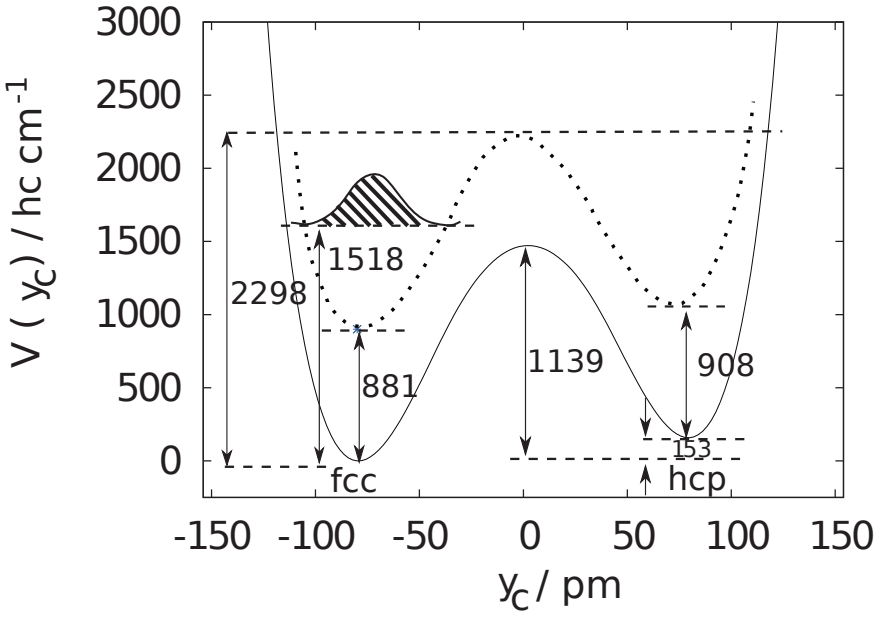

Figure 28 – Schematic representation of the initial wave packet located at the "fcc" site with an energy that equals roughly the zero point energy ($\sim$ 1518 $hc\,\mathrm{cm}^{-1}$). The potential lines are related to the electronic 2D-ZPE adiabatic (dashed) states (see Fig. 8 for an explanation and discussion of the energies).

Fig. 29 shows snapshots of the wave packet evolution for this initial state. The wave packet has sufficient energy ($\simeq$ 1518 $hc\,\mathrm{cm}^{-1}$) to overcome the classical electronic barrier ($\simeq$ 1139 $hc\,\mathrm{cm}^{-1}$). However the wave packet remains localized at the "fcc" site because of the important effective barrier of about 2298 $hc\,\mathrm{cm}^{-1}$ which arises from the variation of the zero point energy along the path linking the two stable sites, see Fig. 28. All energies we refer to, i.e., the energy of the wave packet and characteristic energies of the potential are given with respect to the reference energy at the "fcc" site.

One sees that the wave packet evolves into a breathing motion with some propensity to populate the three channels connecting the initially populated "fcc" site with the next lying "hcp" sites.

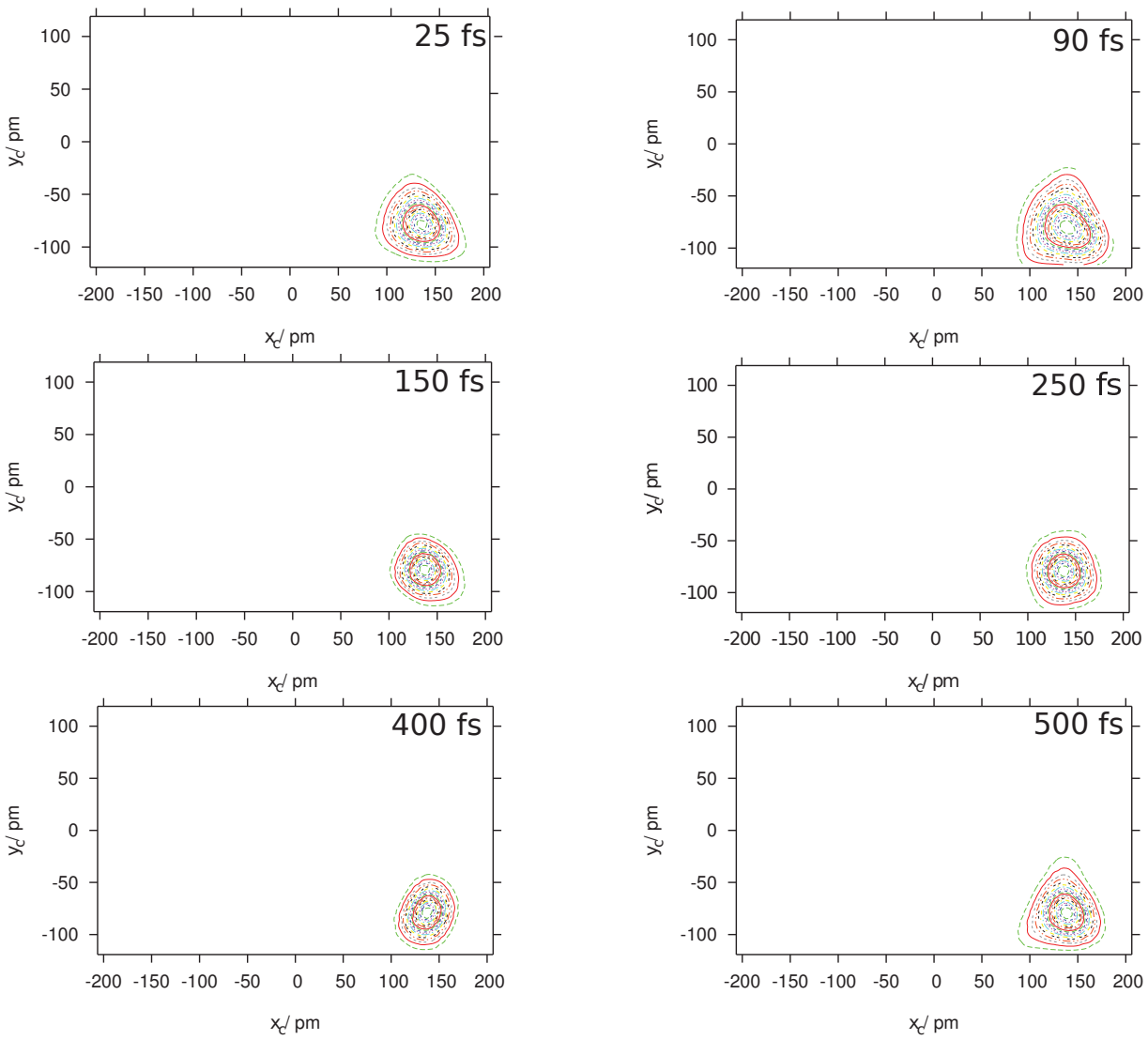

Figure 29 – Snapshots of the wave packet propagation as reduced probability densities in the 2D space of coordinates along the substrate. The initial state is localized at the "fcc" site and is essentially non-excited.

3.2.2 Propagation of H on grid 1 at $\langle E \rangle \simeq 2592\ hc\,\mathrm{cm}^{-1}$

Now, a wave packet propagation was simulated where the perpendicular vibrational mode located at the "fcc" site is initially excited with 1 quantum of energy vibrational perpendicular to the substrate ($\sim 2592\ hc\,\mathrm{cm}^{-1}$), see Fig. 30. In practice, the Gaussian function in the z coordinate is replaced by the eigenfunction $v = 1$ of a harmonic oscillator centered at the "fcc" site and having the harmonic wavenumber 975.5 cm^{-1} (see Tab. 3)

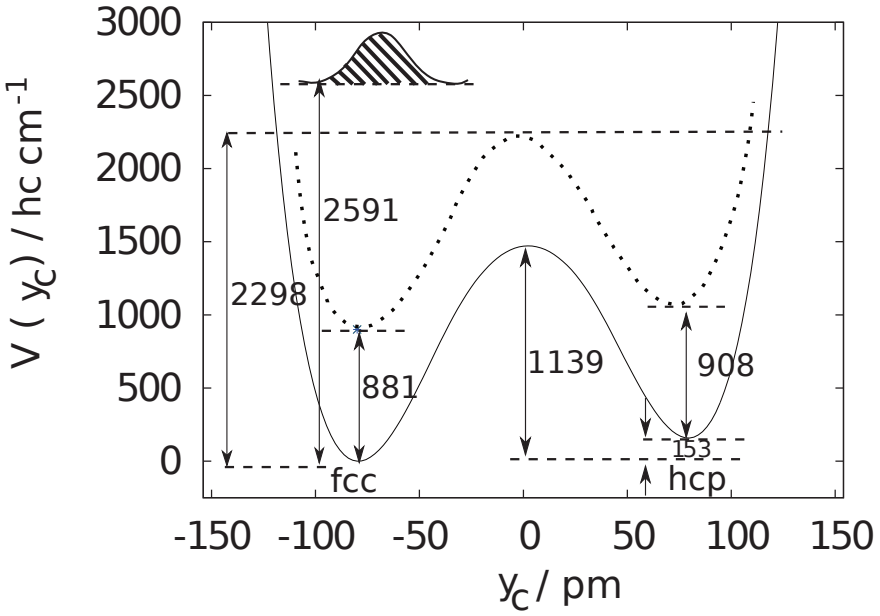

Figure 30 – The centre of the initial wave packet is located at the "fcc" site: the initial state has 1 quantum of energy in the perpendicular vibrational mode ($\simeq 2592\ hc\,\mathrm{cm}^{-1}$).

The initial wave packet is above the effective barrier ($\simeq 2591\ hc\,\mathrm{cm}^{-1}$). It is noted that after 90 fs the hydrogen atom initially located at the "fcc" site starts to move parallelly to the substrate, which corresponds to a lateral diffusion. In fact the initial state contains the perpendicular vibrational mode excited, thus the hydrogen atom should initially be moving perpendicularly to the substrate. The motion shown in Fig. 31 below can not be explained by classical mechanics, because at the same time as the diffusion begins to take place on the "fcc" site, the atom starts to appear on the "hcp" site which is about 200 pm away from the first, Fig. 30. This instant delocalization is characteristic of quantum mechanics, which allows us to say that the spreading of the atom closely follows the rules of this microscopic mechanics. Following this simulation shows that the initial

state is restored partially after two hundred fifty femtoseconds (250 fs) and the diffusion starts over again. This quasi-periodicity of the motion is another feature of the quantum dynamics. The motion would be strictly periodic if it resulted from the superposition of two stationary states only.

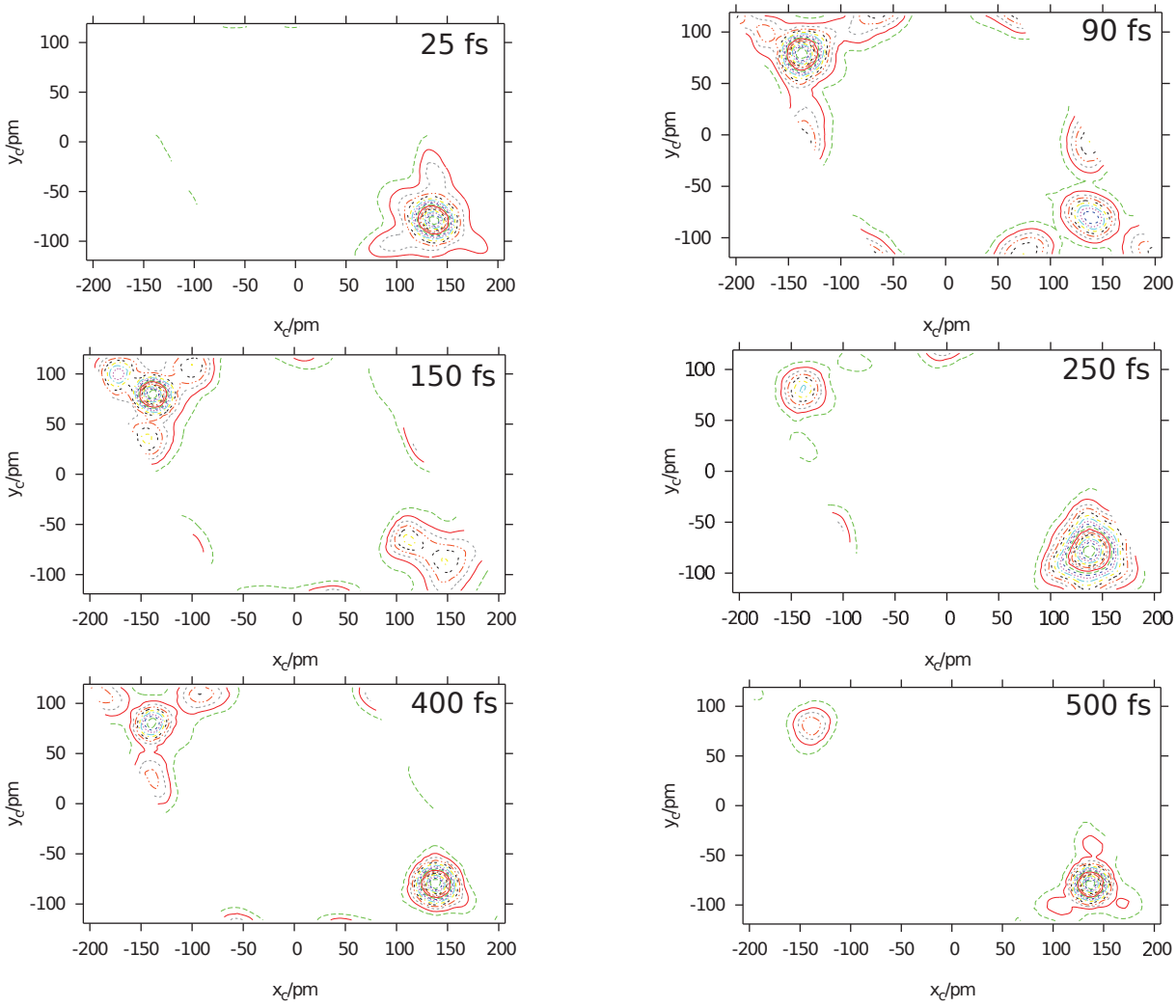

Figure 31 – Snapshots of the wave packet propagation as reduced probability densities in the 2D space of coordinates along the substrate. The hydrogen atom is initially localized at the "fcc" site while its perpendicular mode is excited with 1 quantum of energy ($\simeq$ 2592 $hc\,\mathrm{cm}^{-1}$).

3.2.3 Probabilities of elementary sub-cells for H/Pd(111)

The unit 1×1 cell or grid 1 was divided in 4 sub-cells in the form of small diamonds (see Fig. 9). The probability ($P_i(t)$ with $i = 1, 4$) to find the hydrogen atom in any of these sub-cells as a function of time during the propagation is shown in Fig. 32. Here, one considers the wave packet propagation with 1 quantum of energy in the perpendicular vibrational mode. It is noted that in about 100 fs the probability to find the hydrogen atom in the little diamond 1 (see Fig. (6)) is about 30 %. After 150 fs the probability starts to increase again, showing the recovery of the quasi-periodic motion of this propagation.

On observes at 200 fs that $P_1(t)$ is about 70 %. After 300 fs one observes that $P_1(t)$ decreases again until 400 fs. One observes that in the little diamonds 2 and 4 there is a small probability to find the hydrogen atom, i.e., $P_2(t) \simeq P_4(t) \simeq 10$ %. In the little diamond 3 (see Fig. (6)) is located the "hcp" site and one observes that $P_3(t)$ increases as a function of time. It is noted that in about 100 fs $P_3(t)$ is about 57 %. One observes that $P_3(t)$ decreases again after 200 fs. The quasi-periodic motion of diffusion can be observed again because at 300 fs $P_3(t)$ increases again to decrease again after 400 fs.

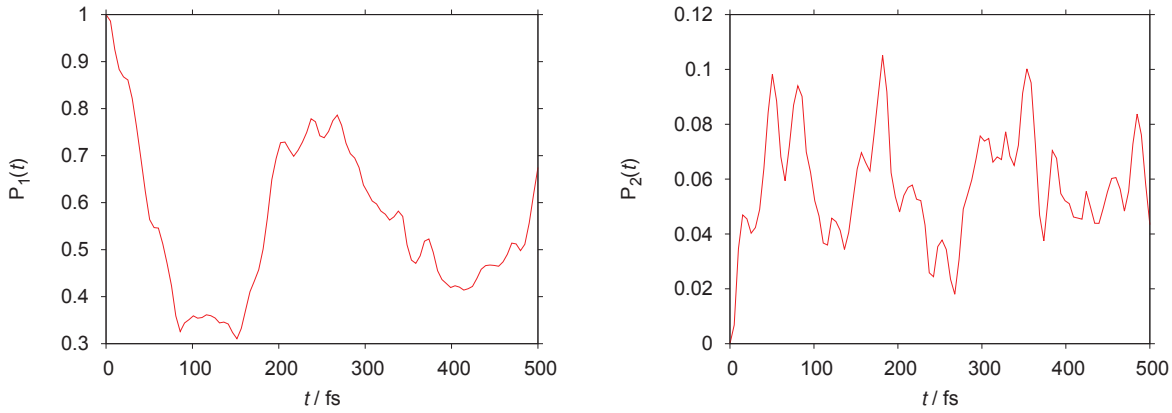

(a) $P_1(t)$ to find the H in little diamond 1.

(b) $P_2(t)$ to find the H in little diamond 2.

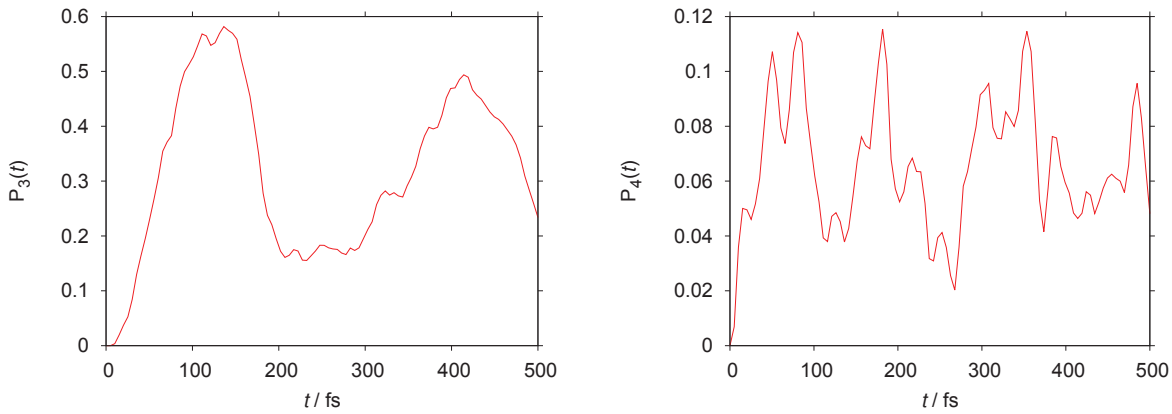

(c) $P_3(t)$ to find the H in little diamond 3.

(d) $P_4(t)$ to find the H in little diamond 4.

Figure 32 – Probability to find the H-atom in each of the elementary sub-cells, also called here little diamonds, during the propagation.

3.2.4 Propagation of H on grid 1 at $\langle E \rangle \simeq 3655\ hc\,\mathrm{cm}^{-1}$

Here a wave packet propagation is simulated where the perpendicular vibrational mode located initially at the "fcc" site is excited with 2 quanta of energy ($\simeq 3655\ hc\,\mathrm{cm}^{-1}$), i.e., well above of effective barrier, see the Fig. 33. Similarly to the study in the section 3.2.2, the initial Gaussian function in the z coordinate is replaced by the eigenfunction $\nu = 2$ of a harmonic oscillator centered at the "fcc" site and having the wave number 975.5 cm^{-1} (see Tab. 3)

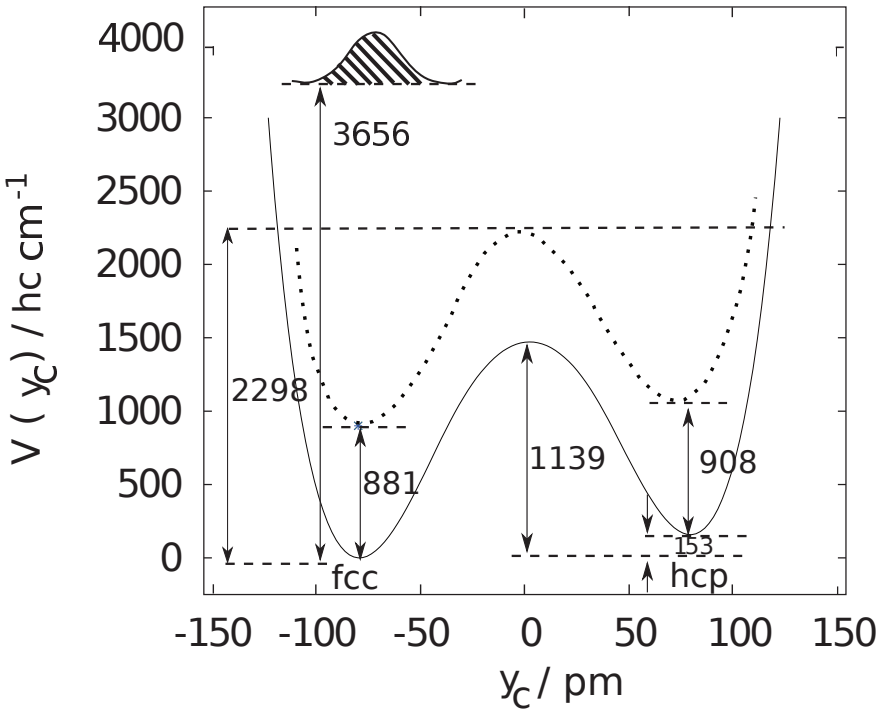

Figure 33 – The centre of the initial wave packet is located at the "fcc" site with 2 quanta of energy in the perpendicular vibrational mode ($\simeq 3655\ hc\,\mathrm{cm}^{-1}$).

It is noted that the lateral diffusion happens very quickly (see Fig. 34). After 25 fs, for example, the "hcp" site is already populated. One observes an important spreading at the "fcc" site. After 90 fs the initial state is restored, showing that this motion is again quasi-periodic. The general form of the evolving wave packet is somewhat more complicated than that of the wave packet shown in section 3.2.2, i.e., where the initial state involved just 1 quantum of perpendicular vibrational motion.

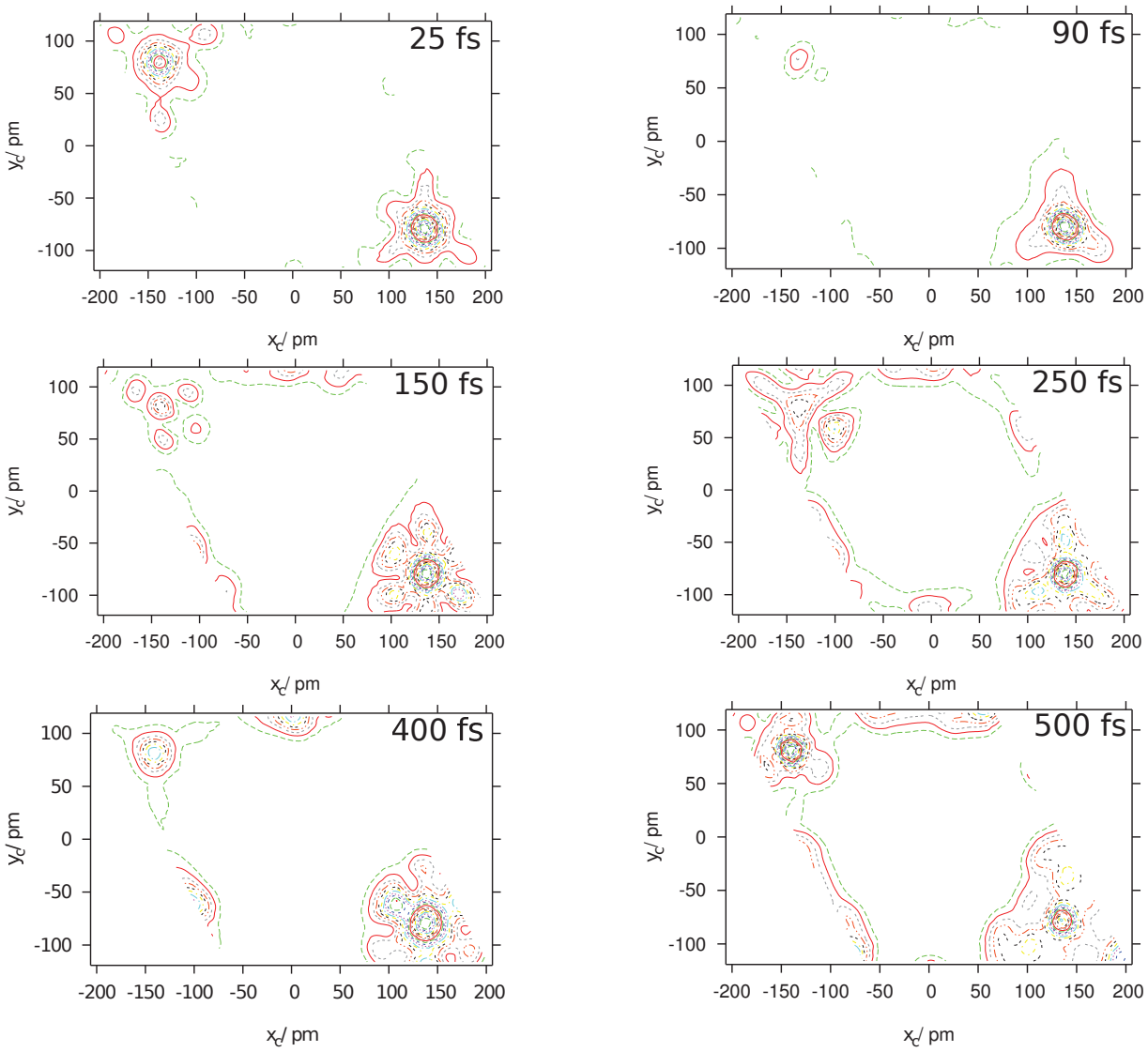

Figure 34 – Snapshots of the wave packet propagation as reduced probability densities in the 2D space of coordinates along the substrate. The perpendicular vibrational mode is initially localized at the "fcc" site and is excited with 2 quanta of energy ($\simeq 3655\ hc\,\mathrm{cm}^{-1}$).

3.2.5 Propagation of H on grid 2 at $\langle E \rangle \simeq 2586\ hc\,\mathrm{cm}^{-1}$

A propagation with 1 quantum of perpendicular vibrational energy ($\simeq 2586\ hc\,\mathrm{cm}^{-1}$) was calculated for grid 2 (see Fig. 10a) which is a (2×2) surface cell grid. One observes that initially the H-atom located at the "fcc" site starts to spread to the 3 closest lying "hcp" sites (see Fig. 35). After 90 fs one observes a local spreading at the "fcc" site while considerably populating the bridge saddle points between the "fcc" and "hcp" sites,

and simultaneously the 3 "hcp" sites become populated. After 150 fs the "fcc" site is almost completely recovered, quite at variance with the previously reported evolution on grid 1 (section 3.2.2), where the recovery happens after about 250 fs, only. After 250 fs one observes that all sites are populated (see Fig.10a) but the initially populated "fcc" site remains the most populated, followed by its nearest "hcp" sites, which, in turn, are followed by their next closest "fcc" sites, and so forth. After 500 fs one observes that the 4 "fcc" sites are more populated that the "hcp" sites. The sequence of snapshots show, however, that their occupation follows the previous occupation of "hcp" sites. Hence, the wave packet motion reminds us of some features of a classical jump mechanism.

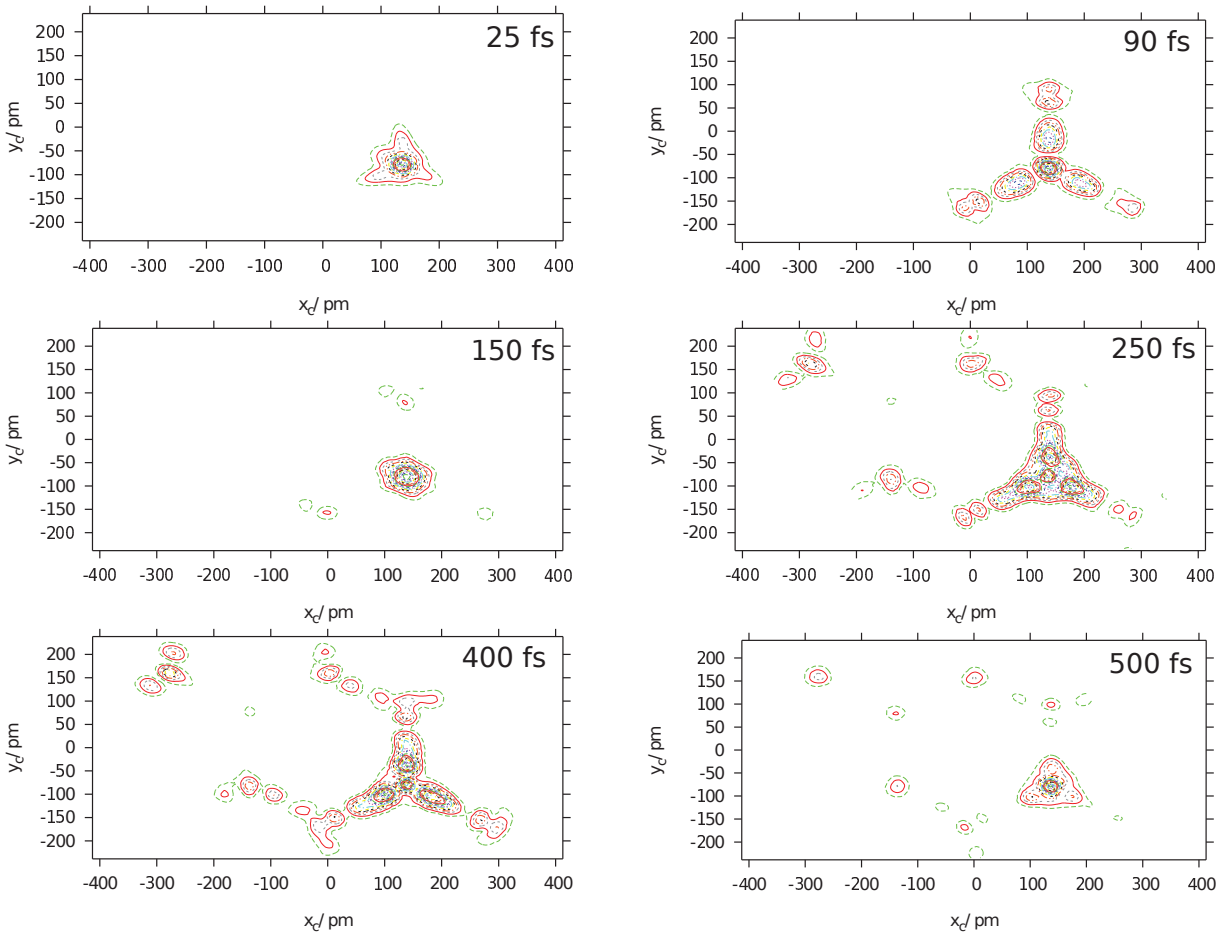

Figure 35 – Snapshots of the wave packet propagation in the (2 × 2) surface cell (grid 2) as reduced probability densities in the 2D space of coordinates along the substrate. The perpendicular vibrational mode is initially excited with 1 quantum of energy ($\simeq$ 2586 $hc\,\mathrm{cm}^{-1}$).

3.2.6 Propagation of H on grid 3 at $\langle E \rangle \simeq 2586\ hc\,\mathrm{cm}^{-1}$

A propagation with 1 quantum of perpendicular vibrational energy ($\simeq 2586\ hc\,\mathrm{cm}^{-1}$) was calculated for the grid 3 (see Fig. 10b), i.e., a (3×3) surface cell grid. Fig. 36, after 90 fs, shows that the 3 "hcp" sites are already populated. After 150 fs, the 3 "hcp" sites are less populated and the initial state is recovered. After 400 fs one observes that the 6 "fcc" sites adjacent to 3 "hcp" sites start to become populated. After 500 fs these sites are less populated and the initial state is recovered.

The motion of the wave packet still has the characteristic quasi-periodic breathing pattern. The adsorbate moves diffusively from the initially populated site to its nearest stable "hcp" sites via the three classically most advantageous channels. However, because of the stronger dilution of adsorbates in grid 3, the number of intermediately unpopulated sites increases and other "fcc" sites, which were importantly populated during the motion on grid 2, remain unpopulated during the evolution on grid 3 at similar initial conditions. One sees that the dilution of the adsorbate makes it stay closer to the initially populated site for longer times.

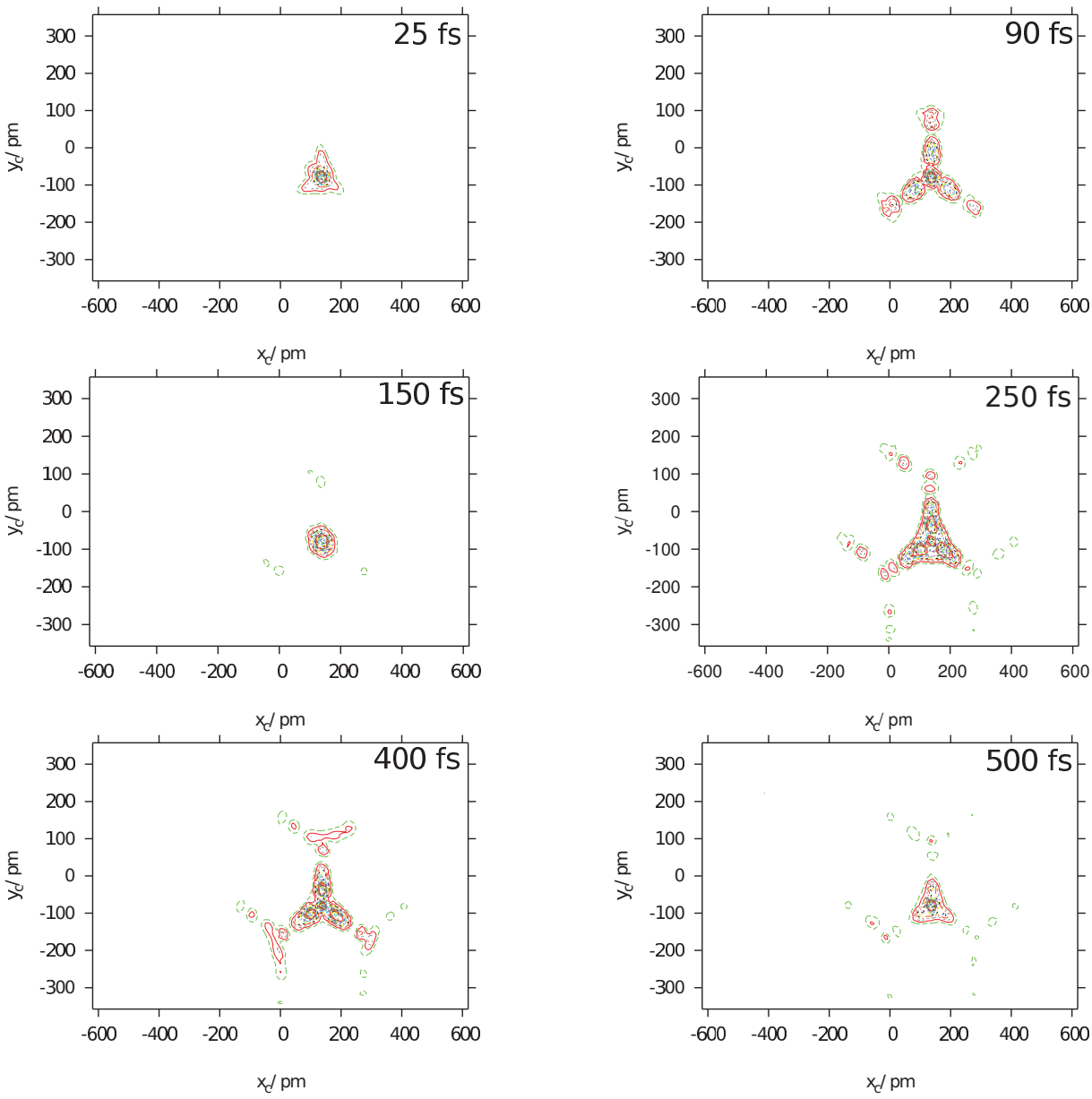

Figure 36 – Snapshots of the wave packet propagation in the (3×3) surface cell (grid 3) as reduced probability densities in the 2D space of coordinates along the substrate. The perpendicular vibrational mode is initially excited with 1 quantum of energy ($\simeq$ 2586 $hc\,\mathrm{cm}^{-1}$) at the "fcc" site.

3.2.7 Propagation of D on grid 1 at $\langle E \rangle \simeq 1801\ hc\,\mathrm{cm}^{-1}$.

Here, the wave packet propagation for the deuterium atom on grid 1 is simulated. Fig. 37 shows a simulation where the perpendicular vibration located at the "fcc" site is excited with 1 quantum of energy ($\simeq 1801\ hc\,\mathrm{cm}^{-1}$). The effective barrier for the D/Pd(111) is $1959\ hc\,\mathrm{cm}^{-1}$, i.e., about $340\ hc\,\mathrm{cm}^{-1}$ smaller than the effective barrier for the H/Pd(111) ($2298\ hc\,\mathrm{cm}^{-1}$, all values given in the harmonic approximation in Tabs. 4 and 2).

Here, too, the effective barrier is significantly larger than the electronic barrier ($\simeq 1139\ hc\,\mathrm{cm}^{-1}$) and the lateral diffusion happens slowly. After 250 fs a small lateral diffusion to the "hcp" site can be observed, the "hcp" site is sparsely populated. One observes that after 500 fs the deuterium atom is found completely in the "fcc" site, performing again a quasi-periodic motion for this lateral diffusion.

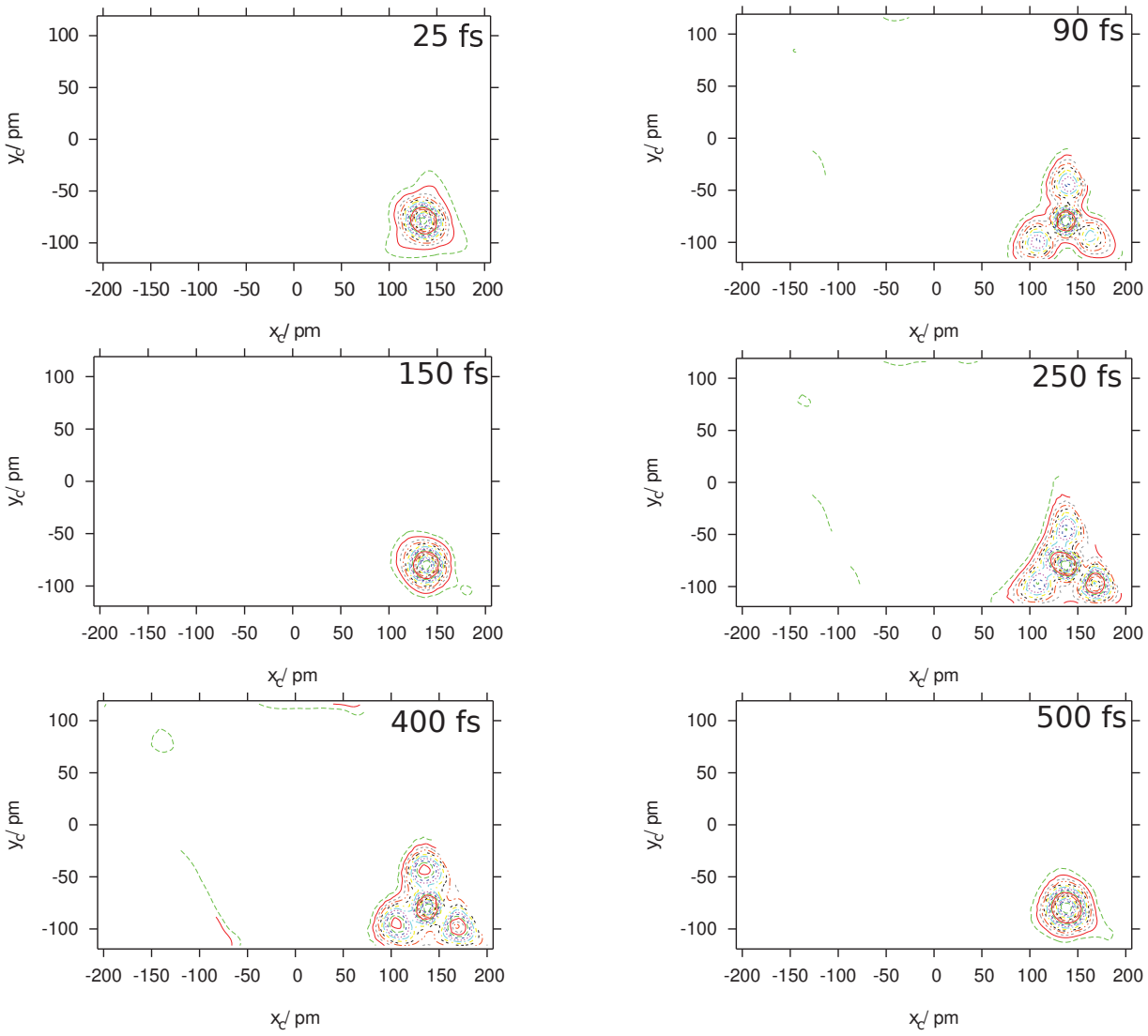

Figure 37 – Snapshots of the wave packet propagation for D/Pd(111) as reduced probability densities in the 2D space of coordinates along the substrate. The perpendicular vibrational mode is initially excited locally at the "fcc" site with 1 quantum of energy ($\simeq 1801\ hc\,\mathrm{cm}^{-1}$).

3.2.8 Propagation of D on grid 1 at $\langle E \rangle \simeq 2560\ hc\,\mathrm{cm}^{-1}$.

Exciting the perpendicular vibrational mode with 2 quanta of energy ($\simeq 2560\ hc\,\mathrm{cm}^{-1}$), locally at the "fcc" site, yelds an initial wave packet that lies energetically above the effective barrier ($\simeq 1959\ hc\,\mathrm{cm}^{-1}$). Subsequently, one notices a fast lateral diffusion (Fig. 38). Readily after 90 fs the "hcp" site becomes clearly populated.

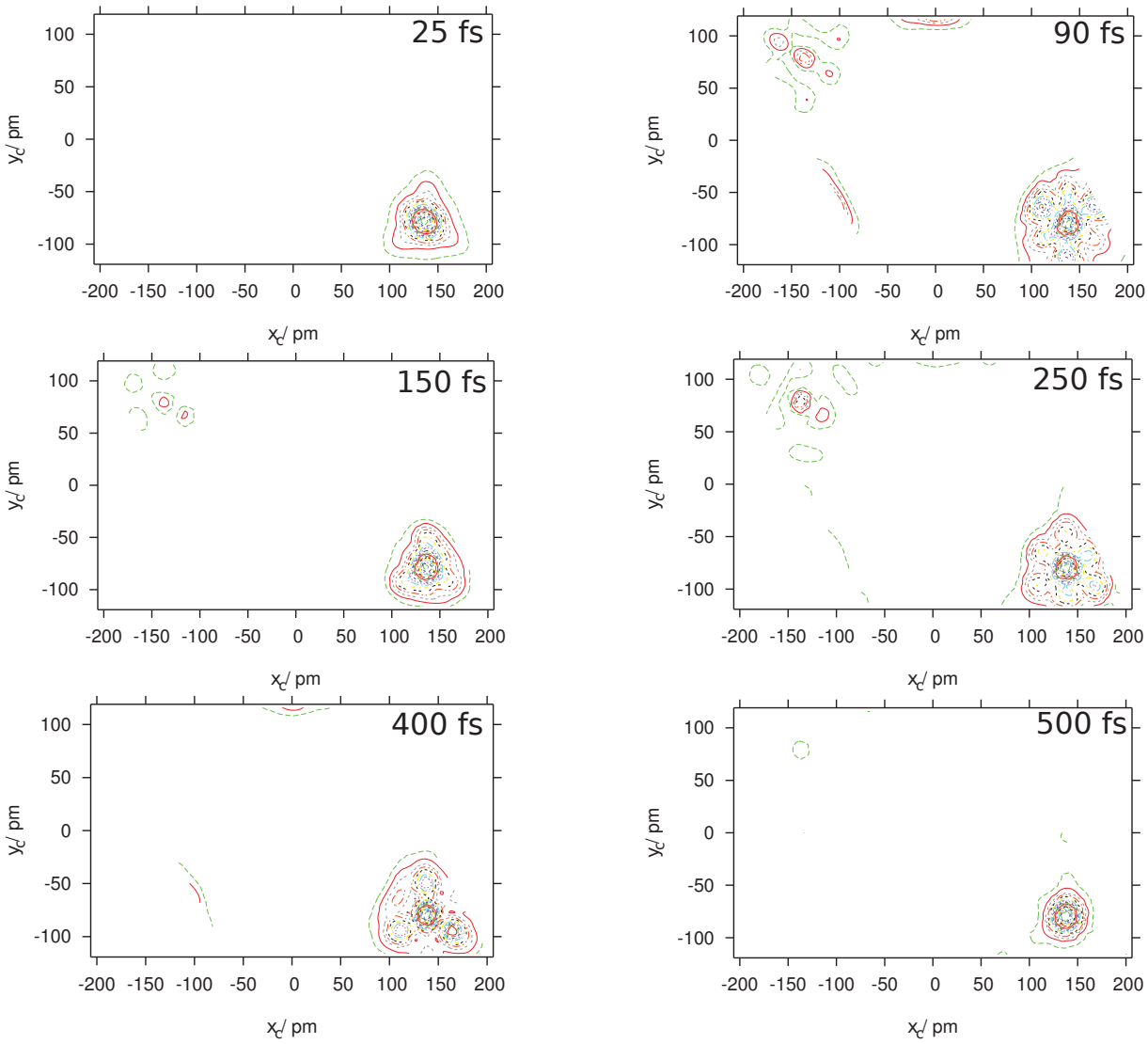

Figure 38 – Snapshots of the wave packet propagation for D/Pd(111) as reduced probability densities in the 2D space of coordinates along the substrate. The perpendicular vibrational mode is excited with 2 quanta of energy ($\simeq 2560\ hc\,\mathrm{cm}^{-1}$).

3.2.9 Probabilities of elementary sub-cells for D/Pd(111)

As in case of H/Pd(111), we calculated the probability to find the deuterium atom in the "little diamonds" defined by the sub-cells of the (1×1) surface cell (see Fig. 9). For this calculation the wave packet was propagated from an initial state where the perpendicular vibrational mode is excited locally at the "fcc" site with 2 quanta of energy ($\simeq 2560\ hc\,\mathrm{cm}^{-1}$). Fig. 39 shows $\mathrm{P}_i(t)$ with $i = 1 - 4$ to find the deuterium atom in the respective sub-cell during the propagation. $\mathrm{P}_2(t) \simeq \mathrm{P}_4(t)$, i.e., the probability to find the deuterium atom in the "little diamonds" 2 and 4 (see Fig. (6)) is very small because the adsorption on the "top" site is not stable. $\mathrm{P}_1(t)$ decreases by ~ 25 % after 200 fs because of the lateral diffusion from the "fcc" site to the "hcp" site. Correspondingly $\mathrm{P}_3(t)$ increases by $\sim$ 25 %. It is noted that the lateral diffusion is quasi-periodic because after 200 fs $\mathrm{P}_1(t)$ increases and $\mathrm{P}_3(t)$) decreases. After 400 fs $\mathrm{P}_1(t)$ decreases and $\mathrm{P}_3(t)$ increases.

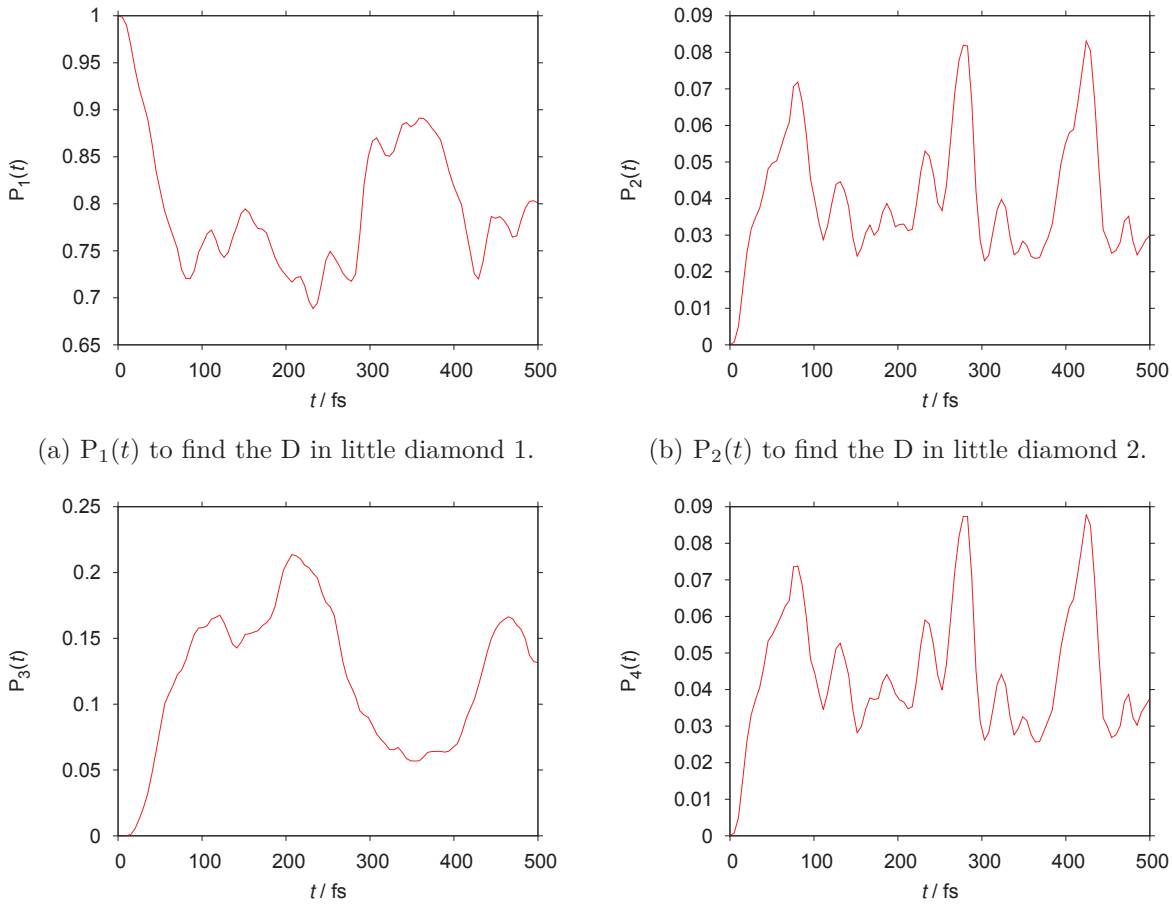

(a) $\mathrm{P}_1(t)$ to find the D in little diamond 1.

(b) $\mathrm{P}_2(t)$ to find the D in little diamond 2.

(c) $\mathrm{P}_3(t)$ to find the D in little diamond 3.

(d) $\mathrm{P}_4(t)$ to find the D in little diamond 4.

Figure 39 – Probability to find the D in each little diamonds during the propagation.

3.2.10 Propagation of T on grid 1 at $\langle E \rangle \simeq 1485\ hc\,\mathrm{cm}^{-1}$.

Similarly, the wave packet propagation for the tritium atom was simulated on grid 1. Fig. 40 shows the wave packet propagation for an initial excitation by 1 quantum of energy in the perpendicular vibration located at the "fcc" site ($\simeq 1485\ hc\,\mathrm{cm}^{-1}$). The effective barrier for T/Pd(111) is 1809 $hc\,\mathrm{cm}^{-1}$, i.e., about 475 $hc\,\mathrm{cm}^{-1}$ smaller than the effective barrier for the H/Pd(111) system. No remarkable lateral diffusion can be observed in the first 500 fs of propagation. One observes nevertheless a feeble breathing motion of the wave packet located at the "fcc" site during the propagation. The breathing extends preferentially along the 3 diffusion channels linking the "fcc" with its neighbouring "hcp" sites.

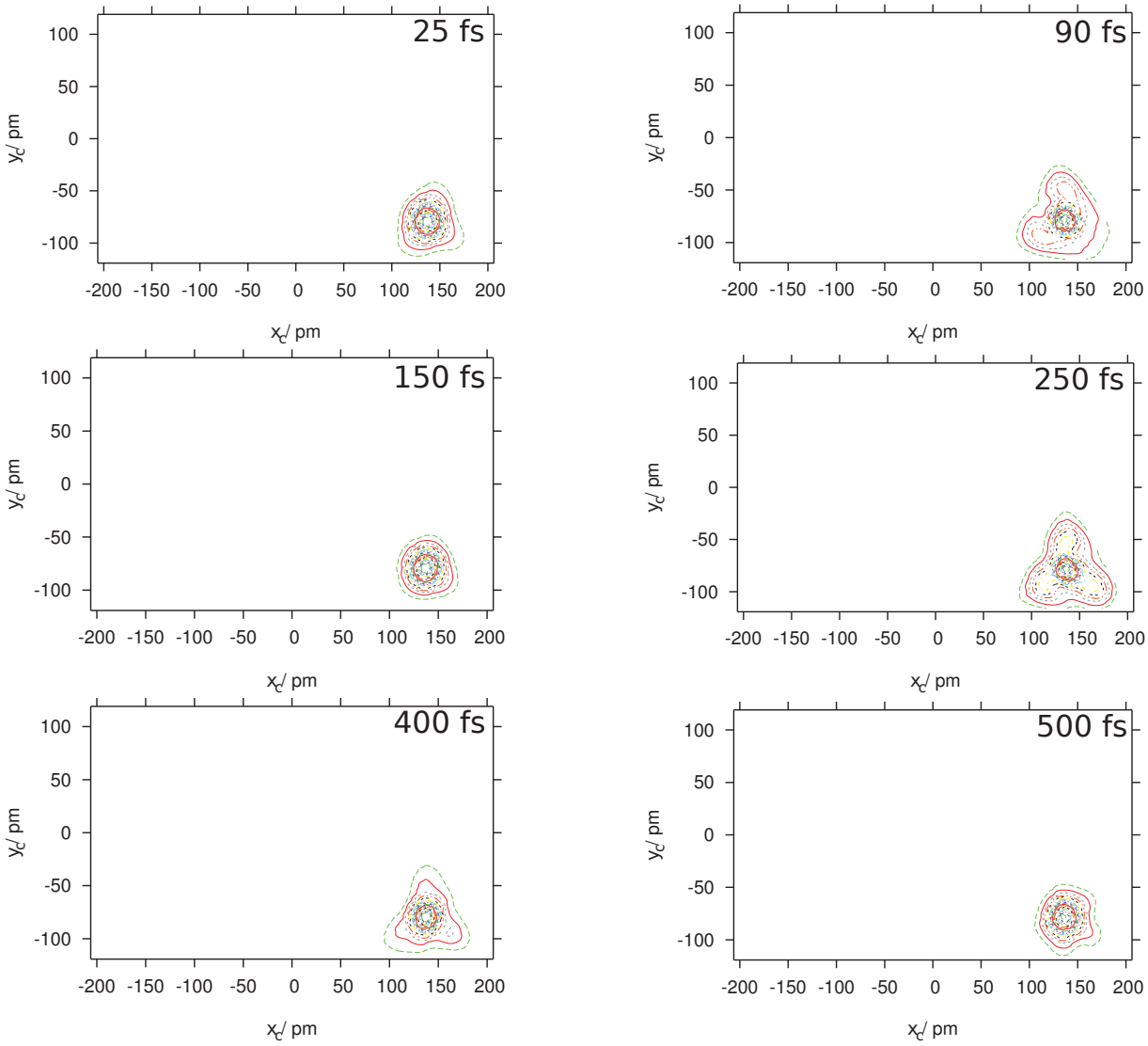

Figure 40 – Snapshots of the wave packet propagation for T/Pd(111) as reduced probability densities in the 2D space of coordinates along the substrate. The perpendicular vibrational mode is initially excited with 1 quantum of energy ($\simeq 1485\ hc\,\mathrm{cm}^{-1}$ above the reference energy at the "fcc" site).

3.2.11 Propagation of T on grid 1 at $\langle E \rangle \simeq 2108\ hc\,\mathrm{cm}^{-1}$.

Upon excitation of the perpendicular vibration localized at the "fcc" site with 2 quanta of energy ($\simeq 2108\ hc\,\mathrm{cm}^{-1}$), i.e. an energy above the effective energy ($\simeq 1809\ hc\,\mathrm{cm}^{-1}$) one observes a very small lateral diffusion. One possible explanation is that the effective barrier for this isotope is still too important for it to perform easily a lateral diffusion. A different explanation is that the eigenstates in the energy range studied here are rather pure states localized at the "fcc" and "hcp" sites. The Fermi resonance mechanism, which was found to be the driving motor of the diffusion process for the H/Pd(111) and, to some extent, also for the D/Pd(111) system, is lacking in the case of the T/Pd(111) system.

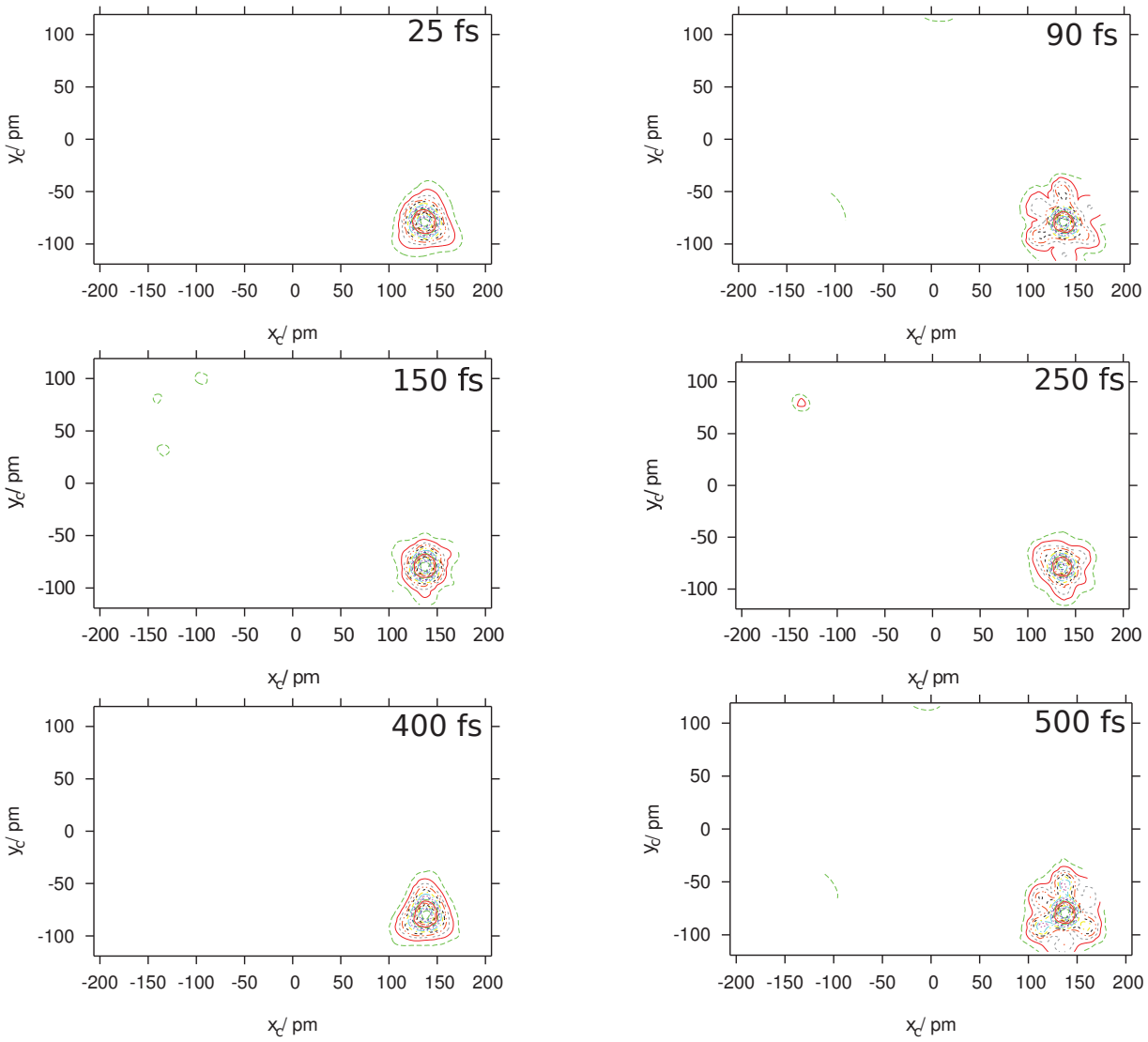

Figure 41 – Snapshots of the wave packet propagation for T/Pd(111) as reduced probability densities in the 2D space of coordinates along the substrate. The perpendicular vibrational mode is initially excited with 2 quanta of energy ($\simeq 2108\ hc\,\mathrm{cm}^{-1}$).

3.3 Thermal wave packet propagation for on grid 1

In this section, a model wave packet evolution is investigated, in which the initial wave packet mimics a thermalized state localized in one stable adsorption site. The model "system" is hence a set of states localized at the "fcc" site, while the "environment" is the set of states that are distributed elsewhere. As the model grid considered here is a (1×1) surface cell grid, the environment is essentially defined by states localized at the "hcp" site.

A thermalized state can be constructed as in section 1.9. In the present model, the eigenfunctions used in Eq. (41) are generated approximately by short time relaxations starting from states that are localized at the "fcc" site. Only four different initial states are considered: three states have each one quantum of vibrational mode along the x, y and z coordinates, respectively; the forth state is the non excited ground state at the "fcc" site. The short time relaxation generates the four states that correspond to a localized ground state and to three localized states with each having nearly one quantum of vibrational excitation. Up to room temperature, higher lying states are expected to have very small populations and are therefore neglected, in this model. Technically, the superposition of the thus obtained functions, which are stored in the restart files, is calculated with the *sumrst* routine of the MCTDH package. The superposition coefficients by which each function is multiplied were generated via the routines for the calculation of Boltzmann weights (Appendix A) and random phases (Appendix B). The energies 0, 744 (2 times) and 1048 $hc\,\mathrm{cm}^{-1}$ were used for the coefficients of theses 4 states.

Fig. 43 shows snapshots of the thermal wave packet evolution at 300 K. After 250 fs the "hcp" site is already populated, showing that a lateral diffusion of hydrogen atoms on Pd(111) might take place at 300 K. Fig. 42 shows the probability ($\mathrm{P}_i(t)$ with $i = 1, 4$) to find the hydrogen atom in the sub-cells defined in Fig. 9 during the propagation. One notes in Fig. 42a a decrease of 8% in the sub-cell where the hydrogen is initially localized , i.e. in the sub-cell defining the "system". That of the "hcp" site increases by 4% (Fig. 42c). Figs. 42b and 42d show that the populations of the remaining sub-cells increase correspondingly.

The global time evolution indicated in these figures suggests that an equilibrium between "system" and "environment" is readily established after about 200 to 300 fs of evolution. The mean asymptotic populations are approximately 92% for the system, and 8% for the environment. The later can be decomposed into 4% for the sub-cell containing the "hcp" site, and $2 \times 2\%$ for those sub-cells containing essentially "top" sites. This result is unexpected, as the thermal population ratio of the ground states at the "hcp" and "fcc" sites is about $\exp(-153/(3/2 \times 300)) \approx 0.47$ at 300 K (see Tab. 1), whereas the present simulation yields a ratio of $4/92 \approx 0.04$. We should therefore conclude that thermalization is far from complete after 10 ps of evolution. Indeed, from the value for the diffusion rate calculated for the same system from a quantum transition state theory in [53], i.e. $D \approx 10^{-5.5}$ cm^2/s at 300 K, we estimate a life time $\tau = \gamma l^2/(2 \times 2 \times D) \approx 9.5$ ps for the population of sub-cell 1; $l = 2h = d/\sqrt{3}$ (see Figs. 4 and 6b), $d \approx 275$ pm is the $\mathrm{Pd} - \mathrm{Pd}$ distance and $\gamma = 3$ is the number of paths linking adjacent sites.

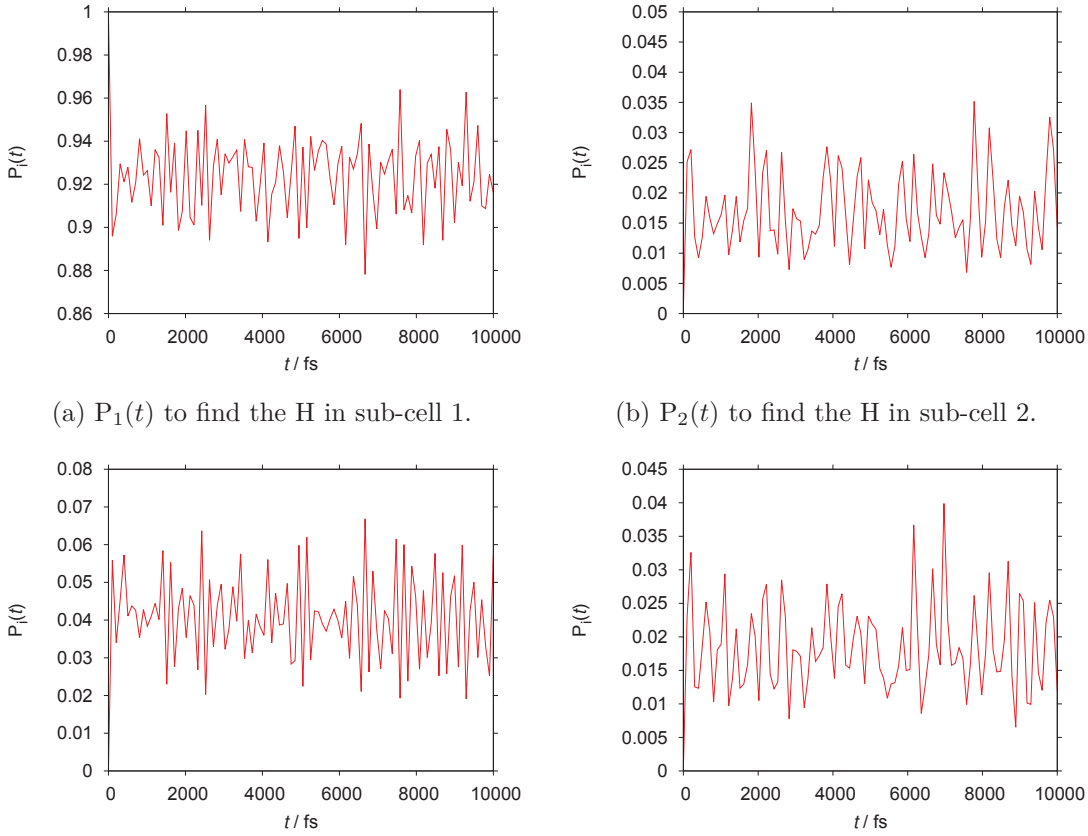

(a) $\mathrm{P}_1(t)$ to find the H in sub-cell 1.

(b) $\mathrm{P}_2(t)$ to find the H in sub-cell 2.

(c) $\mathrm{P}_3(t)$ to find the H in sub-cell 3.

(d) $\mathrm{P}_4(t)$ to find the H in sub-cell 4.

Figure 42 – Probability to find the H in sub-cells defined in Fig. 9. The initial wave packet corresponds to that used in Fig. 43.

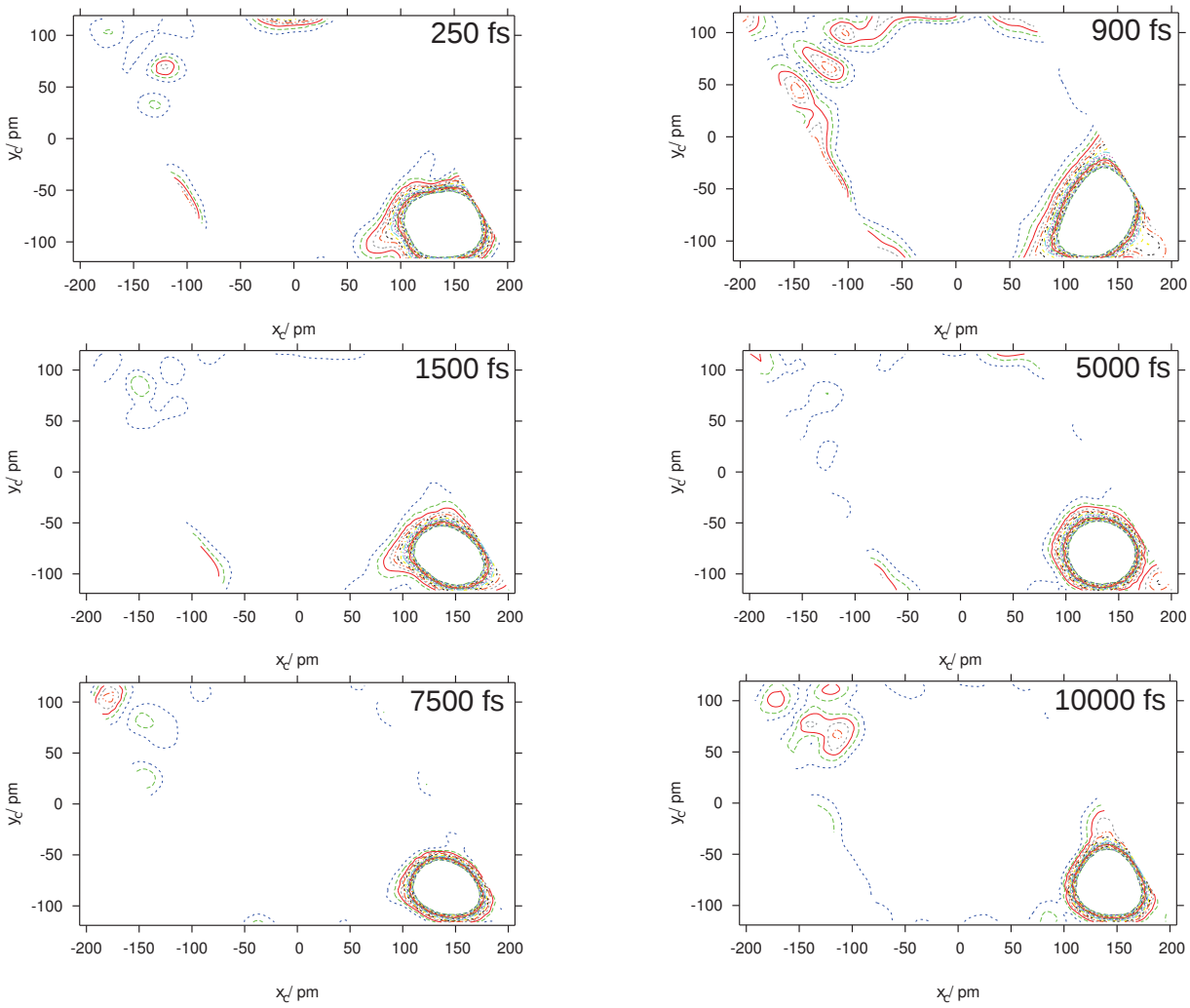

Figure 43 – Snapshots of the wave packet propagation as reduced probability densities in the 2D space of the x_c and y_c coordinates along the substrate. The initial state is a locally thermalized state at the "fcc" site (see text).

Chapter 4

Stationary states of H_2/Pd(111)

4.1 Analysis of the PES for H_2/Pd(111)

The potential energy surface for H_2/Pd(111) is obtained by setting nH = 2 in the REBO subroutine (see section 2.2 and Appendix C). As for H/Pd(111), and, before calculations using the MCTDH code are performed, we tested the PES by reproducing some results that have already been published [1, 12] in order to understand and to ensure the proper implementation of this code. Results will be shown for the routines based on the two units cells, 3 $\times$ 3 and 10 $\times$ 10. Each unit cell has 5 layers, thus the units cells have 45 and 500 atoms of Pd, respectively.

The coordinate system for the interaction of the hydrogen molecule with the surface in six dimensions can be represented by polar coordinates for the internal degrees of freedom and Cartesian coordinates for the center-of-mass motion. See also Figure 44, where x and y are the coordinates for the center-of-mass motion parallel to the substrate, the "frustrated translation", z is the distance from of molecular center to the surface, r is the bond length of H_2, θ is the polar and ϕ the azimuthal angle of orientation of the molecular axis.

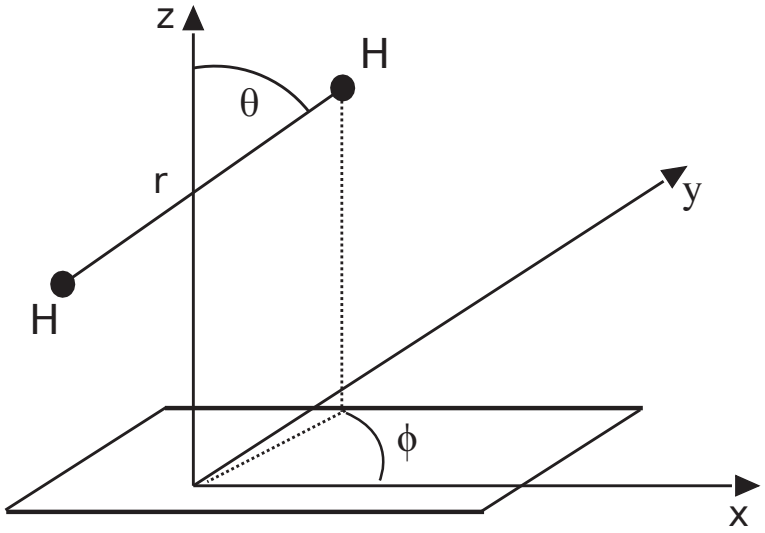

Figure 44 – Coordinate system for dissociation of H_2 on a surface. In the scheme, $x, y,$ and z are the center-of-mass coordinates of H_2, r is the $H-H$ distance, θ is the polar angle of the molecular axis with the z-axis and ϕ is the azimuthal angle.

The following results of PES of H_2/Pd(111) were obtained for the units cells 10×10.

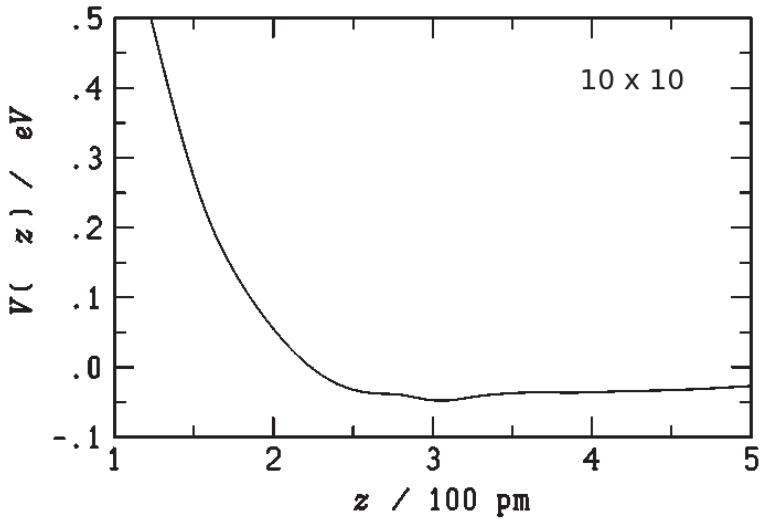

(a) Unit cell 10 × 10.

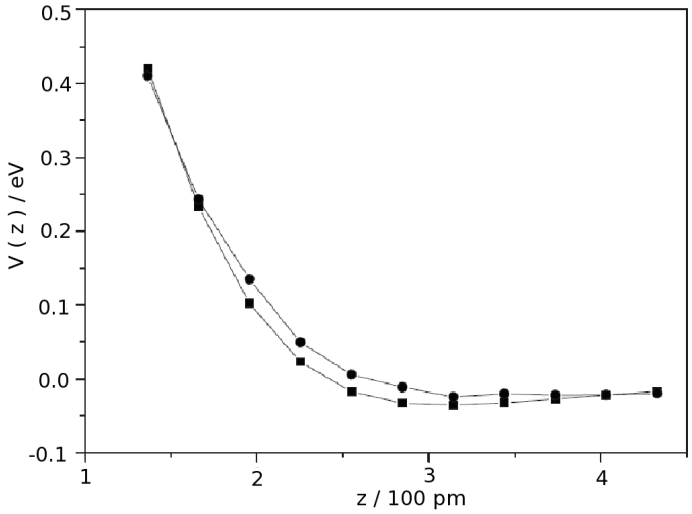

(b) Figure adapted from ref. [1].

Figure 45 – Variation of the potential energy as a function of the distance of H_2 to the surface. The bond length of H_2 is 75 pm and the molecular center is perpendicular to the surface on the so-called "fcc-fcc" site (see text). (a) is the evaluation of the REBO routine along the same section as figure 5 that used in ref. [1], which is reproduced here in (b) (● REBO points and ■ original DFT points) with $x = 279$ pm, $y = 161$ pm, $r = 75$ pm, $\theta = 0^0$ and $\phi = 0^0$. The number of points calculated in the range $1 \leq z/\text{Å} \leq 5$ is 101.

The figure from the original work can be fairly well reproduced by the present evaluation. Our results, obtained by a finer interpolation of the REBO points, indicate that there is some corrugation for both units cells. This corrugation is not visible in the figure 5 of the original article which is a more coarse grained representation of the REBO points.

The figures bellow show the variation of the potential energy as a function of the bond length of H_2 when the molecular axis of H_2 is parallel to the surface on a so-called "fcc-fcc" site for the two units cells. The "fcc-fcc" means that one atom is located on one fcc site, the other atom is located on a next lying fcc site.

It is noted that the PES of H_2/Pd(111) calculated at $z = 250$ pm for the two units cells are slightly different from the one published in [1]. One notes that there is a hump near 200 pm, which is not visible in [1] (figure 46c). In the latter, the number of points at which the potential has been evaluated is smaller than the assessments made in this report. This hump is artificial and may be eliminated for example by reducing the number of evaluations around 200 pm.

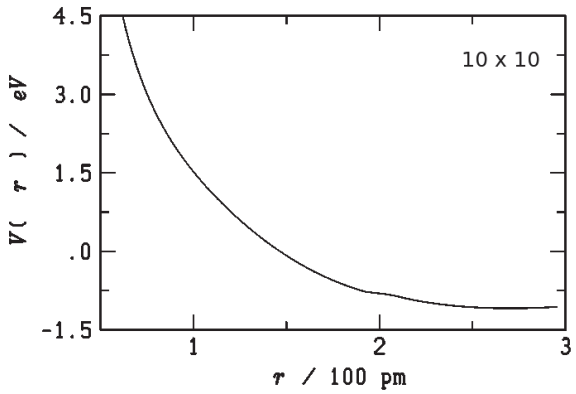

(a) Cut in r when z is 100 pm in unit cell 10 $\times$ 10.

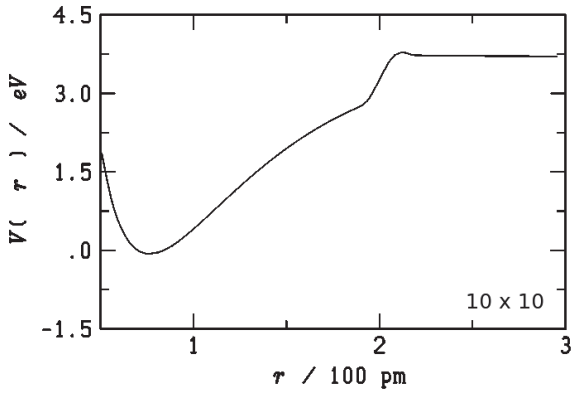

(b) Cut in r when z is 250 pm in unit cell 10 $\times$ 10.

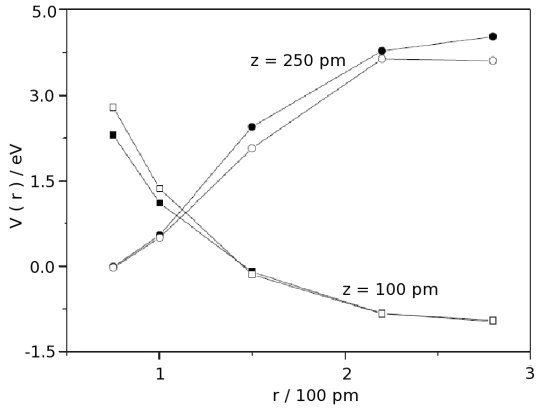

(c) Figure adapted from article [1].

Figure 46 – Variation of the potential energy as a function of r when the molecular axis is parallel to the surface on the "fcc-fcc" site. The figure (c) is adapted from ref. [1].

The Figs. 47a and 47b show the same cuts shown in Fig. 46 but for a larger range in r. Now we can note the periodicity of the unit cell 10 $\times$ 10 along the coordinate r till 1500 pm on the "fcc-fcc" site, with $x = 139$ pm, $y = 161$ pm, $\theta = 90^0$ and $\phi = 0^0$.

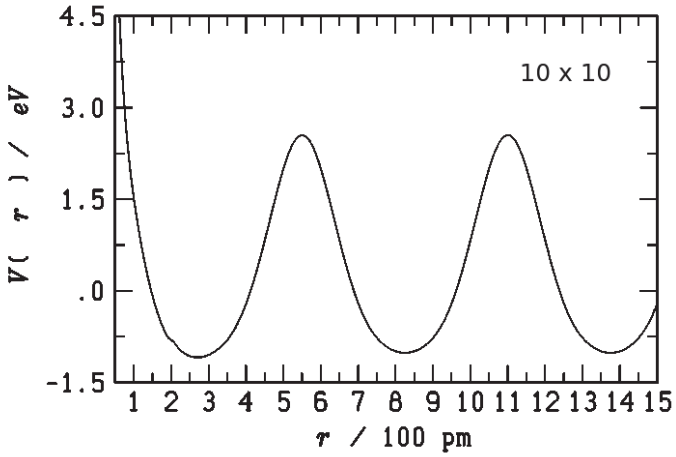

(a) Cut in r when z is 100 pm in unit cell 10 $\times$ 10.

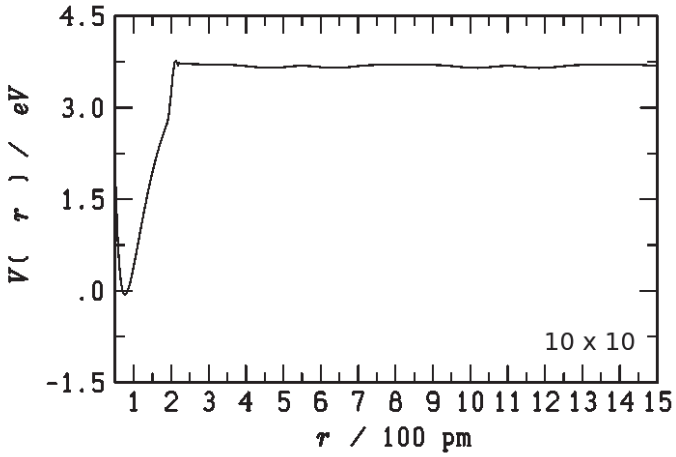

(b) Cut in r when z is 250 pm in unit cell 10 $\times$ 10.

Figure 47 – Variation of the potential energy as a function of r when the molecular axis is parallel to the surface on the "fcc-fcc" site.

We note that the reference state with zero energy is defined in the REBO routine as the state where the hydrogen molecule is desorbed from de substrate ($z \to \infty$) and the interatomic distance is at the gas phase equilibrium value (about 75.14 pm). This means that potential energies at the stable adsorption sites are negative in the original REBO

routine.

It is noted that when H_2 is at $z = 250$ pm, the potential does not look like a simple potential, differentiable, as the Morse potential, what would be expected. The shown discontinuity in the slope seems also to be an artefact and we must then conclude that the potential is not global, in particular for z exceeding 250 pm, the representation cannot be used for dynamical calculations that would involve the dissociation of the diatomic far away from the substrate. These regions of configuration space are hardly probed in the dynamics discussed in the present work, which renders the discontinuities a less severe problem here.

The cuts in Fig. 48 show, for the units cells 10×10, the displacement of H_2 on the Pd(111) surface along of x with $z = 100$ pm, $r = 279$ pm, $\theta = 90^0$ and $\phi = 0^0$. In a) the molecular center is on the "fcc-fcc" site (y =161 pm), and in b) the molecular center is on the so-called "hcp-hcp" site (y =81 pm).

The Fig. 49 shows a cut in y when x is 279 pm. It is noted that there are two wells separated by an energy barrier, as already see in Fig. 8.

The wells observed in Fig. 49 are two most stable adsorption sites for H_2/Pd(111) system, the "fcc-fcc" and "hcp-hcp" sites. It is noted that there is a small difference of energy between the two wells (see also Fig. 8).

In [12] the adsorption energy of H_2/Pd(111) on the "fcc-fcc" site is -0.996 eV, for the "hcp-hcp" site it is -0.892 eV, for the "b-t-b" site is -0.658 eV and for the "top-top" site it is positive: 0.324 eV. The adsorption energy is defined here as the energy difference on the electronic potential energy surface between the adsorbed structure and the isolated molecule in the gas phase when $r = 74$ pm. If one looks at Fig. 49 one can say that the deeper well is the "fcc-fcc" site and the second deeper well is the "hcp-hcp" site. The barrier energy that separate the two wells is the "b-t-b" site.

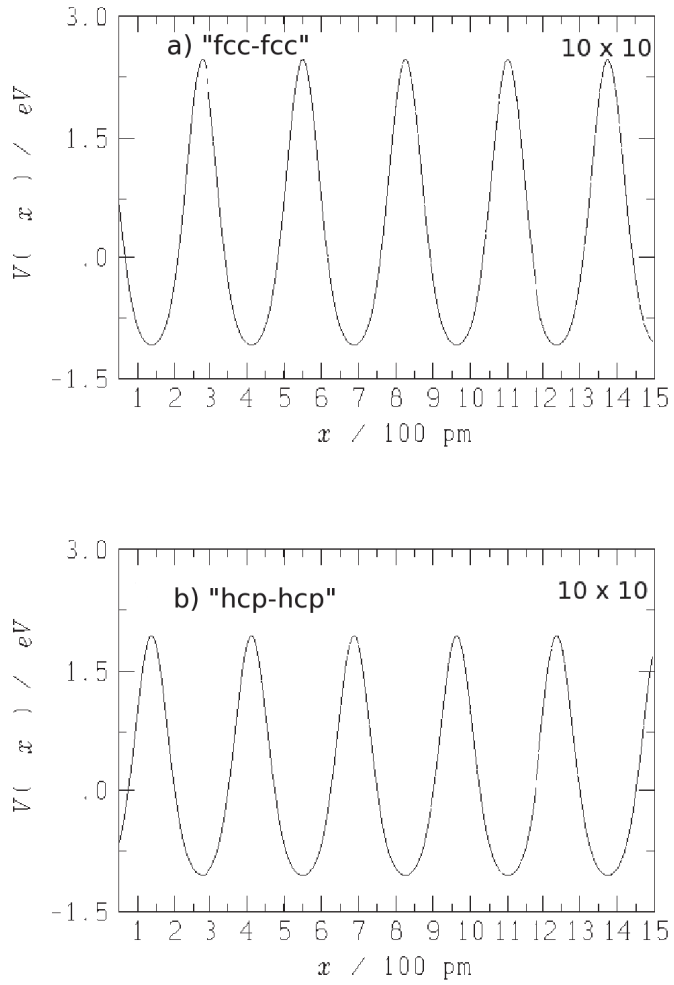

Figure 48 – Variation of the potential energy as a function of x for the unit cell 10×10, with a) $y = 161$ pm, $z = 100$ pm, $r = 279$ pm, $\theta = 90^0$ and $\phi = 0^0$, b) $y = 81$ pm, $z = 100$ pm, $r = 279$ pm, $\theta = 90^0$ and $\phi = 0^0$.

Fig. 50 shows a scheme that helps us to understand the displacement of H_2/Pd(111) along y_c. One can see that after the "hcp-hcp" site, the hydrogen atoms are on the site called "top-top", i.e. each H is on top of a Pd atom. The adsorption is unstable (0.324 eV [12]) at this site.

Tab. 11 summarizes the adsorption energy of H_2/Pd(111) (E_{ad}) at the several sites, the distance between the two hydrogen atoms (d_{H-H}), the distance of the molecular center of H_2 to the surface (h_H) and the distance $H - Pd$ (d_{H-Pd}). All the local minima were calculated with the algorithm described in [4].

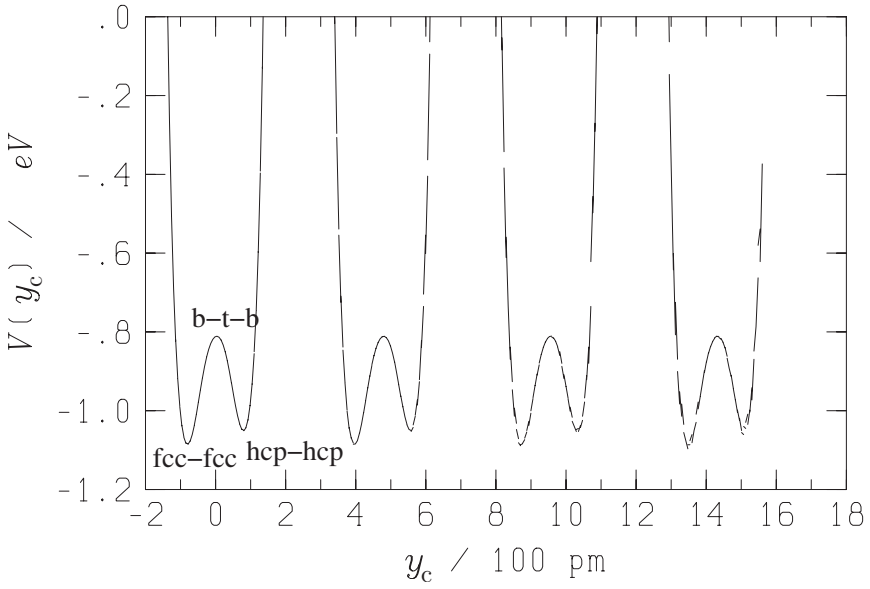

Figure 49 – Variation of the potential energy as a function of y for the two units cells with $x = 279$ pm, $z = 100$ pm, $r = 279$ pm, $\theta = 90^0$ and $\phi = 0^0$.

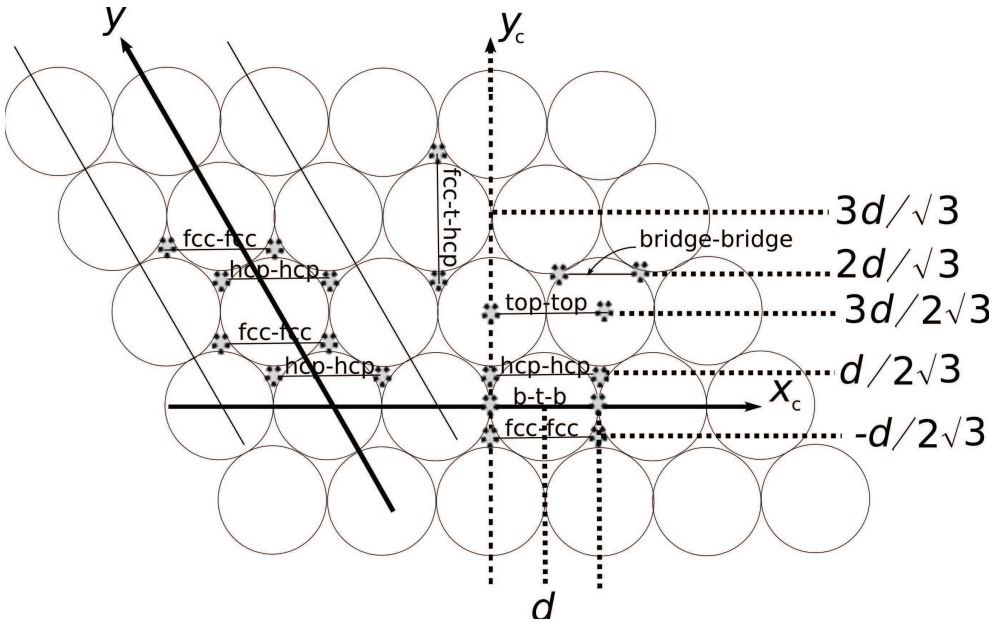

Figure 50 – Different adsorption sites of H_2 on Pd(111).

Table 11 – Adsorption energy E_{ad} for the different reaction sites of Pd(111) (10 × 10 unit cell). The values in parentheses are found in reference [12]. See text and Fig. 50 for the definition of the quantities.

Sites	fcc-fcc	hcp-hcp	b-t-b	fcc-t-hcp	fcc-hcp	bridge-bridge	top-top
E_{ad}/ eV	-1.143	-1.120	-0.829	-1.123	-0.929	-0.193	0.284
	(-0.996)	(-0.892)	(-0.658)	(-0.694)	(-0.694)	(-0.382)	(0.324)
d_{H-H} / Å	2.711	2.705	2.742	3.163	1.880	0.914	2.751
	(2.79)	(2.79)	(2.79)	(2.79)	(1.61)	(1.40)	(2.79)
h_H / Å	0.880	0.873	1.033	0.847	0.853	1.500	1.533
	(0.84)	(0.84)	(1.01)	(0.83)	(0.83)	(1.04)	(1.55)
d_{H-Pd} / Å	1.824	1.788	1.721	2.923	1.939	2.528	1.931
	(1.82)	(1.82)	(1.72)	(1.81)	(1.81)	(1.74)	(1.55)

These results are different from those reported in [12]. For the "fcc-fcc" and "hcp-hcp" sites there is the same qualitative trend. However for the "fcc-t-hcp" there are larger differences. The "fcc-t-hcp" site is as stable as the "hcp-hcp", -1.123 eV and -1.120 eV, respectively.

The most stable site yields hence an adsorption energy of 1.143 eV $\approx$ 9220 $hc\,\mathrm{cm}^{-1}$. The experimental adsorption energy E_{ad} for H_2/Pd(111) obtained by thermal desorption spectroscopy [21] is approximatively 7300 $hc\,\mathrm{cm}^{-1}$. The adsorption energy on the electronic surface is 8100 $hc\,\mathrm{cm}^{-1}$. To estimate the latter, the following zero point energies were assumed the ZPE: 2200 $hc\,\mathrm{cm}^{-1}$ [54] (H_2(g)) and 3000 $hc\,\mathrm{cm}^{-1}$ [22] (2H/Pd(111)(s)).

The experimentally estimated energy on the electronic PES is about 1100 $hc\,\mathrm{cm}^{-1}$ smaller in magnitude than the theoretical value from the H_2/Pd(111) PES. This difference is quite important, which might be related to the quality of the method used to perform the electronic structure on which the REBO potential is used (see Appendix C), or the quality on the REBO representation itself, as discussed above, in particular in relation to the singularity found at $z = 250$ pm (Fig. 47b), or to both.

Table 12 gives the coordinates and the nth order saddle point (n) of each adsorption sites. All the local minima and saddle points were calculated with the algorithm described in [4].

Table 12 – Coordinates for the adsorption sites.

	$x/\ d$	$y/\ d$	$z/$ 100 pm	$r/$ 100 pm	θ/deg	ϕ/deg	$E_{\mathrm{ad}}/$ eV	n
fcc-fcc	$\frac{1}{2}$	$2h$	0.880	2.712	90.000	0.000	-1.143	0
hcp-hcp	1	h	0.873	2.705	90.000	0.000	-1.120	0
b-t-b	$\frac{1}{2}$	$3h$	1.033	2.747	90.000	360.0	-0.829	2
fcc-t-hcp	1	$6h$	0.847	3.163	90.000	90.00	-1.123	0
fcc-hcp	1	$3h$	0.853	1.880	90.000	90.00	-0.929	1
bridge-bridge	$\frac{1}{2}$	$4h$	1.500	0.914	90.000	0.000	-0.193	2
top-top	1	$3h$	1.533	2.751	90.000	0.000	0.284	4

$d = 275.114$ pm, $h = \frac{d}{2\sqrt{3}}$

It is noted that the distance r between the hydrogen atoms when they are on the "fcc-fcc" or "hcp-hcp" site is not equal to $d = 275.114$ pm. There is a difference of 39.14 mm which can be explained by the non-zero distance of the dissociated hydrogen molecule from the substrate at equilibrium.

Fig. 51 is similar to Fig. 7. The one dimensional cut of the potential energy surface along z, Fig. 51, shows the adsorption of H_2 on top of the "fcc-fcc" site in first layer, which is positioned at $z = 0$. The adsorption minimum occurs at about $z = 98$ pm. The adsorption energy is ~ 1.143 eV ($\sim 9220\ hc\,\mathrm{cm}^{-1}$). This well is the deepest of those seen in the figure. The two other wells correspond to sub-layer adsorption and can be considered to be an absorption of H_2, in the bulk. The PES from [12, 28] was not developed to study the absorption of H_2 quantitatively, therefore the range chosen for the dynamical studies carried out in this thesis is $20 \leq\ z/\mathrm{pm} \leq 140$, where there is dissociative adsorption.

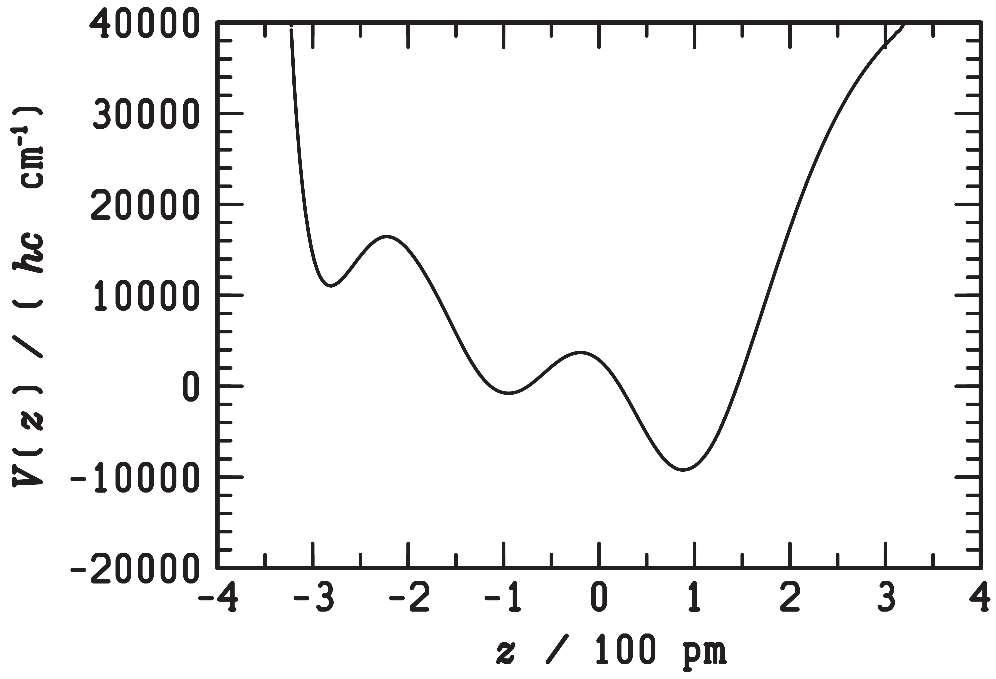

Figure 51 – Variation of the potential energy as a function of z with $x = 275.114$ pm, $y = 158.837$ pm, $r = 275.114$ pm, $\theta = 90^0$ and $\phi = 0^0$.

4.2 Potential representation (POTFIT)

Fig. 52 shows the contour lines representation for H_2/Pd(111). One see two adsorption "fcc-fcc" sites localized at 750 $hc\,\mathrm{cm}^{-1}$, one adsorption "hcp-hcp" site localized at 1100 $hc\,\mathrm{cm}^{-1}$, one adsorption "fcc-t-hcp" site localized at 1450 $hc\,\mathrm{cm}^{-1}$ and three adsorption "fcc-hcp" sites localized at 2500 $hc\,\mathrm{cm}^{-1}$.

To construct potential energy operators for the 6D system to be used in the MCTDH code a relevant region was fitted to a sum-of-products functional form (see Eq. (16)) via the POTFIT routine of the MCTDH program. This region was chosen by the energy bounds -9275.3 $hc\,\mathrm{cm}^{-1}$ $< V < 0$ covering about 18 % of the grids points. The $\mathscr{L}^2$-error for the representation of $V^{\mathrm{app}}(x_1, y_1, z_1, x_2, y_2, z_2)$ in products of bi-dimensional functions (see Eq. (16)) is 82.6 $hc\,\mathrm{cm}^{-1}$.

The $\mathscr{L}^2$-error for this case is larger than that for the 3D system (~ 0.03 $hc\,\mathrm{cm}^{-1}$). Fig. 52

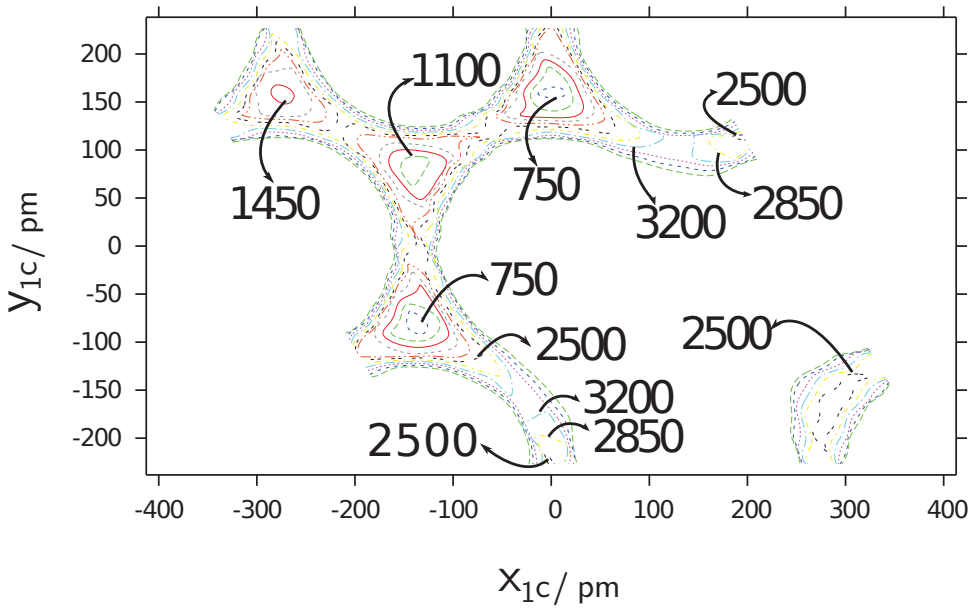

Figure 52 – Contour line representation for H_2/Pd(111). The values on contour lines are in units of $hc\,\mathrm{cm}^{-1}$, $x_{2c} \simeq 120$ pm, $y_{2c} \simeq -70$ pm and $z_{1c} = z_{2c} = 95$ pm.

represents a PES cut , where one hydrogen atom is centred approximately at the "fcc" site ($x_2 \simeq 80$ pm, $y_2 \simeq -80$ pm and $z_2 = 95$ pm) and the other hydrogen atom is free to move in the xy plane, but for constrained to $z_1 = 95$ pm.

The representation is not optimal as we cannot place the hydrogen atom perfectly at the "fcc" site, ($x_2 = 91$ pm, $y_2 = -91$ pm and $z_2 = 95$ pm). To improve this representation it is necessary to increase the expansion orders n_{κ_i} in Eq. (16). However, for a larger number of potential terms, the amount of memory allocated exceeds 0.5 gigabytes and also the calculation becomes more expensive. The time duration to perform this calculation is about 80 hours, on currently available processors (2.4 GHz at 8 GB memory - the routine is currently not parallelized). Parameters needed to obtain the natural potentials are given in Tab. 13.

Table 13 – Calculation parameters for the H_2/Pd(111) system (see also Tab. 6). Parameters apply to a (2×2) surface cell grid and bases 1 to 3 (see text).

grid parameters

coordinate (κ_i)	DVR	DVR-parameters	N_{κ_i} [a)]	M_{κ_i} [a)] $1^{(b)}$	M_{κ_i} [a)] $2^{(b)}$
x_i or y_i	EXP	$x_i^{(\min)} = y_i^{(\min)} = -d$, $x_i^{(\max)} = y_i^{(\max)} = d$ [c)]	21	40	46
z_i	SIN	$z_i^{(\min)} = 20$ pm, $z_i^{(\max)} = 170$ pm	11	18	19

integration parameters

integration or extrapolation scheme	parameters
CMF	initial time interval 1.0 fs; accuracy parameter 10^{-3}
RRDAV/A	maximal order 10000; accuracy 10^{-9}; eps_inv = 10^{-9}
RK8/spf	accuracy 10^{-8}; initial step size 0.1 fs

"potfit" parameters

natural potentials	z_1 and z_2 are "contracted" $x_1 = x_2 = 120$ $y_1 = y_2 = 120$
correlated weights	$-9275.3\ hc\,\mathrm{cm}^{-1} < V < 0$; covering 18 % of the grid points $hc\,\mathrm{cm}^{-1}$
fit characteristics	weighted rms[c)] 82.6 $hc\,\mathrm{cm}^{-1}$ (grid point relevant)

[a)] N_{κ_i} is the number of primitive functions of the coordinate combined κ_i ($\kappa_1 = x_1, y_1; \kappa_2 = x_2, y_2$ and $\kappa_3 = z_1, z_2$), M_{κ_i} is the number of single particle functions.

[b)] basis 1 and basis 2 with the same N_{κ_i}

[c)] $d = 275.114$ pm is the distance between nearest neighbour palladium atoms [45].

[d)] root mean square deviation

4.3 Eigenstates of H_2/Pd(111)

We consider a 2×2 surface cell grid, whose elementary cell is depicted in Fig 53. This cell may be decomposed in 4 elementary cells of the 1×1 surface cell grid, which can be numbered by the digits 1 to 4, as indicated in the figure. Each 1×1 cell hosts a "fcc" (bold circle) and a "hcp" (simple circle) adsorption site. For simplicity, we name the "fcc" sites "A" sites, the "hcp" are the "B" sites. There are hence four A_i and four B_j sites in the 2×2 cell, where i and j range from 1 to 4.

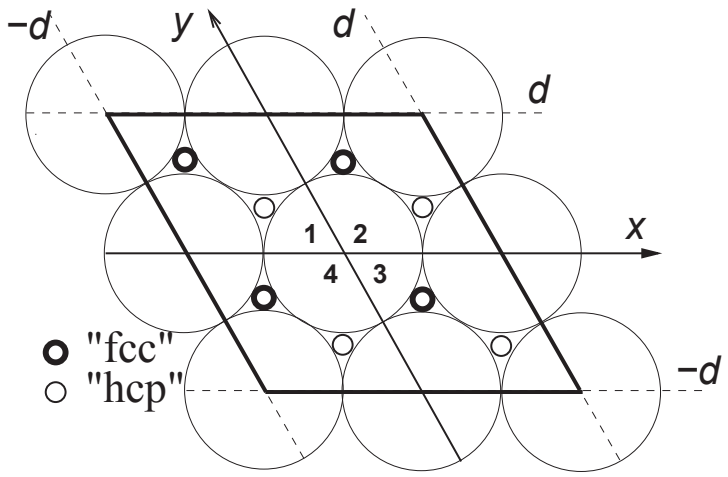

Figure 53 – Scheme of the 2×2 surface cell with numbered 1×1 surface sub-cells as discussed in the text.

There are $12 = 4!/2!$ possibilities to arrange the two hydrogen atoms in the A-sites of the 2×2 cell, which should all minimize the total energy of the system, because the A-site is the energetically most stable site per atom. However, because of the twisted geometry of the cell, only ten out of the 12 sites yield the same interatomic distance, and it turns out that there are indeed 10 states whose energies cluster in a level of lowest energy states. The combination that has a larger interatomic distance can be denoted as A_1A_3, and forcely leads to a higher energy. Note that, because of symmetry, one may find one atom at position A_1 and the other at A_2, or vice-versa, the first at A_2 and the second at A_1. Eigenstates are in fact expected to be symmetric or antisymmetric with respect to the permutation of the two atoms, and the appropriate combination with the antisymmetric (singlet) and symmetric (triplet) spin eigenstates of the protons will finally

lead to distinct para- and ortho-hydrogen states. In the present work, no distinction is made of these modifications.

The first ten eigenstates might therefore be expected to be degenerate. Because of tunneling effects, degeneracy is in fact lifted. Tab 14 summarizes the information about calculated eigenstate energies. Each line in the table lists: a level assignment, which will be explained below; the degeneracy of the level; the lowest eigenvalue of the level, which we define as a *level edge* - in case of the lowest level, the level edge is conventionally taken as zero; the energy difference between the highest and the lowest eigenvalue pertaining to the level, which we define as the *level width*. The table lists values for several bases considered for convergence checks.

Table 14 – Band edges $\tilde{\nu}/\mathrm{cm}^{-1}$, band widths $\Delta\tilde{\nu}/\mathrm{cm}^{-1}$ and band degeneracies g for H/Pd(111).

n	assignment	level degeneracy	basis 1 level edge	basis 1 level width	basis 2 level edge	basis 2 level width	
1	$0_\mathsf{A}0_\mathsf{A}$	10	0.0	11.0	0.0	11.6	
2	$0_\mathsf{A}0_\mathsf{B}$(hex)	6	270.9	3.5	271.0	1.9	
3	$0_\mathsf{B}0_\mathsf{B}$	10	294.1	11.5	293.4	13.2	
4	$0_\mathsf{A}0_\mathsf{A}$(dia)	2	756.8	0.3	757.7	0.04	
5	$0_\mathsf{A}0_\mathsf{B}$(crs)	8	872.9	1.5	873.4	1.7	
6	$2^1_\mathsf{A}0_\mathsf{A}$	40	915.2	151.0	904.8	152.4	
7	$0_\mathsf{B}0_\mathsf{B}$(dia)	2	1114.8	0.2	1115.9	0.3	
8	$2^1_\mathsf{A}0_\mathsf{B}$(hex)+$0_\mathsf{A}2^1_\mathsf{B}$(hex)+$2^1_\mathsf{B}0_\mathsf{B}$	12	1185.5	>550.	1185.1	>550.	
9	$0_\mathsf{A}0_\mathsf{B}$(dia)	2	1196.5	2.9	1197.7	[a]	
10	$1^1_\mathsf{A}0_\mathsf{A}$	20	1291.0	37.7	1290.4	35.8	
11	$1^1_\mathsf{A}0_\mathsf{B}$(hex)+$0_\mathsf{A}1^1_\mathsf{B}$(hex)+$1^1_\mathsf{B}0_\mathsf{B}$	32	1467.9	180.4	1463.2	159.4	
⋮	⋮		⋮		⋮		

[a] the second component of this level could not be firmly assigned

The level assignment is based on both the combinatorial arrangement of atoms on the stable sites, as already outlined above, and on the analysis of the probability density distributions; we also consider as well as the analysis of transition matrix elements involving linear dipole moment operators parallel (x and y coordinates) or perpendicular (z coordinates) to the substrate. Because of the twisted geometry of the coordinates, the following matrix elements have been computed: $M_{nm}^{(\mathrm{par})} = |X_{nm}|^2 - Re(X_{nm}Y_{nm}) + |Y_{nm}|^2$ and $M_{nm}^{(\mathrm{per})} = |Z_{nm}|^2$, where $\kappa_{nm} = \langle\varphi_n|\kappa|\varphi_m\rangle$, and $\kappa = x, y$ or z.

For the assignment, we use symbols related the level assignment introduced above for the H/Pd(111) system. Hence, for the ground state level, we speak of all hydrogen atoms being in the "fcc" (or A-) site, and in their ground state, i.e. in a 0_A nodeless state. We name the level accordingly $0_\mathsf{A}0_\mathsf{A}$, meaning one 0_A for each atom.

Next to this level, a level of 6 nearly degenerate states is found, which corresponds to one atom being in an "fcc" site located around the central palladium atom, the other in the "hcp" site diagonally opposed to it. There are 6 possible configurations of this type, A_2B_4, B_4A_2, A_3B_1, B_1A_3, A_4B_2, B_2A_4. We name this level $0_\mathsf{A}0_\mathsf{B}$(hex). The next level are the 10 configurations of the $0_\mathsf{B}0_\mathsf{B}$ type, which correspond to the $0_\mathsf{A}0_\mathsf{A}$ configurations of the ground level (i.e. all B_iB_j configurations but B_1B_3, with atoms located at the "hcp" sites).

The next level found (level 4) is nearly two-fold degenerate, and corresponds to the configurations where the two hydrogen atoms are in "fcc" sites A_1 and A_3, which are more distant one from the other than the other A_iA_j configurations, which explains the energy difference to the ground level. We call this level $0_\mathsf{A}0_\mathsf{A}$(dia). It is interesting to note that hydrogen atoms still interact rather strongly on the present PES, even if their distance exceeds the Pd-Pd distance.

Level 5 in the table consists of 8 nodeless states corresponding to ground state atoms in the configurations A_1B_2, B_2A_1, A_1B_4, B_4A_1, A_2B_3, B_3A_2, A_4B_3, B_3A_4. We name this level $0_\mathsf{A}0_\mathsf{B}$(crs).

Level 6 contains a first set of states where one hydrogen atom is excited with 1 quantum of a vibrational motion along x or y, i.e. mode 2 according to the nomenclature adopted

previously for the vibrational modes of H on Pd(111). As the lowest level has 10 configurations, and each configuration has 2 x and 2 y components (one per atom), there are 40 possible configurations with one H-atom excited in mode 2. We name this level $2^1_{\mathsf{A}}0_{\mathsf{A}}$. This is the level pertaining to the fundamental parallel transitions from the "fcc" sites.

Level 7 is again a level of nodeless states similar to level 4, but with H-atoms occupying the "hcp" site.

Level 8 contains all states that can be reached from levels 2 and level 3 by a simple excitation of each one of the H-atoms by one quantum of mode 2. Levels 2 and 3 are composed of totally 16 configurations, the total number of simple excitations is therefore 64, which gives the degeneracy of this level. It extends over a broad range of energies that go beyond the energies calculated in this study, and we can only give a lower bound of its width. The states can be rather mixed, we therefore name this level $2^1_{\mathsf{A}}0_{\mathsf{B}}(\mathrm{hex}) + 0_{\mathsf{A}}2^1_{\mathsf{B}}(\mathrm{hex}) + 2^1_{\mathsf{B}}0_{\mathsf{B}}$.

From level 8 on, levels start to mingle. Level 9 is composed of nodeless states corresponding to the configuration A_1B_3.

Level 10 is the level pertaining to the fundamental perpendicular transitions from the "fcc" sites. It contains 20 states, each having one H-atom singly excited in mode 1, following our nomenclature for the vibrational modes of the H/Pd(111) system. We therefore name it $1^1_{\mathsf{A}}0_{\mathsf{A}}$.

Level 11 contains all states that can be reached from levels 2 and level 3 by a simple excitation of a H-atom by one quantum of mode 1. There are 32 states of this type.

Tab 14 does not report on other levels whose edge lies above 1500 $hc\,\mathrm{cm}^{-1}$. There are many states intermingled with the reported levels, which were not considered in the table. In particular, we expect 16 additional levels with nodeless states that lie above 1600 $hc\,\mathrm{cm}^{-1}$. These states correspond to configurations of the type A_1B1, which are clearly too energetic.

The arithmetic center of level 6 is located at 991 $hc\,\mathrm{cm}^{-1}$. That of level 10 is at 1310 $hc\,\mathrm{cm}^{-1}$. This means that the fundamental parallel transition in the H_2/Pd(111) system is about 250 cm^{-1} above the calculated parallel transitions for the H/Pd(111),

and about 200 cm^{-1} above the experimental value for this transition (see Tab. 8). The perpendicular transition is similarly displaced with respect to the data given in Tab. 8. This discrepancy could be related to a lack of convergence of the 6D calculations documented in this section. As the values in Tab. 14 do not change much when the PBF-basis is increased, bad convergence, if at all, could be related to the quality of the POTFIT representation. Further convergence tests must hence be carried out.

However, if convergence is reached, the discrepancy could reveal some odd characteristics of the original REBO representation of the PES. As a third hypothesis, the discrepancy could hint at a real phenomenon, in that the HREELS spectra were recorded under conditions where H-atoms were highly diluted on the substrate so that mono-atomic spectra were recorded. This is interesting, as recent experimental findings report on instantaneous self-assembling of isolated H-atoms on copper [55] and other metallic substrates.

Chapter 5

A brief comment on H_2/Cu(100)

Another system that was initially investigated in the context of this thesis is the H_2/Cu(100) system, for which a PES representation was published quite some time ago, and prominently used in quantum dynamical calculations of the scattering of H_2 on the copper surface, which have lead to a good understanding of measured scattering and sticking probabilities [2, 3]. We have thus initially started to investigate this surface, similarly to the procedure described in section 4.1 above.

One of the original purposes of this thesis was to investigate the influence of different dynamical and structural properties of the adsorbates or their diffusion dynamics on different substrates. It turned out quite readily that a major problem that persists to date is the quality of the underlying potential energy surfaces. The number of available analytical PES representations may be large. However, such representations are too often not appropriate to be used for all kind of calculations. We saw, for instance, that the PES used in the present work for the H_2/Pd(111) system is both qualitatively and quantitatively sufficient to be used for studies of the diffusion dynamics, but it lacks even qualitative criteria at large distances from the substrate.

The routine to calculate the PES for H_2/Cu(100) was provided to us by M. Somers. In reference [2], topic B (2D cuts) pag. 3846, the points were defined in the range ($0 \leq Z \leq 7\ a_0, 0.5\ a_0 \leq r \leq 4.8\ a_0$) and the H_2/Cu(100) PES was determined by spline interpolations. It is noted that the upper limit of r defined in the article ($r \leq 4.8\ a_0$) coincides exactly with the point where the potential becomes constant as the figures shown below indicate.

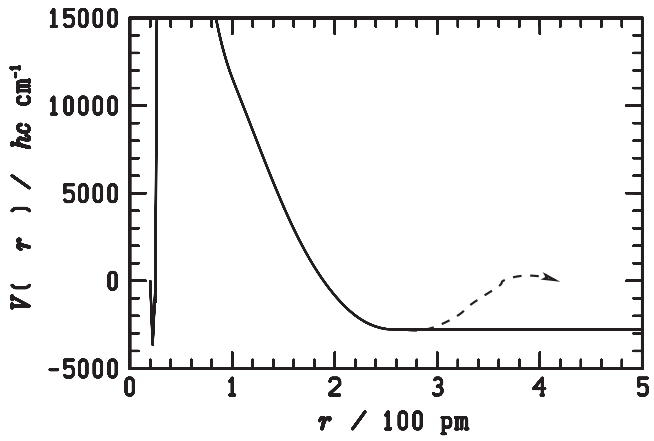

(a) One dimensional section of the PES as function of the coordinate r, with $x = 0.00$ pm, $y = 127.5$ pm, $z = 60$ pm, $\theta = 90^0, \phi = 0^0$. The hand-drawn dashed line represents the expected function (see text).

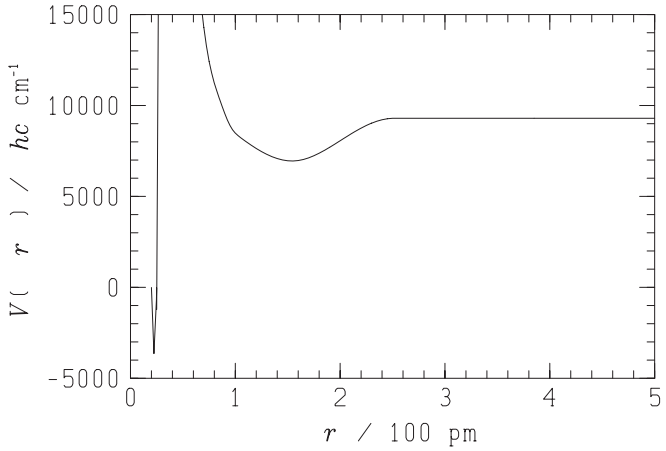

(b) As Figure 54a, but with $x = 127.5$ pm, $y = 127.5$ pm, $z = 60$ pm, $\theta = 90^0, \phi = 0^0$.

Figure 54 – One-dimensional sections of the H_2/Cu(100) potential from [2, 3].

These results for the bridge and hollow sites (Figs. 54a and 54b) show that the potential becomes constant at 4.8 $a_0 \simeq 255$ pm $= d$, where d is the distance between two Cu atoms. When the molecule centre is at a hollow site (Fig. 54b), the potential energy should be maximum (a barrier), because then the H-atoms are closest to the Cu atoms, when $r = d$. But the figure leads us to understand that after 4.8 a_0 atoms behave as free-particles. This is most likely a technical artefact of the representation. The steep decrease of the PES shown in both figures for very short distances of the atoms to the substrate is probably also an artefact. This artefact is less serious here, as we would not intend to probe regions with very small values of r.

The expected function is indicated by the hand drawn dashed line in Fig. 54a. The molecular center is at the bridge site. Here, the PES should increase, when the H atoms are separated beyond r_e, with modulations governed by the H − Cu interaction and the periodicity of the lattice. Very clearly, the PES5 representation from [2,3] is not global, as it does not mimic the expected behaviour even qualitatively. In the quantum dynamical simulation carried out in [3], H_2 molecules were scattered at the Cu substrate and the wave packet was absorbed for r beyond 4.8 a_0 by an optical potential. Such a trick cannot be applied in the context of the present investigation of the frustrated translation.

If one considers the molecular center of mass at the bridge site varying the potential as a function of $H-H$ distance, might result in two situations. The first, depicted schematically in Fig. 55b, in the case where the interaction between the hydrogen atoms can be considered more important than the $H-Cu$ interaction. Here, the PES should increase, when the H atoms are separated beyond r_e, with modulations governed by the $H-Cu$ interaction and the periodicity of the lattice. In the other situation, Fig. 55a, the $H-H$ interaction is weaker than the $H-Cu$ interaction, and here the potential energy function should be periodic with a period $2r_e$.

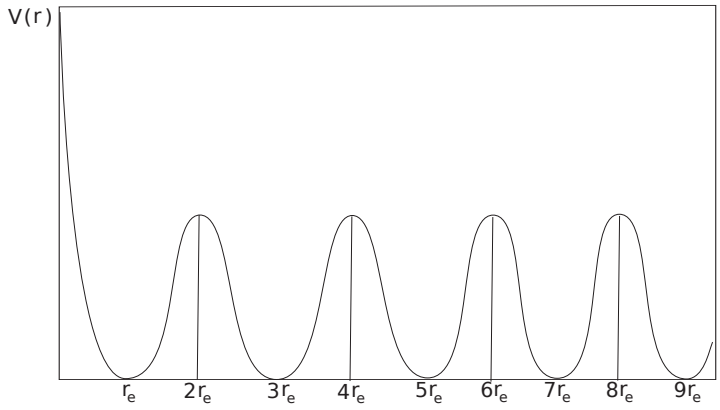

(a) Expected function when $H-H$ interaction is not important.

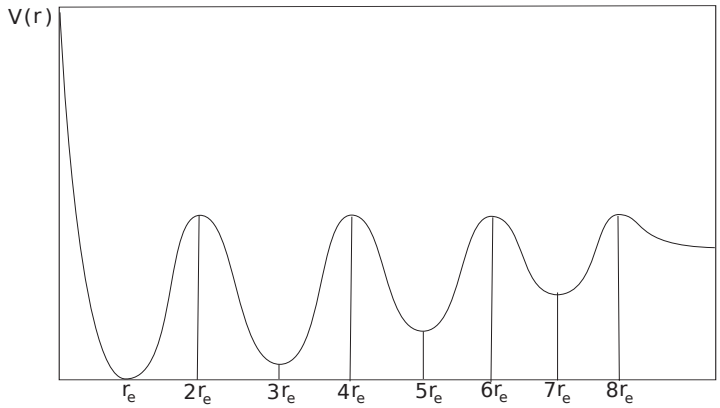

(b) Expected function when $H-H$ interaction is important.

Figure 55 – The two expected functions for the one dimensional in bridge site.

Note that the H2/Pd(111) discussed above yields interaction energies that correspond to the situation depicted in Fig. 55b, i.e., the $H-H$ interaction at the adsorption site is somewhat more important that between H and Pd atoms.

An extension of PES5 to include large positions of the configuration space in x and y is needed before the MCTDH approach can be applied here to study the frustrated translation. The main subject of this project is neither to develop a new PES nor to do calculations of the electronic structure to include more positions and obtain a better description of the configuration space. It is therefore decided to replace the study of the H_2/Cu(100) system by that of H_2/Pd(111), the PES of which is known to have a very suitable analytical representation [12, 28].

The unit cell of Pd(111) chosen to perform calculations of the quantum dynamics of H/Pd(111) or H_2/Pd(111) is 10×10 because the range in which we want to study the adsorption of H_2 presents realistic results and for this range one can consider that this PES [12, 28] is suitable to be used in MCTDH.

Chapter 6

Full quantum calculations of the diffusion rate of adsorbates

This chapter is an extract from [56] and presents some preliminary calculations of the diffusion rate of hydrogen atoms from eigenvalues and eigenfunctions.

The diffusion of adsorbed particles is an important process intervening in heterogeneous catalysis. Yet, and despite the significant progress achieved in the past decades in the domain of surface science, our knowledge about such elementary steps in catalysis remain modest, both experimentally and theoretically. In long time domain of milliseconds to seconds, scanning tunnelling microscopy (STM) is capable of unravelling some of the details of this motion. For instance, Jewel *et. al.* report on quantum tunnelling of isolated hydrogen atoms adsorbed on Cu(111) terraces, which are observed with STM and a spatial resolution of a few tenths of a nanometre [55]. These experiments, carried out at 5 K, show the potential technological application arising from the interaction between the mobile adsorbates leading to the formation of self-assembled clusters. However, the time resolution of these experiments does not allow us to follow the motion of the H atoms in real time, interpreted in these papers as arising from tunnelling.

The motion of hydrogen atoms adsorbed on metal surfaces has been explored with picosecond time in ^{3}He spin-echo experiments for H/Pt(111) [57] and H/Ru(0001) [58]. The primary quantity determined in these experiments is the intermediate scattering function

(ISF) $I(\mathbf{q}, t)$, where $\mathbf{q}$ is the wave vector related to the momentum transferred from the scattered ^{3}He atoms to the hydrogen atoms moving on the surface, and t is the time. In a previous work, Alexandrowicz *et. al.* reported on quasi-elastic broadening measurements from ^{3}He spin-echo experiments on CO/Cu(100) [25]. They observe a quasi-elastic broadening that varies from 0 to about 1 μeV as function of the momentum transferred to the CO molecules along either the $\langle 110 \rangle$ and the $\langle 100 \rangle$ direction.

The observed quasi-elastic energy broadening can in principle be related to the width Γ of the dynamical structure factor (DSF) (DSF) $S(\mathbf{q}, E)$, which is the temporal Fourier transform of the ISF. The ISF is the spatial Fourier transform of the pair correlation function proposed by van Hove [59], who also derived a general expression for the DSF in terms of the eigenvalues and eigenfunctions pertaining to the stationary vibrational states of the adsorbates. This expression was never evaluated, to our knowledge, from within a fully quantum mechanical treatment of the adsobate's dynamics. In the present work, we perform such an evaluation using eigenvalues and eigenfunctions derived from global potential energy surfaces (PES) for the H/Pd(111) system [1, 12, 27]. The problem is treated in full dimensionality for the H_2/Pd and H/Pd systems with static palladium atoms.

A key parameter in the present work is the intrinsic energy broadening Γ_i related to the lifetime $\tau_i \propto 1/\Gamma_i$ of vibrational eigenstates. This finite lifetime can be related to the coupling of the vibrational motion of the adsorbates with either the motion of the substrate atoms (phonons), or to the motion of electrons beyond the Born-Oppenheimer approximation (electron-hole pair formation), or to both. Depopulation of vibrational eigenstates of adsorbates on metal substrates via formation of electron-hole pairs is expected to proceed on the picosecond time scale [60, 61], or even faster [62], which would be much faster than the relaxation due to the coupling to phonons [63]. Note that the picosecond time scale is about the time scale that can be reached with the ^{3}He spin-echo technique. However, lifetime $\tau = 1$ ps corresponds to an energy broadening of 1.3 meV, which is about two to three orders of magnitude larger than the broadening typically observed in the aforementioned ^{3}He spin-echo experiments. We shall see that it is possible

to accommodate the different domains by setting

$$\Gamma = \Gamma_i + \Gamma_d \tag{60}$$

where Γ is the overall width (full width as half maximum, FWHM) of the DSF; Γ_i is the aforementioned intrinsic broadening and Γ_d can be interpreted as the portion of the broadening that is caused by diffusion.

6.1 Dynamical structure factor

The quasi-elastic broadening can be calculated as the width of the dynamical structure factor (DSF) $S(q, E)$ at $E = 0$, see, for instance figure 9 and the corresponding text in [64]. An expression for this quantity was proposed by van Hove in 1954, i.e. equation 4 in [59]:

$$S(\mathbf{q}, E) = \sum_n P_n \sum_m |\langle m|e^{i\mathbf{qx}}|n\rangle|^2 \delta(E - (E_m - E_n)) \tag{61}$$

In this equation, $|n\rangle$ and $|m\rangle$ are eigenstates of the scattering center at energies E_n an E_m; P_n is the Boltzmann population distribution , $\mathbf{x}$ is the position vector of adsorbed particle. If $\mathbf{x}$ is its projection on the direction of the momentum transfer, i.e. parallel to the substrate, $\mathbf{qx} = qx$. In the original equation, matrix elements of a sum over many particles of individual exponential operators (with particle position vectors $\mathbf{x_j}$. In the present work, we shall restrict the study to a single adsorbed particle.

We shall consider that the vibrational eigenstates are not truly stationary but have a individual lifetimes $\tau_n = h/(\pi\gamma_n)$ due to the coupling with a continuous or semi-continuous set of closely lying states pertaining to the motion of other particles (electrons or phonons); h is the Planck constant and γ_n is the width (FWHM) of the energy distribution of this state in the set of the true eigenstates of the full system. Spectral lines such as those occurring in Eq. (61) involve a pair of eigenstates and will hence have an intrinsic width (FWHM) $\Gamma_{nm} = \gamma_n + \gamma_m$. Consequently, we replace the *delta*-function in Eq. (61) by the

Lorentzian distribution

$$L(E;(E_m - E_n, \Gamma_{nm}) = \frac{1}{2\pi} \frac{\Gamma_{nm}}{(E - (E_m - E_n))^2 + \Gamma_{nm}^2/4} \tag{62}$$

In the following, we assume for simplicity that all eigenstates will have the same intrinsic width $\Gamma_{nm} \equiv \Gamma_i$. This very simple model will indeed allow us to extract some interesting conclusions, while more elaborate and more realistic models, which we have considered and which be presented elsewhere, do no alter the qualitative picture of the present results.

Instead of Eq. (61), we shall use hence the following formula to evaluate the DSF:

$$S(\mathbf{q}, E) = \sum_n P_n \sum_m |\langle m|e^{i\mathbf{qx}}|n\rangle|^2 L(E;(E_m - E_n, \Gamma_i) \tag{63}$$

6.2 Results

The eigenfunctions for the H/Pd(111) system were already calculated (see subsection 3.1.1) then the matrix elements of the $e^{\mathbf{qx}}$ operator are calculated for several values of $\mathbf{q}$ with the *crosscorr* utility program contained in the MCTDH program package. We shall evaluate Eq. (63) for a momentum transfer along the surface vector linking two nearest Pd neighbors (which corresponds to the $\langle 11\bar{2}0\rangle$ crystallographic direction in hexagonal closed packed cells). In this direction the scalar product is $\mathbf{qx} = qx_c = q(x - y/2)$. The section of the potential energy surface for H/Pd(111) chosen is represented in 11b. One clearly sees the stable adsorption sites, "fcc" and "hcp", which are also indicated in the scheme 10a. On this PES, the "hcp" site is about 190 $hc\,\mathrm{cm}^{-1}$ less stable than "fcc" site (see Tab. 7) and the barrier between the two sites is at about 1150 $hc\,\mathrm{cm}^{-1}$ above the "fcc" site (see Fig. 8). There are 4 "fcc" and 4 "hcp" sites per unit cell. The "hcp"/"fcc" occupation ratio is about 0.37 at room temperature, and we can therefore assume that the occupation of sites is approximately homogeneous, which makes the present study mimic a coverage degree 12.5 %.

Fig. 56 shows the form of $S(\mathbf{q}, E)$ for this system, when $\Gamma_i = 1$ meV is assumed.

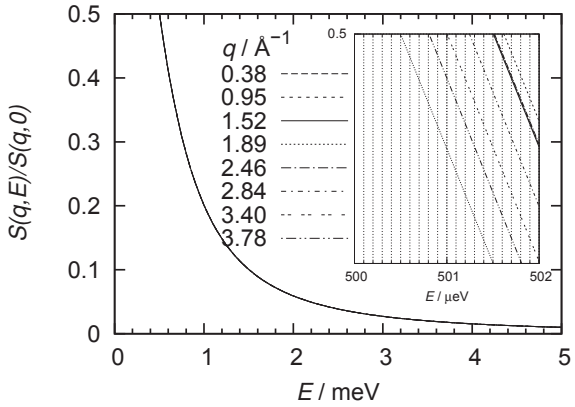

Figure 56 – $S(\mathbf{q}, E)/S(\mathbf{q}, 0)$ for the H/Pd(111) system, assuming as intrinsic broadening $\Gamma_i = 1$ meV. The inset is a magnification of the function in the region of $S(\mathbf{q}, E) \approx 0.5(\mathbf{q}, 0)$. Results are for the $\langle 11\bar{2}0 \rangle$ crystallographic direction, at $T = 250$ K.

Fig. 56 shows this variation in terms of the corresponding diffusion rate, defined here, as $\alpha = \pi\Delta\Gamma/h \approx 0.7596$ ps$^{-1} \times$ $\Delta\Gamma$ /meV, where $\Delta\Gamma = \Gamma - \Gamma_i$. There is currently no experimental result for this function. We may compare the present theoretical result, however, with experimental results for systems that should be rather similar, i.e. H/Ru(0001) [58], (figure 1 therein), and H/Pt(111) [57]: the general behaviour of the rate function show in Fig. 57 reproduces qualitatively very well the form of the experimental functions; however, the variation range for the rate is a factor 10 smaller than that observed for H/Ru(0001, and a factor 100 smaller than what is observed for H/Pt(111).

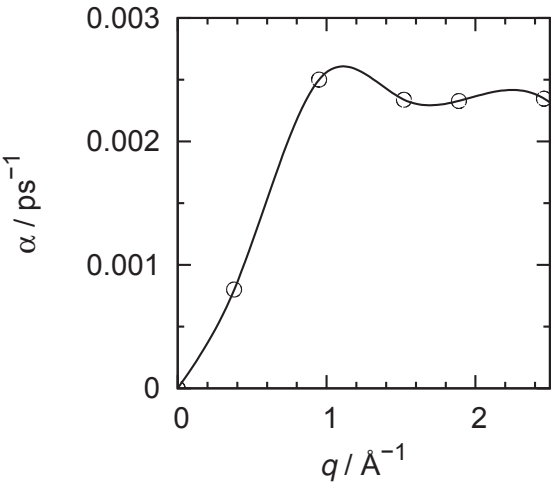

Figure 57 – Calculated diffusion rate $\alpha(q)$ for atomic hydrogen on Pd(111) along the $\langle 11\bar{2}0\rangle$ crystallographic direction, at $T = 250$ K. $\alpha = \pi\Delta\Gamma/h$ and $\Delta\Gamma$ is the differential broadening with respect to Γ_i, obtained as twice the values of the solutions of $S(\boldsymbol{q}, E) = 0.5\, S(\boldsymbol{q}, 0)$ in Fig. 56.

These studies, which include a more realistic modelling of vibrational lifetimes, are currently being carried out. It can be shown that the variation range of the diffusion rate increases, if a much larger value of the intrinsic broadening is assumed, meaning a much shorter relaxation time due to "friction". Relaxation times shorter that those assumed here for hydrogen on ruthenium or palladium can indeed be expected from theory [65].

A second investigation route includes the study of di-hydrogen structures. It is known that hydrogen atoms, even if adsorbed at low coverage degrees, form clusters of di-hydrogen on the substrate [55]. H_2 dissociates upon adsorption on palladium or ruthenium, the adsorbed atoms may interact with each other, however, even at distances larger that the distance between two neighbouring metal atoms.

Chapter 7

Conclusions

The results obtained for the H/Pd(111) system allowed us to improve our theoretical description of this system. The following points summarize the most relevant conclusions:

1 Under the assumption that the vibrational spectrum of H_2/Pd(111) can be confused with that of the H/Pd(111) system at very low coverage degree, since the adsorption of hydrogen molecular is dissociative, this work has provided a somewhat improved theoretical reproduction of the main experimentally available transitions (from HREELS). It has also lead to an important new insight regarding the nature of the vibrational states underlying the observed transitions. In fact, the systematic inspection of reduced probability densities has revealed an important resonance phenomenon between quantum states that are localized on adjacent adsorption sites. Excited vibrational eigenstates of H/Pd(111), and to some extend also those of the D/Pd(111) isotopologue, that involve 1 quantum of the perpendicular vibration, i.e., a vibration of the atom orthogonal to the substrate, are in fact superposition states of states localized on adjacent adsorption sites having 1 quantum of perpendicular vibration and 2 quanta of parallel vibration. For 2 adjacent "fcc" and "hcp" sites, 4 states are strongly mixed. The mixing is the signature of a strong anharmonic coupling that spectroscopists call a Fermi resonance. And the coupling is also an important driving force of a very fast diffusion dynamics that takes place within a few hundred femtoseconds and that was found in this thesis. The resonance is less pronounced for D/Pd(111), and nearly absent

for T/Pd(111) because of mismatching energies of localized states. It should be noted, that the resonance is quite strong for states lying in the vicinity of the diffusion barrier, but a detailed account of the relation between energy barrier and the mixing is not given here.

2 When the coverage degree is large the interactions between the hydrogen atoms may be come important. Investigations of the 6D system, H_2/Pd(111), are appropriate to show whether interactions between the hydrogen atoms on the substrate are important. It was shown that the $H-H$ interactions on the REBO PES for H_2/Pd(111) are indeed quite important. Present results on the vibrational spectrum of H_2/Pd(111) seem to indicate that both the parallel and perpendicular fundamental transition bands are shifted toward higher wave numbers, when compared to those of H/Pd(111) system. The later agree fairly well with experimentally determined values. This result is somehow paradoxical: on one hand the spectrum of H/Pd(111) agrees with the experimental data from HREELS measurements from [22], on the other hand, Jewell *et al* [55] have shown from STM measurements, that hydrogen on copper hardly remains isolated, it rather forms super-molecular clusters. We have not yet fully explored all explanations for this paradox. Admittedly, a potential lack of convergence in the present calculations of H_2/Pd(111) eigenstates could be one trivial explanation. However, we cannot discard some potential failure of the original PES representation used in this work. Finally and hypothetically, one could also argue that hydrogen on palladium might have a different behaviour than on copper, or that the infrared spectrum of larger hydrogen clusters on palladium might be similar to that of a single hydrogen atom, and different from that of the hydrogen molecule. This hypothese need to be further investigated in future work.

3 Using a newly developed idea [56], a full quantum calculation of the diffusion rate of the adsorbate was perfomed, in a simulation of the ^{3}He spin-echo scattering experiments. For this calculation, the eigenfunctions calculated for H/Pd(111) were evaluated in a formula proposed by van Hove in 1954 for the dynamical structure factor. First results are promising but so far predictions are based on vague assumptions and simple models regarding the intrinsic lifetimes of vibrational states. Full 6D treatments of the diffusion dynamics of H_2/Pd(111), in which we shall also consider in a more realistic way lifetimes of vibrational states of the adsorbates will shed more light into the problem. In

particular, such studies would enable us to truly simulate the experimentally determined intermediate scattering function and herewith give accurate values for the diffusion rate of adsorbates from first principle calculations.

```
//!CALCUL DES POIDS DE BOLTZMANN A PARTIR DES ENERGIES
//!DES ETATS PROPRES

#include <stdlib.h>
#include <stdio.h>
#include <math.h>
#include <string.h>

#define kB      0.6950353  //Constante de Boltzmann en hc cm-1 /Kelvin
#define T       300.00     //Temperature en Kelvin

int main ( int argnb , char * arg[] )
{
 //!VARIABLES GENERALES
 int Ntot=64,N;          //Ntot: Nombre total d'etats␣propres
␣char␣strtmp[400];

␣//!RECUPERATION␣DES␣ENERGIES␣DES␣ETATS␣PROPRES
␣double␣E[Ntot];␣//Energie␣des␣etats␣propres␣en␣hc␣cm-1
␣FILE␣*IN;
␣IN=fopen("Energy","r");//Adresse␣du␣fichier␣contenant␣les
␣//energies␣des␣etats␣propres

␣for␣(N=0;N<Ntot;N++)␣␣␣//Lecture␣des␣energies␣en␣hc␣cm-1.
␣//des␣etats␣allant␣de␣0␣a␣Ntot-1
␣␣␣␣␣␣␣␣{
␣␣␣␣␣␣␣␣␣fscanf(IN,"%[^=]=%lf",&strtmp,&E[N]);
␣␣␣␣␣␣␣␣␣fgets(strtmp,400,IN);
␣␣␣␣␣␣␣␣}
␣fclose(IN);
```

```
␣//!CALCUL␣DE␣LA␣FONTION␣DE␣PARTITION
␣double␣Z=0.;␣␣␣//Fonction␣de␣partition
␣for␣(N=0;N<Ntot;N++)␣Z+=exp(-(E[N]-E[0])/(kB*T));␣//La␣reference
␣//en␣energie␣(E=0)␣est␣l'energie du premier etat qui correspond
 // a l'energie␣de␣point␣zero

␣//!CALCUL␣DES␣POIDS␣DE␣BOLTZMANN
␣FILE␣*OUT;
␣sprintf(strtmp,"BoltzmannWeight%.0f",T);␣//Adresse␣du␣fichier␣de␣sortie
```

```
//!CALCUL DES Coeficients A PARTIR DES poids DES ETATS
//!PROPRES à une certaine température


#include <math.h>
#include <cmath>
#include <iostream>
#include <fstream>
#include <stdlib.h>

#define Pi 3.14159265359
#define urf  Pi/180.

using namespace std;

int main ( int argc , char * argv[] )
{
 //!VARIABLES GENERALES
 int Ntot=64,N; //Ntot: Nombre total d'etats␣propres
␣int␣istate;

␣if␣(␣argc␣<␣2␣)
␣{
␣␣␣cout␣<<␣"!!!!!!␣Arguments␣missing␣!!!!!!!!!!!"␣<<␣endl;
␣␣␣cout␣<<␣"Usage:␣$PATH/BoltzmannWeight.exe␣file␣"␣<<␣endl;
␣␣␣return␣1;
␣}

␣ifstream␣traj_file;
␣traj_file.open(␣argv[1],␣ifstream::binary);
```

```
 //!RECUPERATION DES ENERGIES ET DES POIDS DES ETATS PROPRES
 double E[Ntot]; // Energie des etats propres en u.a.
 double W[Ntot]; // Poids des etats propres
 double RC[Ntot]; // Coefficient réel
 double IC[Ntot]; // Coefficient imaginaire
 double phase[Ntot];
 srand (time(NULL));

 N=0;
 if (traj_file.is_open())
 {
    while (!traj_file.eof())
    {
      traj_file >> istate >> E[N] >> W[N];
      N+=1;
    }
 }
 else
 {
    cout << "unable to open file" << endl;
    return 1;
 }
 traj_file.close();


 //!CALCUL DES COEFF.
 for (N=0; N< Ntot; N++)
 {
    phase[N]=(rand()*1.)/ (1.*RAND_MAX)*360.0;
    RC[N] = sqrt(W[N]) * cos(phase[N]*urf);
    IC[N] = sqrt(W[N]) * sin(phase[N]*urf);
```

```
␣␣␣cout␣<<␣phase[N]␣<<␣"␣coeff=␣"␣<<␣RC[N]␣<<␣IC[N]␣<<␣endl;
␣}

␣ofstream␣out_file;
␣out_file.open("coef.dat");
␣for␣(int␣i␣=␣0;␣i␣<␣Ntot;␣i++)
␣{
␣␣␣out_file␣<<␣i␣<<"␣␣␣"<<␣E[i]␣<<␣"␣␣␣␣"␣<<␣W[i]␣<<␣"␣␣␣␣"␣<<␣phase[i]␣<<␣"
␣}
␣out_file.close();

␣return(0);
```

```
      SUBROUTINE POSITIONS(XA,YA,ZA)
      double precision xa(1000),ya(1000),za(1000),a(100),yf,esma
      integer np,nh,nq
      np=500    ! number of Pd atoms
      nh=2      ! number of H atoms
      DO j=1,np     !!!  np=500
!read the parameters of positions 1500 of Pd atoms
      XA(   1) = 0.0666666666666663
      YA(   1) = 0.0333333333333334
      ZA(   1) = 0.0000000000000000
      XA(   2) = 0.0666666666666665
      YA(   2) = 0.1333333333333330
*************************************************************************
! H2Pd111 help files
! coordinates: nq,np,xa,ya,za,a,yf
! lengths are in bohr, angles in rad
! xyz are the coordinates of the molecular centre
! PES is returned in hartree
      SUBROUTINE H2Pd111au(X,Y,Z,R,T,P,V)
      IMPLICIT REAL*8 (A-H,O-Z)
      INTEGER np,nh,nq
      DIMENSION XA(1000),YA(1000),ZA(1000),a(100)
!     parameter (tocm=219474.6314,toev=27.21138,a0=0.5291772085)
      parameter (tocm=8065.544647,toev=27.21138,a0=0.5291772085)
      np=500
      nh=2
      nq=np+nh
      rx=R*dsin(T)*dcos(P)
      ry=R*dsin(T)*dsin(P)
      rz=R*dcos(T)
      X1=(X)+0.5*(rx)
```

```
      Y1=(Y)+0.5*(ry)
      Z1=(Z)+0.5*(rz)
      X2=(X)-0.5*(rx)
      Y2=(Y)-0.5*(ry)
      Z2=(Z)-0.5*(rz)
      CALL POSITIONS(XA,YA,ZA)
!       aa=27.5114              !the unit is angstron
      aa=27.5114/a0           !the unit is now bohr
      zamax=0.39066
      ZA(NP+1)=zamax+Z1/aa/0.836017
      YA(NP+1)=Y1/aa
      XA(NP+1)=X1/aa
      ZA(NP+2)=zamax+Z2/aa/0.836017
      YA(NP+2)=Y2/aa
      XA(NP+2)=X2/aa
      CALL func(nq,np,xa,ya,za,a,yf)        ! call subroutine which is to cal

!La valeur choisie comme étant le zero d'énergie, soit, la molecule de H2 is
      V=YF/toev + 92.09875
      RETURN
      END SUBROUTINE H2Pd111au
!*****************************************************************************
! HPd111 help files
! coordinates: nq,np,xa,ya,za,a,yf
! lengths are in bohr, angles in rad
! xyz are the coordinates of the molecular centre
! PES is returned in hartree
      SUBROUTINE HPd_3dt(X,Y,Z,V)
      IMPLICIT REAL*8 (A-H,O-Z)
      INTEGER np,nh,nq
      DIMENSION XA(1000),YA(1000),ZA(1000),a(100)
```

```
!       parameter (tocm=219474.6314,toev=27.21138,a0=0.5291772085)
        parameter (tocm=8065.544647,toev=27.21138,a0=0.5291772085)
        np=500
        nh=1
        nq=np+nh
        X1=X
        Y1=Y
        Z1=Z
        CALL POSITIONS(XA,YA,ZA)
!         aa=27.5114              !the unit is angstron
        aa=27.5114/a0           !the unit is now bohr
        zamax=0.39066
        ZA(NP+1)=zamax+Z1/aa/0.836017
        YA(NP+1)=Y1/aa
        XA(NP+1)=X1/aa
        CALL func(nq,np,xa,ya,za,a,yf)          ! call subroutine which is to cal
        V=YF/toev + 91.8855
        RETURN
        END SUBROUTINE HPd_3dt
```

Thermodynamic cycle

We have 4 reactions

$$H_2(g) + Pd(s) \rightleftharpoons 2\,H/Pd(s) \qquad \Delta_1 H \tag{64}$$

$$H(g) + Pd(s) \rightleftharpoons H/Pd(s) \qquad \Delta_2 H \tag{65}$$

$$H/Pd(s) + H/Pd(s) \rightleftharpoons 2\,H/Pd(s) \qquad \Delta_3 H \tag{66}$$

$$H_2(g) \longrightarrow 2\,H(g) \qquad \Delta_4 H \tag{67}$$

Hess yields:

$$\Delta_1 H = \Delta_4 H + 2\Delta_2 H + \Delta_3 H$$

The Tab. 15 shows the enthalpy for the reactions (64), (65) and (67) with and without ZPE inclusion. $\Delta_2 H$ was estimated from the experimental data [21,66] assuming $\Delta_3 H = 0$. To estimate the latter from the former (originally measured data), the following (approx) zero point energies are assumed (in $hc\,\mathrm{cm}^{-1}$): 2000 [54] (H_2(g)), 1500 [22] (H/Pd(111)(s)), 3000 [22] (2H/Pd(111)(s)).

Table 15 – Experimental enthalpy of reactions in $hc\,\mathrm{cm}^{-1}$.

	values with ZPE	values without ZPE
$\Delta_1 H$	-7300 [21]	-8300
$\Delta_2 H$	-21710	-23210
$\Delta_4 H$	36100 [66]	38100

The experimental value of $\Delta_1 H$ is about $\simeq 1000\ hc\,\mathrm{cm}^{-1}$ smaller in magnitude than the theoretical value from the H_2/Pd(111). This difference is quite important. One should also note that the experimental value is old and probably not very certain either. Theoretically, we have the following values (in $hc\,\mathrm{cm}^{-1}$) :

Table 16 – Theoretical enthalpy of reactions in $hc\,\mathrm{cm}^{-1}$.

	Values
$\Delta_1 H$	-9220
$\Delta_2 H$	-27700
$\Delta_3 H$	8100
$\Delta_4 H$	38100

Here, we assume that $\Delta_4 H$ is as from the experiment, and obtain $\Delta_3 H$ from the above equation. The latter value is too large, but more problematic is the sign: one should expect a negative enthalpy of coalescence [55]. Hence, either the assumption on $\Delta_4 H$ is totally wrong, but that in unrealistic, or the value for $\Delta_2 H$ is not correct. We may estimate a value for $\Delta_2 H$ from the experimental data, assuming that $\Delta_3 H = -1000\ hc\,\mathrm{cm}^{-1}$ (which is a reasonable assumption, given the eigenvalues for H_2/Pd that we obtained in 6D):

$$\begin{aligned} 2\Delta_2 H &= \Delta_1 H - \Delta_4 H - \Delta_3 H \\ \Delta_2 H &= -22700\ hc\,\mathrm{cm}^{-1} \end{aligned}$$

If the enthalpy of coalescence is not considered, the enthalpy of reaction (65) is given as

$$\begin{aligned} 2\Delta_2 H &= \Delta_1 H - \Delta_4 H \\ \Delta_2 H &= -23200\ hc\,\mathrm{cm}^{-1} \end{aligned}$$

Brief overview of Density Functional Theory

Several methods based on the calculation of the electronic wavefunction (see for instance [29, 67–69]) allow a high level treatment of the important electronic correlation problem. Some of these are the MPn ($n = 2, 3, 4$) [70,71], the CISD [69], the CASPT2 [72], and the CCSD(T) [69, 73] methods. However, these are all limited to small systems. A way to study larger systems is to use Density Functional Theory (DFT) [74, 75].

The database used for developing the H/Pd(111) and H_2/Pd(111) contain the DFT [12] calculations obtained with the help of the Vienna *ab initio* package (VASP) [76]. The valence orbitals are expanded in a plane-wave basis, with the electron-ion interaction described by the ultrasoft pseudopotentials optimized by Kresse and Hafner [77]. The results are obtained within the framework of the generalized gradient approximation (GGA) and the exchange-correlation-functional of Perdew and Wang (PW91) [78].

The general idea of Density Functional Theory (DFT) is that the exact ground-state electronic energy E (Eq. (1)) can be represented by the ground-state electronic density $\rho(r)$, according to the first and second Hohenberg-Kohn theorem [74]. The first Hohenberg-Kohn theorem shows that the electron density $\rho(r)$ related to the exact ground-state wave function ψ (Eq. (1)) is uniquely determined by the external potential of the electrons. Moreover, the second Hohenberg-Kohn theorem shows that the electron density can be also used as basic variable in order to reach n_0 variationally. The electron density fixes the number of electrons n of the system according to Eq. (68)

$$n = \int \rho(r) dr \tag{68}$$

where $\rho(r)$ is the electron density and r is the (3D) coordinate of an electron. The electron density can be decomposed into spin densities ρ_α and ρ_β

$$\rho(r) = \rho_\alpha(r) + \rho_\beta(r) \tag{69}$$

The total electron energy is a functional of densities, $E[\rho]$. Closed-shell and open-shell energies are expressed in a similar manner. This energy is written as

$$\bar{E}[\rho] = \bar{T}[\rho] + \bar{E}_{\mathrm{ne}}[\rho] + \bar{E}_{\mathrm{ee}}[\rho] \tag{70}$$

where $\bar{T}[\rho]$ is the kinetic energy, $E_{\mathrm{ne}}[\rho]$ the nuclei-electrons interaction energy and $E_{\mathrm{ee}}[\rho]$ the electron-electron interaction energy. The last term can be divided into a Coulomb and Exchange interactions, $J[\rho]$ and $K[\rho]$. The nuclei-electrons interaction energy is written

$$E_{\mathrm{ne}}[\rho] = \sum_{\mathrm{a}} \int \frac{Z_{\mathrm{a}}\rho(r)}{|R_{\mathrm{a}} - r|} d^3r \tag{71}$$

and the Coulomb interaction is

$$J[\rho] = \frac{1}{2} \int \int \frac{\rho(r)\rho(r')}{|r - r'|} d^3r d^3r' \tag{72}$$

The kinetic energy and the exchange energy functionals can be evaluated by solving a set self-consistent equations which include, in an approximative way, exchange and correlation effects. In the most and approximation, one considers a gas of n electrons without interaction [75]. The basic idea of this approximation, also called the Kohn and Sham (KS) formalism, is splitting the kinetic energy functional into two parts, one of which can be calculated exactly, and a presumably small correction term [29]. Considering a gas of n electrons with non interaction between then, the density is written in terms of a set of auxiliary one-electron functions, orbitals, as

$$\rho(r) = \sum_{i=1}^{N} |\phi_i(r)|^2 \tag{73}$$

The exact kinetic energy is

$$T_{\mathrm{S}}[\rho] = \sum_i \langle \phi_i | \frac{p^2}{2} | \phi_i \rangle \tag{74}$$

The orbitals are obtained from the solution of differential equation. The equation for the system with non interacting electrons is

$$\left[\frac{p^2}{2} + V_{\mathrm{S}}(r)\right]\phi_i = \varepsilon_i\phi_i \tag{75}$$

where $V_{\mathrm{S}}(r)$ is the mean field potential resulting to the electron gas and experienced by any electron. The total energy for this electron gas system is given by

$$E_{\mathrm{S}}[\rho] = T_{\mathrm{S}}[\rho] + E_{\mathrm{ne}}[\rho] \tag{76}$$

In reality the electrons are interacting and the energy $E_{\mathrm{S}}[\rho]$ does not provide the total kinetic energy. However, just as Hartree-Fock (HF) theory the solutions of Eq. (75) provide $\sim 99\%$ of the total energy. It is necessary to include the explicit interaction of electrons (the same as in HF theory, one has to include the electronic correlation). Then, the energy $E[\rho]$ (Eq. (70)) can be re-written according to $T_{\mathrm{S}}[\rho]$ and $J[\rho]$

$$E[\rho] = T_{\mathrm{S}} + E_{\mathrm{ne}}[\rho] + J[\rho] + E_{XC}[\rho] \tag{77}$$

where $E_{XC}[\rho]$ is the energy expressing the electron exchange correlation

$$E_{XC}[\rho] = (T[\rho] - T_{\mathrm{S}}[\rho]) + (E_{\mathrm{ee}}[\rho] - J[\rho]) \tag{78}$$

The first term in the parenthesis is the kinetic energy correlation (the difference between the exact kinetic energy and that of a system with non interacting of electrons) and the second term in the parenthesis is the exchange energy containing the correlation energy. The exchange-correlation potential is

$$V_{XC}(r) = \frac{dE_{XC}[\rho]}{d\rho(r)} \tag{79}$$

The correlation between electrons of parallel spin is different from that between electrons of opposite spin. The exchange energy is "by definition" given as a sum of contributions from the α and β spin densities, as exchange energy only involves electrons of the same spin. The kinetic energy, the nuclear-electron attraction and Coulomb terms are trivially separable [29].

$$\begin{aligned} E_{\mathrm{X}}[\rho] &= E_{\mathrm{X}}^{\alpha}[\rho_\alpha] + E_{\mathrm{X}}^{\beta}[\rho_\beta] \\ E_{\mathrm{C}}[\rho] &= E_{\mathrm{C}}^{\alpha\alpha}[\rho_\alpha] + E_{\mathrm{C}}^{\beta\beta}[\rho_\beta] + E_{\mathrm{C}}^{\alpha\beta}[\rho_\alpha, \rho_\beta] \end{aligned} \tag{80}$$

Now we must resolve a set of equations given by

$$\left[\frac{p^2}{2} + V_{\mathrm{ne}}(r) + \int \frac{\rho(r')}{|r - r'|} d^3r' + V_{XC}(r)\right] \phi_i(r) = \varepsilon_i \phi_i(r) \tag{81}$$

The resulting pseudo-eigenvalue equations are known as the Kohn-Shan equations

$$h_{\mathrm{KS}} \phi_i = \varepsilon_i \phi_i \tag{82}$$

The problem is how to find an exchange-correlation potential $V_{XC}[\rho]$ that it can be used for an universal system. Today there are many functionals that describe more or less well the $V_{XC}[\rho]$ term. According to different approximations, these functionals are divided in :

- Local Density Approximation (LDA); the density is treated locally as a uniform electron gas and the density is a slowly varying function [29]. In this approximation, the exchange energy, $E_x[\rho]$ depends on the local spin densities only at r : this approach is valid for slowly varying densities and the performance is reasonably good for the description of atomic and molecular systems, but the accuracy of energy parameters is not always sufficient [75]. The exchange energy for a uniform electron gas is given by the Dirac model [79]. Improvements over the LDA reflect the strongly inhomogeneous densities of real systems.

- The Generalized Gradient Approximation (GGA) methods are also sometimes referred to as non local methods; one considers a non-uniform electron gas. The GGA was devised where the exchange energy, $E_x[\rho]$, depends not only on the spin densities at r but also on the derivatives of the density. The GGA improves over the LDA [78, 80, 81].
- Hybrid Functionals : This approximation has a degree of precision higher because it combines exchange and correlation energies obtained by GGA with a certain fraction of exchange energy given by Hartree-Fock theory [29].

The exchange functional proposed by Perdew and Wang in [78] (PW91 functional) is given by

$$E_x^{\mathrm{PW91}} = E_x^{\mathrm{LDA}} \left(\frac{1 + x a_1 \sinh^{-1}(x a_2) + (a_3 + a_4 \exp^{-b x^2}) x^2}{1 + x a_1 \sinh^{-1}(x a_2) + a_5 x^2} \right) \tag{83}$$

where $a_i (i = 1, 2, ..., 5)$ and b is suitable parameters and x is defined in Eq. (84), that is a dimensionless gradient variable, and a, b and c again are suitable parameters [82].

$$\begin{aligned} E_x^{\mathrm{PW86}} &= E_x^{\mathrm{LDA}} (1 + a x^2 + b x^4 + c x^6)^{\frac{1}{15}} \\ x &= \frac{|\nabla \rho|}{\rho^{\frac{4}{3}}} \end{aligned} \tag{84}$$

Brief overview of group theory

The concept of molecular symmetry is very useful in spectroscopy to study the spectra of atoms and molecules. Therefore we use group theory to label and classify the energy levels of the vibrations of H/Pd(111). The idea of molecular symmetry can be quantified by the introduction of symmetry operations that means to do a geometry action (such as a reflection) that leaves the molecule in equivalent positions. These geometrical operations can be classified into four types: reflections ($\hat{\sigma_v}$), rotations ($\hat{C}_n$), rotations-reflections ($\hat{S}_n$), and inversions ($\hat{i}$). For mathematical reasons a fifth operation, the "do nothing" operation of identity ($\hat{E}$), needs to be added. Associated with each symmetry operation (except the identity) is a symmetry element [83].

The point group associated with the ammonia molecule is the C_{3v} group is has six members, $\{\hat{E}, \hat{C}_3, \hat{C}_3^{-1}, \hat{\sigma_v}', \hat{\sigma_v}'', \hat{\sigma_v}'''\}$, associated with three vertical planes of symmetry, where the identity $\hat{E}$ operator leaves the hydrogen located at "fcc" site unchanged (see Fig. 12 the blue circle), the $\hat{C}_3$ operator rotates the channels of diffusion by $2\pi/3 = 120^0$ in a clockwise direction about the $\hat{C}_3$ axis out of the plane. The clockwise direction is defined by viewing the model (Fig. 12) from de $+z$ direction toward the xy-plane of model. The $\hat{C}_3^{-1}$ operator rotates the channels in the counter-clockwise direction (that is, by $-2\pi/3 = -120^0$). The reflection operator $\hat{\sigma_v}$ (subscript v means the vertical mirror plane), reflects the channels at a plane containing the z-axis and one of the channels. Three equivalent channels exist at the "hcp" site (see Fig. 12, the red circles) [83].

The C_{3v} point group is of order 6 and it is divided in three classes ($3\hat{\sigma_v}, 2\hat{C}_3$ and $\hat{E}$). The first column block of the Tab. 17 shows the three symmetry species. It is seen that all elements of each symmetry class have the same symmetry characters. The symmetry species E is a double degenerate one. The second column block lists the characters of the matrices (of smallest possible dimension) that describes the symmetry of operations. The third column block indicated which of the irreducible representations correspond to translations (unit x, y, z vectors) and rotations. The forth column block gives the corresponding information for quadratic functions that is used for building the molecular orbitals or selection rules in Raman spectroscopy.

Table 17 – Character table for C_{3v} point group.

C_{3v}	$\hat{E}$	$2\hat{C}_3$	$3\hat{\sigma}_v$	linear functions	quadratic functions
A_1	1	1	1	z	$(x^2+y^2);(z^2)$
A_2	1	1	-1	R_z	-
E	2	-1	0	$(x,y);(R_x,R_y)$	$(x^2-y^2,xy);(xz,yz)$

The quadratic functions representation space for C_{3v} has dimension 9. The reduction yields a six-dimensional space which splits into a two-dimensional space of type A_1 and a two-dimensional space of type E [84,85]. The A_1 symmetry adapted are (x^2+y^2) and (z^2), the E symmetry adapted are (x^2-y^2,xy) and (xz,yz).

Reduced probability densities for T/Pd(111)

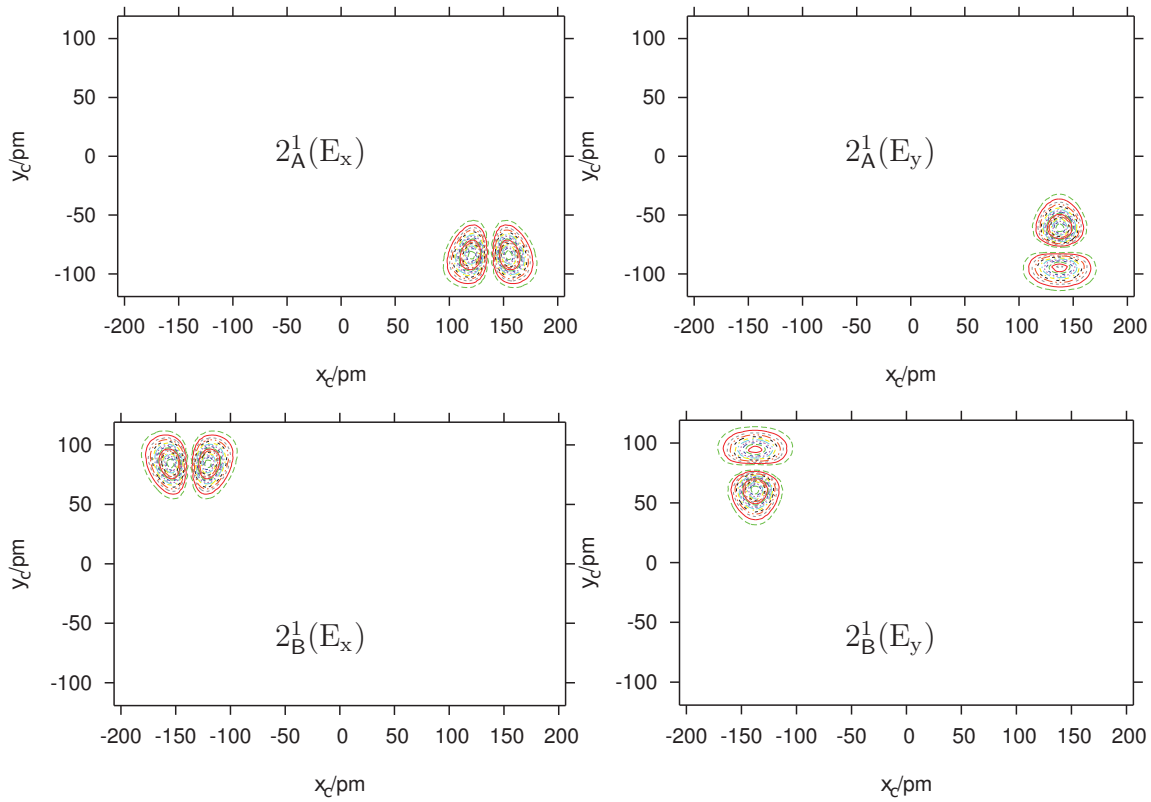

Figure 58 – Reduced probability density for the third and fifth level (471.2 and 660.1 $hc\,\mathrm{cm}^{-1}$, respectively) that represent parallel modes with 1 quantum of energy (2^1_B and 2^1_B) in "fcc" and "hcp" sites, respectively, in the $x_c y_c$ plan.

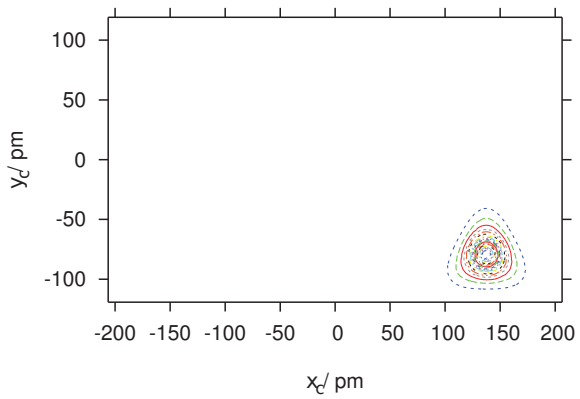

(a) Reduced probability density in $x_c y_c$ plan.

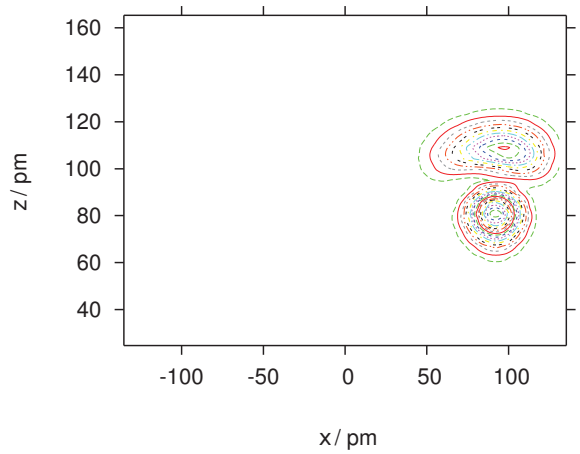

(b) Reduced probability density in xz plan.

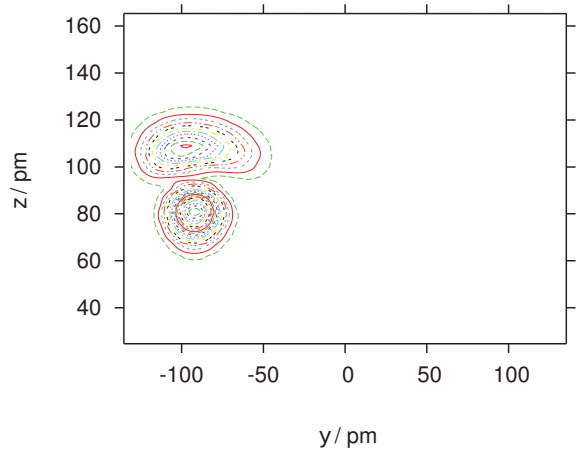

(c) Reduced probability density in yz plan.

Figure 59 – Reduced probability density for the fourth level at 650.4 $hc\,\mathrm{cm}^{-1}$ assigned as $1^1_{\mathsf{A}} + (2^2_{\mathsf{A}})$. The 2^2_{A} component is visibly very weak.

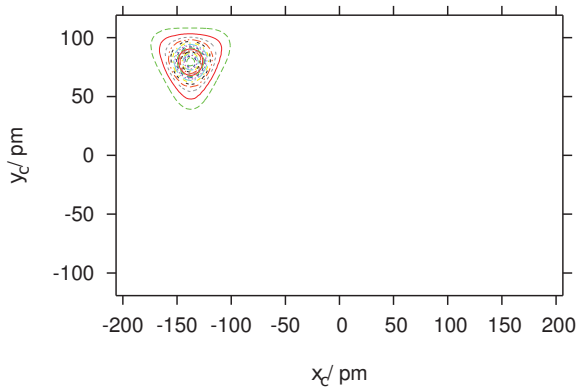

(a) Reduced probability density in $x_c y_c$ plan.

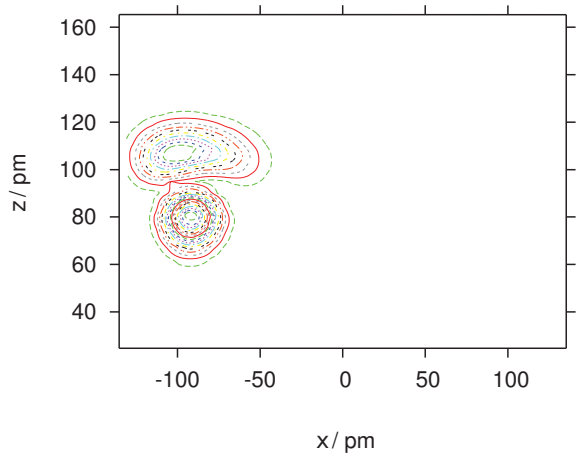

(b) Reduced probability density in xz plan.

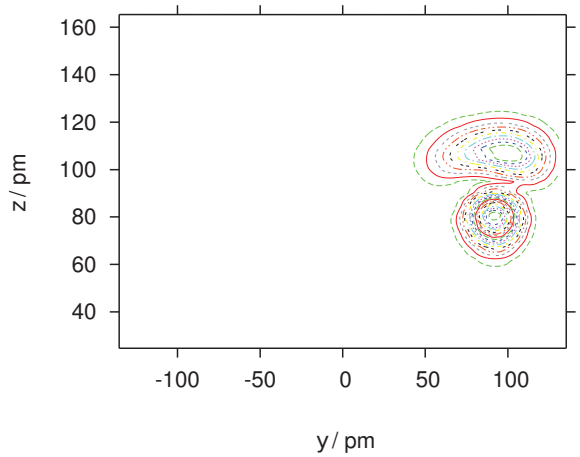

(c) Reduced probability density in yz plan.

Figure 60 – Reduced probability density for the sixth level (837.1 $hc\,\mathrm{cm}^{-1}$) assigned as $1^1_{\mathrm{B}} + (2^2_{\mathrm{B}})$, its label of symmetry is A_1(the 2^2_{B} component is very weak).

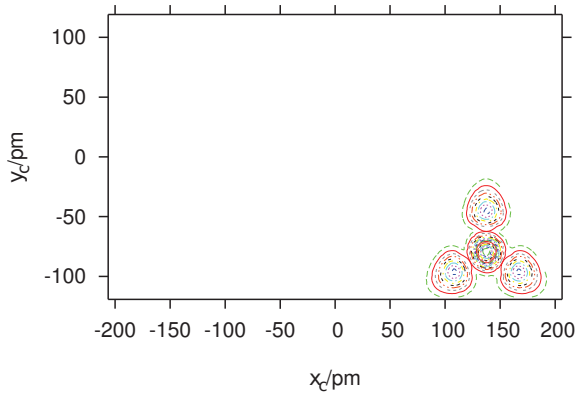

(a) Reduced probability density in $x_c y_c$ plan.

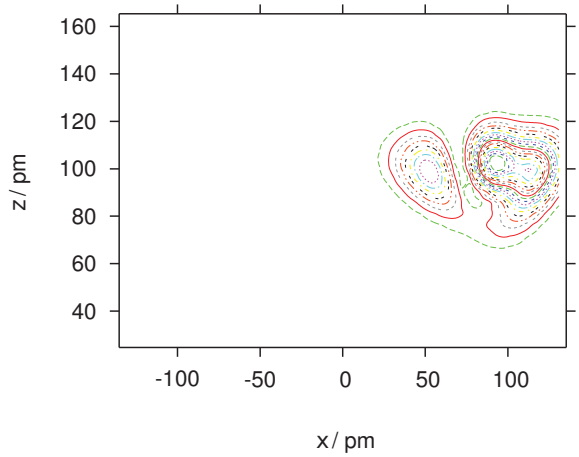

(b) Reduced probability density in xz plan.

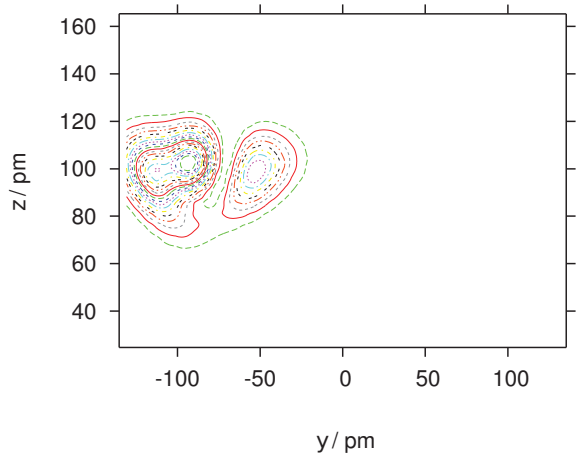

(c) Reduced probability density in yz plan.

Figure 61 – Reduced probability density for the seventh level (873.7 $hc\,\mathrm{cm}^{-1}$) assigned as $1^1_{\mathrm{A}} + 2^2_{\mathrm{A}}$, its label of symmetry is A_1.

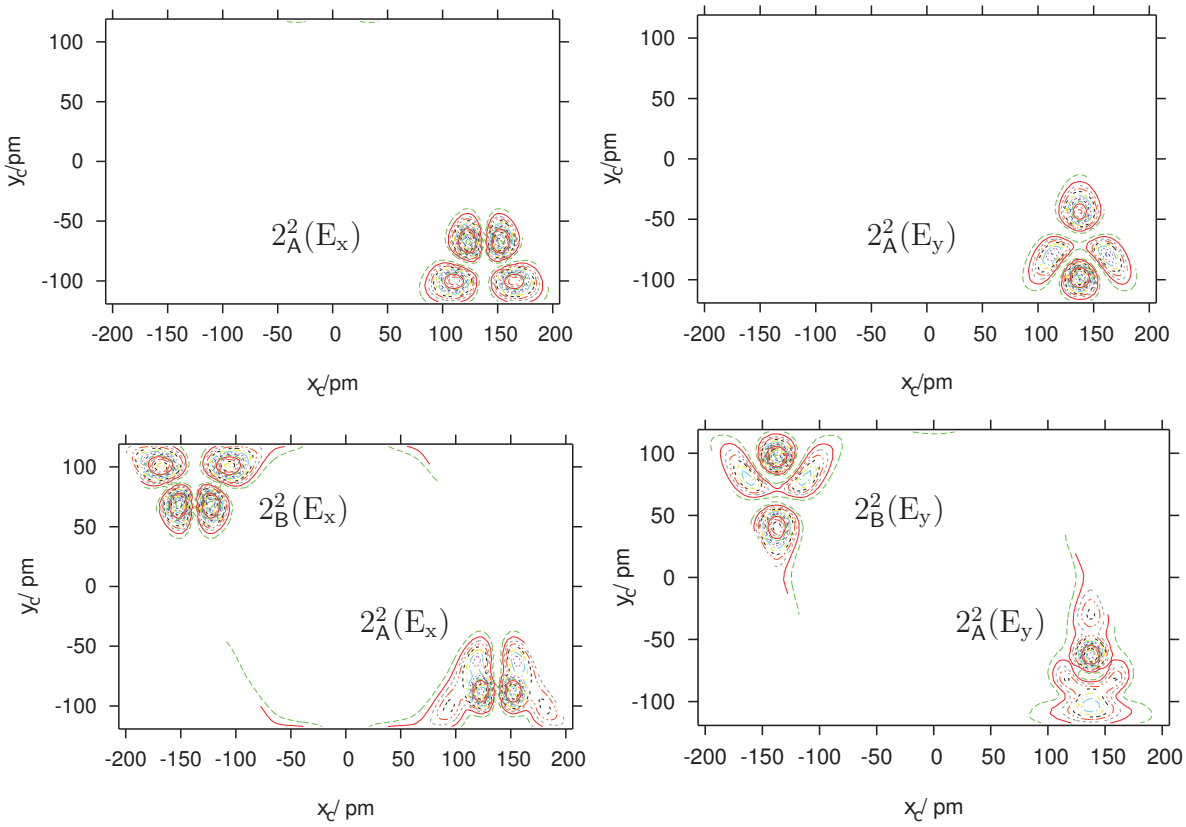

Figure 62 – Reduced probability density for the eighth and tenth levels (912.1 and 1085.7 $hc\,\mathrm{cm}^{-1}$, respectively) that represent the vibrational parallel modes with 2 quanta of energy. At 912.1 $hc\,\mathrm{cm}^{-1}$ the mode is localized at "fcc" site (2^2_A) and at 1085.7 $hc\,\mathrm{cm}^{-1}$ the mode is delocalized in two sites (2^2_A+2^2_B).

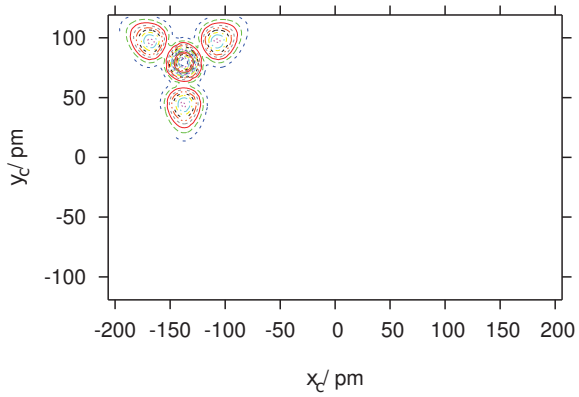

(a) Reduced probability density in $x_c y_c$ plan.

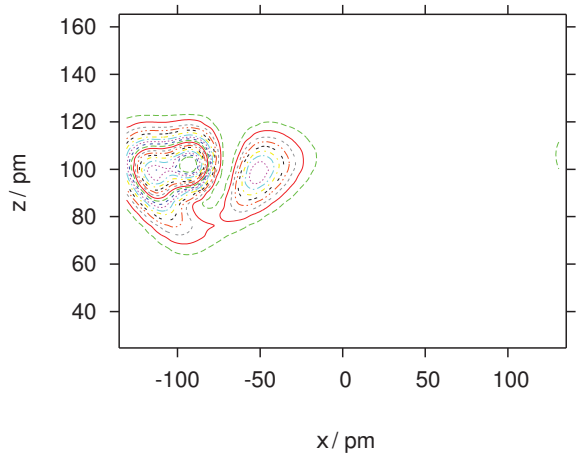

(b) Reduced probability density in xz plan.

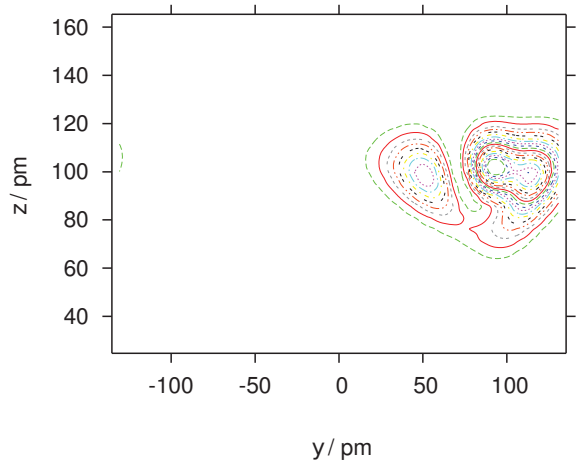

(c) Reduced probability density in yz plan.

Figure 63 – Reduced probability density for the ninth level (1049.9 $hc\,\mathrm{cm}^{-1}$) assigned as $1^1_{\mathsf{B}} + 2^2_{\mathsf{B}}$, its label of symmetry is A_1.

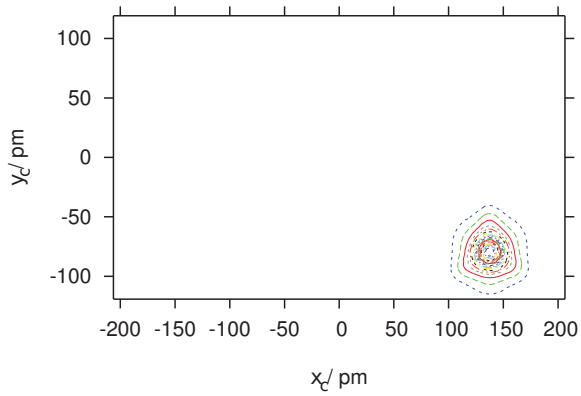

(a) Reduced probability density in $x_c y_c$ plan.

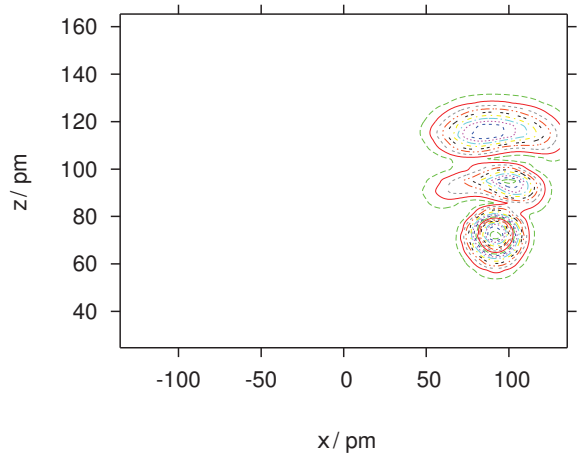

(b) Reduced probability density in xz plan.

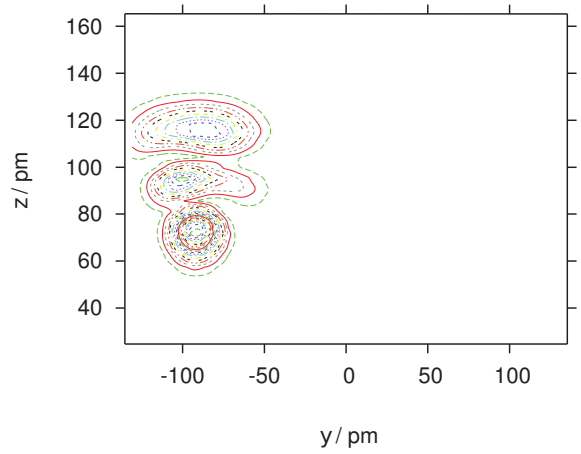

(c) Reduced probability density in yz plan.

Figure 64 – Reduced probability density for the twenty second band (1311.9 $hc\,\mathrm{cm}^{-1}$) assigned as $1^2_{\mathrm{A}} + (2^2_{\mathrm{A}})$, its label of symmetry is A_1(the 2^2_{A} component is weak).

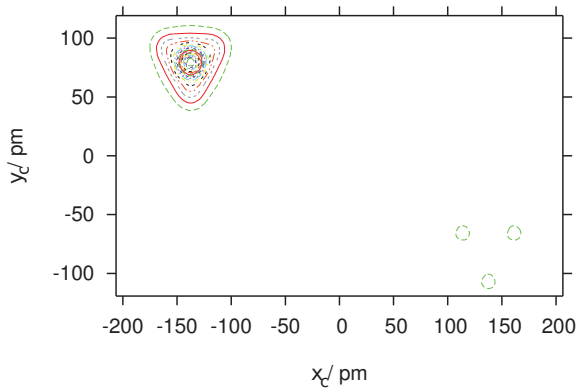

(a) Reduced probability density in $x_c y_c$ plan.

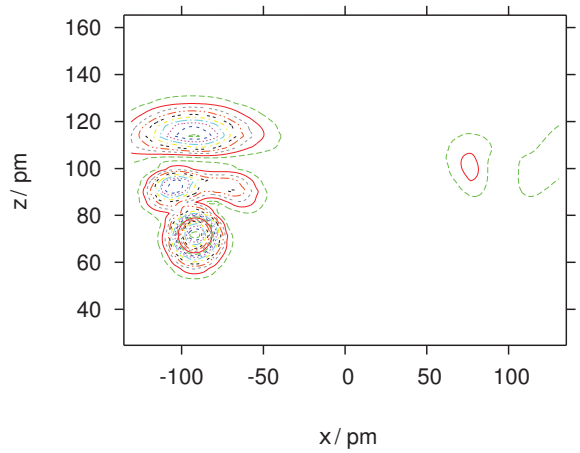

(b) Reduced probability density in xz plan.

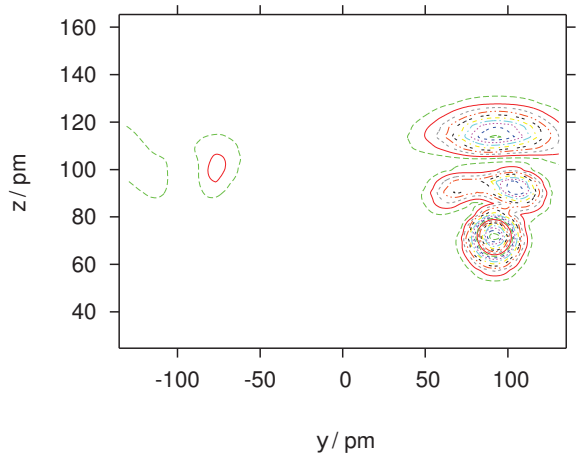

(c) Reduced probability density in yz plan.

Figure 65 – Reduced probability density for the twenty ninth level (1490.9 $hc\,\mathrm{cm}^{-1}$)assigned as $1^1_B + (2^2_B)$, its label of symmetry is A_1(the 2^2_B component is weak.

Bibliography

[1] Y. Xiao, W. Dong, and H. Busnengo, "Reactive force fields for surface chemical reactions: A case study with hydrogen dissociation on Pd surfaces," *J. Chem. Phys.*, vol. 132, no. 1, 2010.

[2] R. A. Olsen, H. F. Busnengo, A. Salin, M. F. Somers, G. J. Kroes, and E. J. Baerends, "Constructing accurate potential energy surfaces for a diatomic molecule interacting with a solid surface: H_2-Pt(111) and H_2-Cu(100)," *J. Chem. Phys.*, vol. 116, no. 9, pp. 3841–3855, 2002.

[3] M. F. Somers, R. A. Olsen, H. F. Busnengo, E. J. Baerends, and G. J. Kroes, "Reactive scattering of H_2 from Cu(100): Six-dimensional quantum dynamics results for reaction and scattering obtained with a new, accurately fitted potential-energy surface," *J. Chem. Phys.*, vol. 121, no. 22, p. 11379, 2004.

[4] A. Banerjee, N. Adams, J. Simons, and R. Shepard, "Search for Stationary Points on Surfaces," *J. Phys. Chem.*, vol. 89, no. 1, pp. 52–57, 1985.

[5] S. Holloway, "Dynamics of gas-surface reactions," *Surf. Sci.*, vol. 299-300, no. 0, pp. 656 – 666, 1994.

[6] G.-J. Kroes, A. Gross, E.-J. Baerends, M. Scheffler, and D. A. McCormack, "Quantum theory of dissociative chemisorption on metal surfaces," *Acc. Chem. Res.*, vol. 35, no. 3, pp. 193–200, 2002.

[7] E. Fromm, *Kinetics of metal-gas interactions at low temperatures: hydriding, oxidation, poisoning*. Springer series in surface sciences, Berlin: Springer, 1998.

[8] G. Wiesenekker, G. J. Kroes, E. J. Baerends, and R. C. Mowrey, "Dissociation of H_2 on Cu(100): Dynamics on a new two-dimensional potential energy surface," *J. Chem. Phys.*, vol. 102, no. 9, pp. 3873–3883, 1995.

[9] B. E. J. Wiesenekker G., Kroes G. J., "An analytical six-dimensional potential energy surface for dissociation of molecular hydrogen on Cu(100)," *J. Chem. Phys.*, vol. 104, no. 18, p. 7344, 1996.

[10] B. E. J. Mowrey R. C., Kroes G. J., "Dissociative adsorption of H_2 on Cu(100): Fixed-site calculations for impact at hollow and top sites," *J. Chem. Phys.*, vol. 108, no. 16, p. 6906, 1998.

[11] D. A. McCormack, G.-J. Kroes, R. A. Olsen, J. A. Groeneveld, J. N. P. van Stralen, E. J. Baerends, and R. C. Mowrey, "Quantum dynamics of the dissociation of H_2 on Cu(100): Dependence of the site-reactivity on initial rovibrational state," *Faraday Discuss.*, vol. 117, pp. 109–132, 2000.

[12] W. Dong and J. Hafner, "H_2 dissociative adsorption on Pd(111)," *Phys. Rev. B*, vol. 56, no. 23, p. 15396, 1997.

[13] R. Marquardt, F. Cuvelier, R. Olsen, E. Baerends, J. Tremblay, and P. Saalfrank, "A new analytical potential energy surface for the adsorption system CO/Cu(100)," *J. Chem. Phys.*, vol. 132, no. 7, p. 74108, 2010.

[14] G. Ertl, "Primary steps in catalytic synthesis of ammonia," *J. Vac. Sci. Technol., A*, vol. 1, no. 2, pp. 1247–1253, 1983.

[15] G. Ertl, "Elementary steps in heterogeneous catalysis," *Angew. Chem. Int. Ed.*, vol. 29, no. 11, pp. 1219–1227, 1990.

[16] V. A. Blagojević, D. M. Minić, D. G. Minić, and J. G. Novaković, *Hydrogen Economy: Modern Concepts, Challenges and Perspectives.* InTech, DOI: 10.5772/46098. Available from: `http://www.intechopen.com/books/hydrogen-energy-challenges-and-perspectives`, 2012.

[17] G. A. Somorjai, *Introduction to Surface Chemistry and Catalysis.* John Wiley and Sons, New York, 1994.

[18] N. Sheppard, "Surface studies by IR spectroscopy," in *Encyclopedia of Spectroscopy and Spectrometry (Second Edition)* (J. C. Lindon, ed.), pp. 2813 – 2821, Oxford: Academic Press, second edition ed., 1999.

[19] M. Jo, Y. Kuwahara, M. Onchi, and M. Nishijima, "Adsorbed states of hydrogen on Pd(110): Vibrational electron energy loss spectroscopy and low-energy electron diffraction studies," *Solid State Commun.*, vol. 55, no. 7, pp. 639 – 642, 1985.

[20] V. H. Grassian and E. L. Muetterties, "Vibrational electron energy loss spectroscopic study of benzene, toluene, and pyridine adsorbed on Pd(111) at 180 K," *J. Phys. Chem.*, vol. 91, no. 2, pp. 389–396, 1987.

[21] H. Conrad, G. Ertl, and E. Latta, "Adsorption of hydrogen on palladium single crystal surfaces," *Surf. Sci*, vol. 41, no. 2, pp. 435 – 446, 1974.

[22] H. Conrad, M. Kordesch, R. Scala, and W. Stenzel, "Surface resonances on H/Pd(111) observed with HREELS," *J. Electron. Spectrosc. Relat. Phenom.*, vol. 38, no. 0, pp. 289 – 298, 1986.

[23] T. Ellis and M. Morin, "The vibrational modes of hydrogen adsorbed on Pd(110)," *Surf. Sci. Lett.*, vol. 216, no. 1-2, pp. L351 – L356, 1989. 330.

[24] R. A. Scott and C. M. Lukehart, *Applications of Physical Methods To Inorganic and Bioinorganic Chemistry.* Wiley-Interscience, 2007.

[25] G. Alexandrowicz, A. P. Jardine, P. Fouquet, S. Dworski, W. Allison, and J. Ellis, "Observation of microscopic CO dynamics on Cu(001) using ^{3}He spin-echo spectroscopy," *Phys. Rev. Lett.*, vol. 93, p. 156103, Oct 2004.

[26] X. J. Shen, W. Dong, Y. Xiao, and X. H. Yan, "Comment on reactive force fields for surface chemical reactions: A case study with hydrogen dissociation on Pd surfaces," *J. Chem. Phys.*, vol. 135, no. 16, p. 167101, 2011.

[27] Y. Xiao and W. Dong, "Molecular dynamics simulation of a complex surface reaction: The effect of coverage on H_2 dissociation on Pd(111)," *Phys. Rev. B*, vol. 83, p. 125418, 2011.

[28] X. Shen, Y. Xiao, W. Dong, X. Yan, and H. Busnengo, "Molecular dynamics simulations based on reactive force-fields for surface chemical reactions," *Comput. Theor. Chem.*, vol. 990, no. 0, pp. 152 – 158, 2012.

[29] F. Jensen, *Introduction to Computational Chemistry.* John Wiley & Sons, 1999.

[30] G. A. Worth, M. H. Beck, A. Jäckle, , and H.-D. Meyer, MCTDH *package, version 8.4.* See `http://mctdh.uni-hd.de/`, 2013.

[31] H.-D. Meyer, U. Manthe, and L. Cederbaum, "The multi-configurational time-dependent hartree approach," *Chem. Phys. Lett.*, vol. 165, no. 1, pp. 73 – 78, 1990.

[32] M. Beck, A. Jäckle, G. Worth, and H.-D. Meyer, "The multiconfiguration time-dependent hartree (MCTDH) method: a highly efficient algorithm for propagating wavepackets," *Phys. Rep.*, vol. 324, no. 1, pp. 1 – 105, 2000.

[33] H.-D. Meyer, F. Gatti, and G. A. Worth, *Multidimensional Quantum Dynamics:* MCTDH *Theory and Applications.* Wiley-VCH Verlag GmbH & Co. KGaA, 2009.

[34] R. Marquardt, "Theoretical methods for ultrafast spectroscopy," *ChemPhysChem*, vol. 14, no. 7, pp. 1350–1361, 2013.

[35] A. Jäckle and H.-D. Meyer, "Reactive scattering using the multiconfiguration time-dependent hartree approximation: General aspects and application to the collinear H + H_2 –> H_2 + H reaction," *J. Chem. Phys.*, vol. 102, no. 14, pp. 5605–5615, 1995.

[36] A. Jäckle and H.-D. Meyer, "Product representation of potential energy surfaces," *J .Chem. Phys.*, vol. 104, no. 20, pp. 7974–7984, 1996.

[37] A. Jäckle and H.-D. Meyer, "Product representation of potential energy surfaces. II," *J. Chem. Phys.*, vol. 109, no. 10, pp. 3772–3779, 1998.

[38] H.-D. Meyer and G. A. Worth, "Quantum molecular dynamics: propagating wavepackets and density operators using the multiconfiguration time-dependent hartree method.," *Theor. Chem. Acc.*, vol. 109, no. 5, pp. 251 – 267, 2003.

[39] H.-D. Meyer, F. L. Quéré, C. Léonard, and F. Gatti, "Calculation and selective population of vibrational levels with the multiconfiguration time-dependent hartree (MCTDH) algorithm," *Chem. Phys.*, vol. 329, no. 1-3, pp. 179–192, 2006.

[40] F. Richter, F. Gatti, C. Léonard, F. Le Quéré, and H.-D. Meyer, "Time-dependent wave packet study on trans-cis isomerization of HONO driven by an external field," *J. Chem. Phys.*, vol. 127, no. 16, p. 164315, 2007.

[41] L. J. Doriol, F. Gatti, C. Iung, and H.-D. Meyer, "Computation of vibrational energy levels and eigenstates of fluoroform using the multiconfiguration time-dependent hartree method," *J. Chem. Phys.*, vol. 129, no. 22, p. 224109, 2008.

[42] Q. Meng and H.-D. Meyer, "MCTDH study on vibrational states of the CO/Cu(100) system," *J. Chem. Phys.*, vol. 139, no. 16, p. 164709, 2013.

[43] E. R. Davidson, "The iterative calculation of a few of the lowest eigenvalues and corresponding eigenvectors of large real-symmetric matrices," *J. Comput. Phys.*, vol. 17, no. 1, pp. 87 – 94, 1975.

[44] J. L. Bonnardet and G. Papin, *État solide*. BRÉAL, 2003.

[45] N. D. Mermin and N. W. Ashcroft, *Solid State Physics*. Holt-Saunders Internation Editions, New York, 1976.

[46] D. W. Brenner, O. A. Shenderova, J. A. Harrison, S. J. Stuart, B. Ni, and S. B. Sinnott, "A second-generation reactive empirical bond order (REBO) potential energy expression for hydrocarbons," *J. Phys. : Condens. Matter*, vol. 14, no. 4, p. 783, 2002.

[47] N. Ozawa, N. B. A. Jr, T. A. Roman, H. Nakanishi, W. A. Diño, and H. Kasai, "Quantum states of hydrogen atom motion on the Pd(111) surface and in the subsurface," *J. Phys.: Condens. Matter*, vol. 19, no. 36, p. 365214, 2007.

[48] N. Ozawa, T. A. Roman, H. Nakanishi, H. Kasai, N. B. Arboleda, and W. A. Diño, "Potential energy of hydrogen atom motion on Pd(111) surface and in subsurface: A first principles calculation," *J. Appl. Phys.*, vol. 101, no. 12, pp. 123530–123530–6, 2007.

[49] J. C. Tremblay and P. Saalfrank, "Selective subsurface absorption of hydrogen in palladium using laser distillation," *J. Chem. Phys.*, vol. 131, no. 8, p. 084716, 2009.

[50] E. Fermi, "über den ramaneffekt des kohlendioxyds," *Zeitschrift für Physik*, vol. 71, no. 3-4, pp. 250–259, 1931.

[51] G. Herzberg, *Electronic Spectra and Electronic Structure of Polyatomic Molecules*. No. vol. 2 in Electronic Spectra and Electronic Structure of Polyatomic Molecules, Krieger Publishing Company, 1991.

[52] E. R. Cohen, T. Cvitas, J. G. Frey, B. Holmström, K. Kuchitsu, R. Marquardt, I. Mills, F. Pavese, M. Quack, J. Stohner, H. L. Strauss, M. Takami, and A. J. Thor, *Quantities, Units and Symbols in Physical Chemistry*. RSC Publishing, Cambridge, UK, 3 ed., 2007.

[53] I. Nikitin, W. Dong, H. Busnengo, and A. Salin, "Diffusion of a hydrogen atom on the Pd(111) surface: quantum transition state wave packet approach," *Surf. Sci.*, vol. 547, no. 1-2, pp. 149 – 156, 2003.

[54] K. K. Irikura, "Experimental Vibrational Zero-Point Energies: Diatomic Molecules," *J. Phys. Chem. Ref. Data*, vol. 36, no. 2, pp. 389–397, 2007.

[55] A. D. Jewell, G. Peng, M. F. G. Mattera, E. A. Lewis, C. J. Murphy, G. Kyriakou, M. Mavrikakis, and E. C. H. Sykes, "Quantum tunneling enabled self-assembly of hydrogen atoms on Cu(111)," *ACS Nano*, vol. 6, no. 11, pp. 10115–10121, 2012.

[56] T. Firmino, R. Marquardt, F. Gatti, D. Zanuttini, and W. Dong, "Full quantum calculations of the diffusion rate of adsorbates," in *Frontiers in Quantum Methods and Applications in Chemistry and Physics: Selected and Edited Proceedings of QSCP-XVIII*, (Paraty, Brazil), Springer-Verlag GmbH Berlin, December 2013.

[57] A. P. Jardine, E. Y. M. Lee, D. J. Ward, G. Alexandrowicz, H. Hedgeland, W. Allison, J. Ellis, and E. Pollak, "Determination of the quantum contribution to the activated motion of hydrogen on a metal surface: H/Pt(111)," *Phys. Rev. Lett.*, vol. 105, p. 136101, Sep 2010.

[58] E. M. McIntosh, K. T. Wikfeldt, J. Ellis, A. Michaelides, and W. Allison, "Quantum effects in the diffusion of hydrogen on Ru(0001)," *J. Phys. Chem. Letters*, vol. 4, no. 9, pp. 1565–1569, 2013.

[59] L. Van Hove, "Correlations in space and time and born approximation scattering in systems of interacting particles," *Phys. Rev.*, vol. 95, pp. 249–262, Jul 1954.

[60] M. Morin, N. J. Levinos, and A. L. Harris, "Vibrational energy transfer of CO/Cu(100): Nonadiabatic vibration/electron coupling," *J. Chem. Phys.*, vol. 96, no. 5, pp. 3950–3956, 1992.

[61] C. Frischkorn and M. Wolf, "Femtochemistry at metal surfaces: Nonadiabatic reaction dynamics," *Chem. Rev.*, vol. 106, no. 10, pp. 4207–4233, 2006.

[62] T. Vazhappilly, S. Beyvers, T. Klamroth, M. Luppi, and P. Saalfrank, "Vibrationally enhanced associative photodesorption of molecular hydrogen from Ru(0001)," *Chem. Phys.*, vol. 338, no. 2-3, pp. 299 – 311, 2007.

[63] M. Head-Gordon and J. C. Tully, "Vibrational relaxation on metal surfaces: Molecular-orbital theory and application to CO/Cu(100)," *J. Chem. Phys.*, vol. 96, no. 5, p. 963939, 1992.

[64] A. Jardine, H. Hedgeland, G. Alexandrowicz, W. Allison, and J. Ellis, "Helium-3 spin-echo: Principles and application to dynamics at surfaces," *Prog. in Surf. Sci.*, vol. 84, no. 11-12, pp. 323 – 379, 2009.

[65] J. C. Tremblay, "A unifying model for non-adiabatic coupling at metallic surfaces beyond the local harmonic approximation: From vibrational relaxation to scanning tunneling microscopy," *J. Chem. Phys.*, vol. 138, no. 24, pp. 244106–1–244106–15, 2013.

[66] Y. P. Zhang, C. H. Cheng, J. T. Kim, J. Stanojevic, and E. E. Eyler, "Dissociation energies of molecular hydrogen and the hydrogen molecular ion," *Phys. Rev. Lett.*, vol. 92, p. 203003, May 2004.

[67] A. Szabo and N. S. Ostlund, *Modern Quantum Chemistry: Introduction to Advanced Electronic Structure Theory (Dover Books on Chemistry)*. Dover Publications, new edition ed., july 1996.

[68] T. Helgaker, P. Jørgensen, and J. Olsen, *Molecular Electronic Structure Theory*. Chichester: John Wiley & Sons, LTD, 2000.

[69] R. J. Bartlett and J. F. Stanton, *Applications of Post-Hartree-Fock Methods: A Tutorial*, pp. 65–169. John Wiley & Sons, Inc., 2007.

[70] C. Møller and M. S. Plesset, "Note on an approximation treatment for many-electron systems," *Phys. Rev.*, vol. 46, pp. 618–622, Oct 1934.

[71] R. J. Bartlett, "Many-body perturbation theory and coupled cluster theory for electron correlation in molecules," *Annu. Rev. Phys. Chem.*, vol. 32, no. 1, pp. 359–401, 1981.

[72] K. Andersson, P.-Å. Malmqvist, and B. O. Roos, "Second-order perturbation theory with a complete active space self-consistent field reference function," *J. Chem. Phys.*, vol. 96, no. 2, pp. 1218–1226, 1992.

[73] K. Raghavachari, G. W. Trucks, J. A. Pople, and M. Head-Gordon, "A fifth-order perturbation comparison of electron correlation theories," *Chem. Phys. Lett.*, vol. 157, no. 6, pp. 479 – 483, 1989.

[74] P. Hohenberg and W. Kohn, "Inhomogeneous electron gas," *Phys. Rev.*, vol. 136, pp. B864–B871, Nov 1964.

[75] W. Kohn and L. J. Sham, "Self-consistent equations including exchange and correlation effects," *Phys. Rev.*, vol. 140, pp. A1133–A1138, Nov 1965.

[76] G. Kresse and J. Hafner, "*Ab initio* molecular dynamics for liquid metals," *Phys. Rev. B*, vol. 47, pp. 558–561, 1993.

[77] W. Dong, G. Kresse, J. Furthmüller, and J. Hafner, "Chemisorption of H on Pd(111): An *ab initio* approach with ultrasoft pseudopotentials," *Phys. Rev. B*, vol. 54, pp. 2157–2166, Jul 1996.

[78] J. P. Perdew, J. A. Chevary, S. H. Vosko, K. A. Jackson, M. R. Pederson, D. J. Singh, and C. Fiolhais, "Atoms, molecules, solids, and surfaces: Applications of the generalized gradient approximation for exchange and correlation," *Phys. Rev. B*, vol. 46, pp. 6671–6687, Sep 1992.

[79] P. A. Dirac, "Note on exchange phenomena in the thomas atom," *Math. Proc. Cambridge*, vol. 26, p. 376, 1930.

[80] J. P. Perdew, "Density-functional approximation for the correlation energy of the inhomogeneous electron gas," *Phys. Rev. B*, vol. 33, pp. 8822–8824, Jun 1986.

[81] J. P. Perdew and W. Yue, "Erratum: Accurate and simple density functional for the electronic exchange energy: Generalized gradient approximation," *Phys. Rev. B*, vol. 40, pp. 3399–3399, Aug 1989.

[82] J. P. Perdew and W. Yue, "Accurate and simple density functional for the electronic exchange energy: Generalized gradient approximation," *Phys. Rev. B*, vol. 33, pp. 8800–8802, Jun 1986.

[83] P. F. Bernath, *Spectra of Atoms and Molecules*. Oxford: Oxford Univ. Press, USA, 2005.

[84] J. Duncan and I. Mills, "The calculation of force constants and normal coordinates-IV XH_4 and XH_3 molecules," *Spectrochim. Acta*, vol. 20, no. 3, pp. 523 – 546, 1964.

[85] R. Marquardt and K. Sagui, "A complete list of symmetry adapted expressions to the fourth power for compact bending potentials in molecules with and symmetry from a general symbolic algebra program," *Mol. Phys.*, vol. 105, no. 9, pp. 1157–1169, 2007.

Thiago Diamond REIS FIRMINO

The quantum dynamics of the diffusion of dissociatively adsorbed diatomic molecules

Résumé

Les travaux réalisés au cours de cette thèse portent sur la dynamique quantique de diffusion d'atomes d'hydrogène sur une surface de palladium (111). L'étude du système 3D a permis de détailler le spectre infrarouge de H/Pd(111) en mettant en évidence l'existence sur différents sites d'adsorption d'états localisés fortement couplés (résonance de Fermi). Ce phénomène gouverne la diffusion des atomes d'hydrogène sur une échelle de temps ultra-rapide (fs).

L'étude du système 6D (H_2/Pd(111)) a montré que les transitions observées sont, en fait, des bandes de transition entre plusieurs états d'adsorption quasi-dégénérés. L'accord entre les valeurs calculées et mesurées est, par contre, significativement moins bon qu'entre celles calculées pour le système 3D et les données mesurées. Est-ce que l'hydrogène adsorbé sur le palladium existe sous la forme d'une molécule diatomique faiblement lié? Cette thèse a fourni certains éléments de réponse à cette question, qui reste cependant encore ouverte.

Mots-clés : Adsorption dissociative, diffusion quantique, MultiConfiguration Time-Dependent Hartree (MCTDH), Surface d'Énergie Potentielle, Spectroscopie Vibrationnelle, résonance de Fermi, Spectromètre de pertes d'énergie d'électrons à haute résolution (HREELS).

Résumé en anglais

The work carried out during this thesis focuses on the quantum dynamics of the diffusion of hydrogen atoms on a surface of palladium (111). The study of the 3D system allowed us to detail the infrared spectrum of H/Pd (111), showing the existence of different adsorption sites on which localized states exist that are strongly coupled (Fermi resonance). This phenomenon governs the diffusion of hydrogen atoms in an ultra-fast time scale (fs).

The study of the (6D) H_2/Pd(111) system has shown that the transitions observed are in fact transition bands between several quasi-degenerate adsorption states. The agreement between the calculated and measured values is significantly less good than that between the data calculated for the 3D system and the measured data. Does adsorbed hydrogen on palladium exist in the form of a weakly bound H_2 molecule? This thesis has provided some answers to this question, which remains open, hovewer, to some extent.

Keywords: Dissociative adsorption, quantum diffusion, Multiconfiguration Time-Dependent Hartree (MCTDH), Surface Potential Energy, Vibrational Spectroscopy, Fermi resonance, High resolution electron energy loss spectroscopy (HREELS).